

NUMERICAL SOLUTION OF  
THE TURBULENT-BOUNDARY-LAYER  
EQUATIONS

BY

A. M. O. SMITH, and T. CEBECI

AD656430

Prepared Under Navy Contract N0w 66-0324-c,  
Administered Under Technical Direction of  
The Naval Ordnance Systems Command, Weapon  
Dynamics Division, Code ORD-035.

Distribution of this document  
is unlimited

RECEIVED

AUG 21 1967

CFS11



Report No. DAC 33735  
May 29, 1967

NUMERICAL SOLUTION OF  
THE TURBULENT-BOUNDARY-LAYER  
EQUATIONS

BY

A. M. O. SMITH, and T. CEBECI

Prepared Under Navy Contract N0w 66-0324-c,  
Administered Under Technical Direction of  
The Naval Ordnance Systems Command, Weapon  
Dynamics Division, Code ORD-035.

Distribution of this document  
is unlimited

**BLANK PAGE**

PREFACE

This report is written in fulfillment of the requirements of U.S. Navy Contract NOW 66-0324c. The contract is a "level of effort" type, and the objectives are covered by the following work statement, taken from the contract.

"Develop and verify an accurate, general, and rapid method of calculating axially symmetric and two-dimensional turbulent boundary-layer flows. The specific phases of the work are as follows:

(a) Semi-empirical expressions will be developed for the turbulent transport properties, such as eddy viscosity, for use in solution of the flow equations.

(b) Solutions of the complete partial differential equations will be obtained for incompressible flow, covering problems of flow in water and in air.

(c) Solutions will also be obtained for compressible flow, applicable to air.

(d) Illustrative applications of the method will be performed to provide information on velocity profiles, boundary-layer thickness, skin friction and heat transfer.

(e) Accuracy will be checked by solution of a variety of flow problems and comparison with experimental data."

Under this type of contract, when the due date arrives, accomplishments are reported whether the ultimate goals have been reached or not. In the present case, as might be expected, the studies are not complete. The problem of incompressible flow has been rather well explored, although more remains to be done. The results have been surprisingly good. The equations governing compressible flow have all been programmed and the method is working, but time was available to calculate only a few cases of flat-plate flow, with and without heat transfer. Much more work remains to be done, and the gratifying results for incompressible flow supply a firm foundation for continuation, which should follow. The present method has been programmed on the IBM 709<sup>4</sup> under the number 57EB. The program can be obtained by qualified requesters from "Commander, Naval Ordnance Laboratory, White Oak, (Code 330), via Commander, Naval Ordnance Systems Command (Code ORD-035)".

The authors and their company wish to express gratitude for the support supplied by the U.S. Navy. Without it, it is unlikely the work would ever have been accomplished.

## 1.0 SUMMARY

This report presents a numerical solution of turbulent boundary-layer equations for both compressible and incompressible flows. An eddy viscosity concept is used to eliminate the Reynolds shear-stress term, and an eddy-conductivity concept is used to eliminate the time mean of the product of fluctuating velocity and temperature. The turbulent boundary layer is regarded as a composite layer consisting of inner and outer regions, and a separate expression for eddy viscosity is used in each region. The ratio of eddy-viscosity to eddy conductivity is assumed to be constant. An implicit finite-difference method is used in the solution of both momentum and energy equations after they are linearized.

A variety of flows have been computed by this method, and comparisons with experimental data and various correlations have been very encouraging. The results described in this report do not represent a finished development but only what has already been accomplished by using one particular formulation of eddy viscosity and constant turbulent Prandtl number.

2.0 TABLE OF CONTENTS

	<u>Page No.</u>
1.0 Summary	2
2.0 Table of Contents	3
3.0 Index of Figures	5
4.0 Principal Notation	8
5.0 Introduction	11
6.0 Description of Method of Solution	16
6.1 Equations of the Compressible Turbulent Boundary Layer	16
6.2 Formulation of Eddy Viscosity and Turbulent Prandtl Number	21
6.2.1 Viscosity in the Inner Region	21
6.2.2 Viscosity in the Outer Region	22
6.2.3 Definition of Inner and Outer Regions	23
6.2.4 Turbulent Prandtl Number	24
6.3 Transformation of Boundary-Layer Equations	24
6.4 Transformation of Eddy-Viscosity Equations	30
6.5 Fluid Properties	30
6.6 Overall Method of Solution	31
6.6.1 Solution of Momentum Equation	34
6.6.1.1 Finite-Difference Representation of $\xi$ -Derivatives	34
6.6.1.2 Linearization of Momentum Equation	34
6.6.1.3 Variable-Grid Spacing in the $\eta$ -Direction	37
6.6.1.4 Method of Solution	39
6.6.2 Solution of Energy Equation	45
6.6.2.1 Finite-Difference Representation of $\xi$ -Derivatives	45
6.6.2.2 Method of Solution	46
6.6.3 Outline of Procedure for Solving Momentum and Energy Equations Simultaneously at $\xi = \xi_n$	48
6.6.4 Starting the Solution at the Leading Edge or at the Stagnation point, $\xi = 0$	52
6.7 Boundary-Layer Parameters	54
7.0 Comparison of Calculated and Experimental Results	58
7.1 Incompressible Flows	60

	<u>Page No.</u>
7.1.1 Flat-Plate Flow	60
7.1.2 Flat-Plate Flow with Mass Transfer	63
7.1.2.1 Uniform Blowing (Mickley and Davis)	64
7.1.2.2 Uniform Suction (Tennekes)	64
7.1.3 Equilibrium Flows in Favorable and in Adverse Pressure Gradients	65
7.1.3.1 Equilibrium Flow in a Favorable Pressure Gradient (Herring and Norbury)	65
7.1.3.2 Equilibrium Flow in an Adverse Pressure Gradient (Clauser)	66
7.1.3.3 Equilibrium Flow Recovering to Constant Pressure Flow (Bradshaw and Ferriss)	67
7.1.4 Nonequilibrium and Separating Flows	69
7.1.4.1 Favorable and Adverse Pressure Gradients on an Airfoil-like Body (Schubauer and Klebanoff)	69
7.1.4.2 Adverse Pressure Gradient on a Body of Revolution (Moses)	70
7.1.4.3 Adverse Pressure Gradient on an Airfoil (Von Doenhoff and Tetervin)	71
7.2 Compressible Flows	72
7.2.1 Flat-Plate Flow with Adiabatic Wall	72
7.2.2 Flat-Plate Flow with Heat Transfer	75
8.0 Concluding Statements	76
9.0 Technological Forecast	78
9.1 Problem	78
9.2 State of the Art, Solution and Forecast	78
9.3 Suggestions and Implications	78
10.0 Acknowledgments	82
11.0 References	83
Appendix A. Behavior of the Eddy Viscosity Very Close to the Wall	87
Appendix B. Modification of the Inner Eddy-Viscosity Equation for Compressible Flow	91
Appendix C. Variable-Grid Differentiation Formulas	94

3.0 INDEX OF FIGURES

<u>No.</u>	<u>Title</u>	<u>Page No.</u>
1.	A turbulent boundary-layer velocity profile.	12
2.	Eddy-viscosity distribution across a boundary layer.	14
3.	Boundary layer on a body of revolution. Coordinate system	17
4.	Coordinates for axially symmetric body.	25
5.	Finite-difference variable-grid system in the $\eta$ -direction.	39
6.	Finite-difference molecule for the momentum equation at $(n, i)$ .	40
7.	Finite-difference molecule for the momentum equation at $(n, N-1)$ .	41
8.	Finite-difference molecule for the energy equation at $(n, i)$ .	46
9.	Flow-diagram for solving the boundary-layer equations at station $n$ , $\xi = \xi_n$ .	51
10.	Diagram showing the method of generating the initial coefficients of the momentum equation at station $n$ .	52
11.	Flow diagram for solving the boundary-layer equations at $\xi = 0$ .	53
12.	Results of calculations for a flat-plate flow.	100-109
13.	Results of calculations for the flat plate with two uniform blowing rates, $v_w/u_e = 0.001$ and $0.002$ (Experimental data of Mickley and Davis).	110-112
14.	Results of calculations for the flat plate with two uniform suction rates, $v_w/u_e = -0.00312$ and $-0.00429$ (Experimental data of Tennekes).	113-115
15.	Velocity distribution used to match the momentum thickness for the experimental data of Herring and Norbury.	66
16.	Results of calculations for an equilibrium flow in a favorable pressure gradient with $E = -0.35$ (Experimental data of Herring and Norbury).	116-118
17.	Velocity distribution used to match the defect-shape factor for the experimental data of Clauser's P.D.1.	67
18.	Results of calculations of an equilibrium flow in an adverse pressure gradient (Experimental data of Clauser's P.D.1).	119-121
19.	Velocity distribution used to match the momentum thickness for the experimental data of Bradshaw and Ferriss.	68

<u>No.</u>	<u>Title</u>	<u>Page No.</u>
20.	Results of calculations of an equilibrium flow recovering to constant pressure flow (Experimental data of Bradshaw and Ferriss, $\alpha = -0.255 \rightarrow 0$ ).	122-123
21.	Results of calculations for favorable and adverse pressure gradients on an airfoil like body (Experimental data of Schubauer and Klebanoff).	124-126
22.	Velocity distribution used to match the momentum thickness for the experimental data of Moses' P.D.2.	70
23.	Results of calculations for a nonequilibrium flow in an adverse pressure gradient (Experimental data of Moses' P.D.2.).	127-129
24.	Results of calculations for an airfoil with separation (Experimental data of von Doenhoff and Tetervin's NACA 65(216)-222 Airfoil).	130-133
25.	Comparison of calculated and experimental local skin-friction coefficients for an adiabatic flat plate at $M = 2.8$ (Experimental data of Spivack).	134-135
26.	Comparison of calculated and experimental average skin-friction coefficients for an adiabatic flat plate at $M = 0.81, 2.5,$ and $3.6$ (Experimental data of Chapman and Kester).	136
27.	Comparison of calculated and experimental local skin-friction coefficients for an adiabatic flat plate at $M = 0.20, 2.95,$ and $4.20$ (Experimental data of Matting et al.).	137
28.	Comparison of calculated and experimental boundary layer Mach number profiles and velocity profiles (Experimental data of Matting et al.).	138-139
29.	Comparison of calculated and experimental average skin-friction coefficients for a flat plate with heat transfer at $M = 1.69$ (Experimental data of Pappas).	140
30.	Comparison of calculated and experimental local Stanton number for a flat plate with heat transfer at $M = 1.69$ (Experimental data of Pappas).	141
31.	Comparison of skin-friction variation with Mach number.	142

<u>No.</u>	<u>Title</u>	<u>Page No.</u>
32.	Turbulent Prandtl numbers of boundary layers on a cooled flat plate, $M \sim 5.1$ , $(T_e - T_w)/T_e \sim 0.35$ .	80

Appendix

C1.	Variable-grid system for three points.	95
C2.	Variable-grid system for five points.	95

4.0 PRINCIPAL NOTATION

$c_f$	local skin-friction coefficient, eq.(6.113)
$\bar{c}_f$	average skin-friction coefficient
$c_p$	specific heat at constant pressure
$c_{\tau_L}$	local shear-stress coefficient for laminar flow, eq.(6.114)
$c_{\tau_T}$	local shear-stress coefficient for turbulent flow, eq.(6.115)
$C$	$\frac{\rho \mu}{\rho_e \mu_e}$ , viscosity-density parameter
$E$	equilibrium boundary-layer parameter, $\frac{\delta^*}{\tau_w} \frac{dp}{dx}$
$f$	dimensionless stream function, eq.(6.46)
$g$	dimensionless total-enthalpy ratio, eq.(6.54), where applicable
$G$	defect-shape factor, eq.(6.122)
$h$	specific enthalpy
$H$	total enthalpy, $h + \frac{1}{2} u^2$ or shape factor, eq.(6.121), where applicable
$K$	variable-grid-system parameter
$l$	mixing length
$L$	reference body length
$M$	Mach number
$p$	pressure
$Pr$	Prandtl number
$q$	local heat-transfer rate per unit area
$r$	radial distance from axis of revolution
$r_o$	radius of body of revolution
$Re_x$	Reynolds number, $u_e x / \nu_e$
$Re_\theta$	Reynolds number, $u_e \theta / \nu_e$
$St$	Stanton number, eq.(6.118)

t	transverse-curvature term, eq.(6.42), where applicable
T	absolute temperature
u	x-component of velocity
$u^*$	friction velocity, $\sqrt{\tau_w/\rho}$
v	y-component of velocity
x	distance along surface measured from leading edge or from stagnation point
y	distance normal to x
$\alpha$	angle between normal to the surface y and the radius r, fig. 4
$\beta$	dimensionless velocity-gradient term, eq.(6.53).
$\gamma$	intermittency factor, eq.(6.26), or convergence criterion, where applicable
$\delta$	boundary-layer thickness
$\Delta$	defect-displacement thickness, eq.(6.123)
$\epsilon$	eddy viscosity
$\eta$	transformed y-coordinate
$\theta$	momentum thickness, eq.(6.111)
$\lambda$	thermal conductivity
$\mu$	dynamic viscosity
$\nu$	kinematic viscosity
$\xi$	transformed x-coordinate
$\rho$	density
$\tau$	shear stress
$\varphi$	perturbation quantity, $f - f_0$
$\psi$	stream function
$\omega$	vorticity

SUBSCRIPTS

c evaluated at the switching point of the boundary layer

e evaluated at outer edge of boundary layer

w evaluated at wall

oo evaluated at free-stream or reference conditions

Primes on  $f$  denote differentiation with respect to  $\eta$

## 5.0 INTRODUCTION

The boundary-layer concept, first introduced in 1904 by Prandtl, divides the flow past a body into two regions: an inviscid region, governed by the Euler equations of motion, and a thin viscous region in the neighborhood of the body, governed by the boundary-layer equations. For laminar flow, the existence of a known relationship between the shear stress and the velocity gradient completes a set of partial differential equations, and exact solution of the boundary-layer equations is mathematically possible. Highly accurate solutions exist for some simple flows, such as similar flows, which are especially important. With the advent of high-speed computers, quite satisfactory results for a variety of general flows have been obtained.

For turbulent flows, on the other hand, because of the limited understanding of the turbulent process, the exact solutions of the boundary-layer equations are not possible. The usual boundary-layer equations for such flows contain a term involving the time mean of the product of two fluctuating velocities, which is known as the turbulent shear stress, and a term involving the time mean of the product of a fluctuating velocity and a fluctuating temperature. At the present, these terms have not been rigorously related to the mean velocity and mean temperature distributions. Thus, exact solutions of the boundary-layer equations for turbulent flows are not possible. In order to proceed at all, the solutions must depend on some empirical information. Even then the solution of boundary-layer equations is not easy. For this reason, most of the work on turbulent flows has been centered on empirical correlations together with integral methods. In general, the approaches followed in these methods vary widely. In one approach, for example, Head's method [1], the boundary-layer parameters are obtained by solving the momentum integral equation with two empirical expressions called auxiliary equations. These equations consist of an expression for local skin-friction coefficient ( $c_f$ ) and an expression for shape factor ( $H$ ). In another approach, for example, Truckenbrodt's method [2], the boundary-layer parameters are obtained by solving both the momentum and energy integral equations by using an empirical expression for the dissipation integral and by introducing further approximations in the solution. These methods were recently

reviewed by Thompson [3] for two-dimensional incompressible turbulent flows and were found to give widely differing and often inaccurate results.

A more fundamental approach to the solution of turbulent boundary layers is to regard the turbulent boundary layer as a composite layer and to characterize it by inner and outer regions (see figure 1). The existence of two

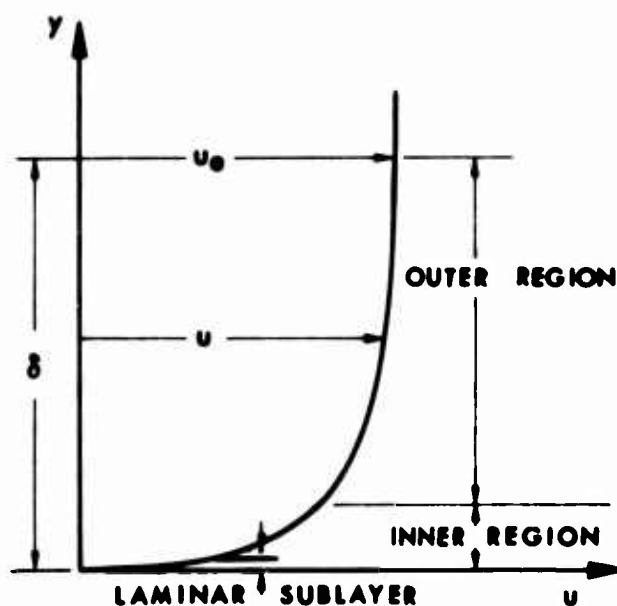


Figure 1.-A turbulent-boundary-layer velocity profile.

regions is due to the different response to shear and pressure gradient by the fluid near the wall. The inner region, whose thickness is approximately 0.1 to 0.2  $\delta$ , depends primarily on the wall shear stress and fluid viscosity. The mean velocity distribution in this region responds rapidly to changes in these wall conditions because the eddies in this region are very small. The mean velocity distribution may be described by the so-called "law of the wall":

$$\frac{u}{u^*} = \phi_1 (yu^*/\nu)$$

This relation was originally obtained by Prandtl from a mixing-length concept [4]. In addition, if an expression for eddy viscosity is introduced in the inner region, it can be shown that eddy viscosity in this region varies almost linearly with distance.

In the case of a smooth wall, the inner region contains a layer, commonly called the laminar sublayer, adjacent to the wall, where the flow is primarily viscous and the mean velocity increases linearly with distance from the wall. The thickness of this layer is of the order of 0.001 to 0.01  $\delta$ .

The outer region, on the other hand, contains 80 to 90 percent of the boundary layer thickness. The flow in this region is independent of the fluid viscosity, but is dependent on the wall shear stress, and it is highly affected by conditions in the free stream such as streamwise pressure gradient. The mean velocity distribution is conveniently described by the so-called "velocity-defect law":

$$\frac{u_e - u}{u^*} = \varphi_2(y/\delta)$$

The flow in the outer region shows some similarity to wake flow. Near the outer edge, it has an intermittent character. The turbulence is characterized by large eddies. The response of the mean velocity distribution to changes in its determining conditions is much slower than that of the inner region. In addition, an eddy viscosity, if introduced, shows a nearly constant value across the region. For example, as suggested by Clauser [5], the eddy viscosity for the so-called "equilibrium" boundary layers is

$$\epsilon = k_2 \rho u_e \delta^*$$

where  $k_2$  was empirically determined to be 0.018.

The approach in which the turbulent boundary layer is regarded as a composite layer consisting of inner and outer regions was followed in [6] and [7] for incompressible flows. In both references, the Reynolds shear-stress term was eliminated through the use of an eddy-viscosity concept. The main difference between the two approaches is the expression used for eddy viscosity in each region. Another difference is the transformation used to stretch the coordinate normal to the flow direction to reduce the variation of the boundary-layer thickness and to remove the singularity at the leading edge or at the stagnation point. A third difference is the method used to solve the boundary-

layer equations. In reference [7] the momentum equation was solved in its non-linear form by an integration technique; in reference [6] the momentum equation was solved in a linearized form.

The approach used in this report is the one used in reference [7]. Again the Reynolds shear-stress term in the momentum equation is eliminated through the use of an eddy-viscosity concept, and a separate expression for eddy viscosity is used in each region (see figure 2). However, this time the expressions are

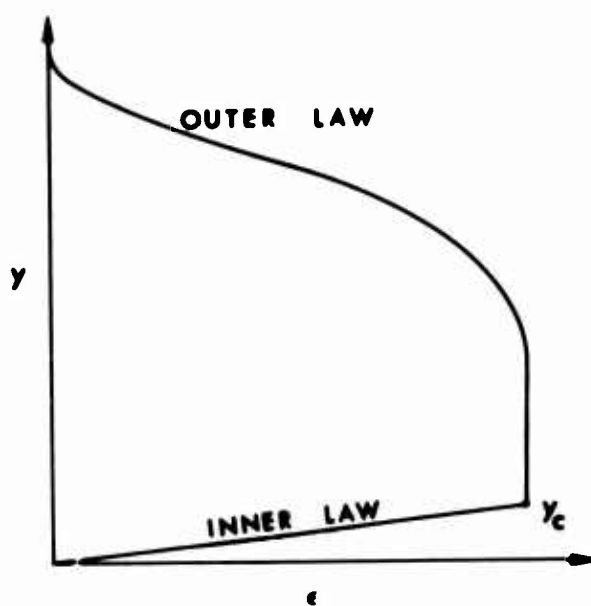


Figure 2.- Eddy-viscosity distribution across a boundary layer.

slightly modified, to account for the compressibility effect. In addition, the time mean of the product of a fluctuating velocity and a fluctuating temperature in the energy equation is eliminated through the use of an eddy-conductivity concept and is introduced into the energy equation through the definition of turbulent Prandtl number:

$$\text{Pr}_T = \frac{c_p \epsilon}{\lambda_T}$$

As an initial step, the turbulent Prandtl number is assumed to be constant. Note that the present framework is general and that it can handle widely varying eddy-viscosity and turbulent Prandtl number formulations.

The method used to solve the boundary-layer equations here is different from the one used in previous studies [7 through 13]. Again the streamwise derivatives in both momentum and energy equations are replaced by finite differences. However, unlike the previous studies, in this study the momentum equation is solved in a linearized form, and the previous integration technique is replaced by an implicit finite-difference technique. A variety of flows has been computed by this method, and comparisons with experimental data and various established correlations are made. The results presented in this report do not represent a finished development, but are only the results obtained so far by one particular eddy-viscosity and constant turbulent Prandtl number formulation, in fact the first one tried.

## 6.0 DESCRIPTION OF METHOD OF SOLUTION

### 6.1 Equations of the Compressible Turbulent Boundary Layer

The governing equations describing the flow about two-dimensional and axisymmetric bodies at high Reynolds numbers and constant pressure within the boundary layer are [11]:

#### CONTINUITY

$$\frac{\partial \rho}{\partial t} + \frac{1}{r^k} \left\{ \frac{\partial}{\partial x} (r^k \rho u) + \frac{\partial}{\partial y} (r^k \rho v) \right\} = 0 \quad (6.1)$$

#### MOMENTUM

$$\rho \frac{\partial u}{\partial t} + \rho u \frac{\partial u}{\partial x} + \rho v \frac{\partial u}{\partial y} = - \frac{dp}{dx} + \frac{1}{r^k} \frac{\partial}{\partial y} \left( r^k \mu \frac{\partial u}{\partial y} \right) \quad (6.2)$$

#### ENERGY

$$\rho \frac{\partial H}{\partial t} + \rho u \frac{\partial H}{\partial x} + \rho v \frac{\partial H}{\partial y} = \frac{1}{r^k} \frac{\partial}{\partial y} r^k \left\{ \frac{\mu}{Pr} \frac{\partial H}{\partial y} + \mu \left( 1 - \frac{1}{Pr} \right) u \frac{\partial u}{\partial y} \right\} \quad (6.3)$$

where  $k = 0$  for two-dimensional flow and  $k = 1$  for axisymmetric flow.

The basic notation and scheme of coordinates are shown in figure 3, where  $u_\infty$  is a reference velocity and  $u_e(x)$  is the velocity just outside the boundary layer. The term  $H_e$ , which is a constant, is the total enthalpy outside the boundary layer. Local enthalpy outside the boundary layer, namely,  $h_e$ , is given by

$$H_e = h_e + \frac{1}{2} u_e^2$$

The coordinates are a curvilinear system in which  $x$  is distance along the surface measured from the stagnation point or leading edge. The dimension  $y$  is measured normal to the surface. Within the boundary layer, the velocity components in the  $x$ - and  $y$ -directions are  $u$  and  $v$ , respectively. The body radius is  $r_0$ .

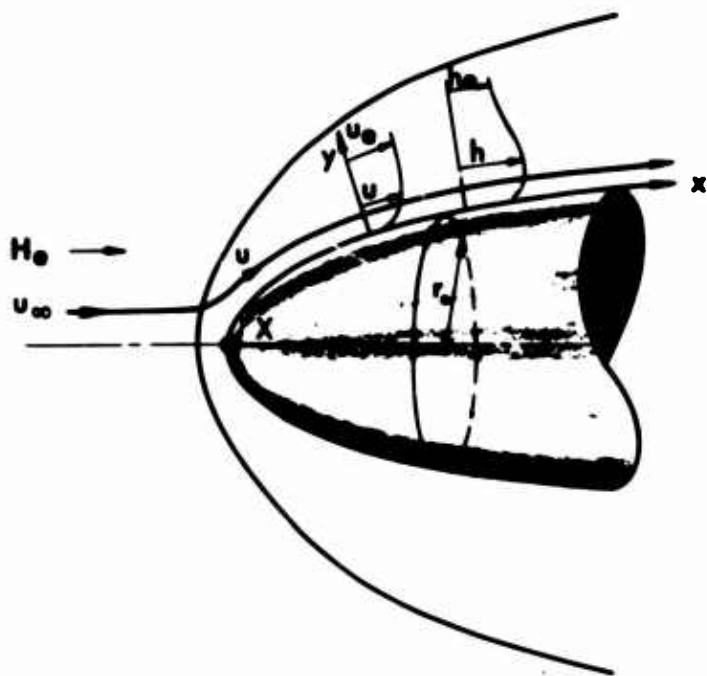


Figure 3.-Boundary layer on a body of revolution. Coordinate system.

In these equations, the transverse-curvature terms, which are of second order, are retained because of their importance in predicting boundary-layer growth on long slender bodies such as certain missiles or at the tail of a streamlined body of revolution.

The equations (6.1), (6.2), and (6.3) apply to turbulent as well as to laminar flows, providing the dependent variables - velocity, density, and enthalpy - are replaced by their instantaneous values for turbulent flow. The procedure is due to O.Reynolds. With instantaneous values, (6.1), (6.2), and (6.3) become

$$\frac{\partial \rho_i}{\partial t} + \frac{1}{r^k} \left\{ \frac{\partial}{\partial x} (r^k \rho_i u_i) + \frac{\partial}{\partial y} (r^k \rho_i v_i) \right\} = 0 \quad (6.4)$$

$$\rho_i \frac{\partial u_i}{\partial t} + \rho_i u_i \frac{\partial u_i}{\partial x} + \rho_i v_i \frac{\partial u_i}{\partial y} = - \frac{dp_i}{dx} + \frac{1}{r^k} \frac{\partial}{\partial y} \left( r^k \mu \frac{\partial u_i}{\partial y} \right) \quad (6.5)$$

$$\rho_i \frac{\partial H_i}{\partial t} + \rho_i u_i \frac{\partial H_i}{\partial x} + \rho_i v_i \frac{\partial H_i}{\partial y} = \frac{1}{r^k} \frac{\partial}{\partial y} r^k \left\{ \frac{\mu}{Pr} \frac{\partial H_i}{\partial y} + \mu \left( 1 - \frac{1}{Pr} \right) u_i \frac{\partial u_i}{\partial y} \right\} \quad (6.6)$$

Let the instantaneous values be denoted by their average and fluctuating values, as follows:

$$\begin{aligned} u_i &= u + u' & v_i &= v + v' & \rho_i &= \rho + \rho' \\ p_i &= p + p' & H_i &= H + H' \end{aligned} \quad (6.7)$$

Introducing the first three expressions defined by (6.7) into (6.4) and averaging with respect to time gives

$$\frac{\partial}{\partial x} r^k (\rho u + \overline{\rho' u'}) + \frac{\partial}{\partial y} r^k (\rho v + \overline{\rho' v'}) = 0 \quad (6.8)$$

By time average is meant, for example,

$$u = \frac{1}{t} \int_0^t u_i(t + \tau) d\tau$$

with  $t$  large compared with the time scale of the turbulent motions. For the fluctuating values, say  $u'$ , the average value,  $\overline{u'}$ , is

$$\overline{u'} = \frac{1}{t} \int_0^t u' d\tau = 0$$

The momentum equation for steady compressible turbulent flow can be obtained as follows. Multiplying (6.4) by  $u_i$ , (6.5) by  $r$ , and adding the resulting equations gives

$$\begin{aligned} r^k \rho_i u_i \frac{\partial u_i}{\partial x} + r^k \rho_i v_i \frac{\partial u_i}{\partial y} + u_i \frac{\partial}{\partial x} (r^k \rho_i u_i) + u_i \frac{\partial}{\partial y} (r^k \rho_i v_i) \\ = - r^k \frac{dp_i}{dx} + \frac{\partial}{\partial y} (r^k \mu \frac{\partial u_i}{\partial y}) \end{aligned} \quad (6.9a)$$

which can be written as

$$\frac{\partial}{\partial x} (r^k \rho_i u_i u_i) + \frac{\partial}{\partial y} (r^k \rho_i v_i u_i) = - r^k \frac{dp_i}{dx} + \frac{\partial}{\partial y} (r^k \mu \frac{\partial u_i}{\partial y}) \quad (6.9b)$$

Introducing the first four expressions defined by (6.7) into (6.9b), averaging with respect to time, and using (6.8) gives

$$\begin{aligned}
 (\rho u + \overline{\rho'u'}) \frac{\partial u}{\partial x} + (\rho v + \overline{\rho'v'}) \frac{\partial u}{\partial y} &= -\frac{dp}{dx} - \frac{1}{r^k} \frac{\partial}{\partial x} r^k (\rho \overline{u'^2} + u \overline{\rho'v'} + \overline{\rho'u'^2}) \\
 + \frac{1}{r^k} \frac{\partial}{\partial y} r^k \left\{ \mu \frac{\partial u}{\partial y} - \rho \overline{v'u'} - v \overline{\rho'u'} - \overline{\rho'v'u'} \right\} &\quad (6.10)
 \end{aligned}$$

The energy equation for compressible turbulent flow can be obtained in a similar way. Multiplying (6.4) by  $H_i$ , (6.6) by  $r$ , and adding the resulting equations gives

$$\begin{aligned}
 H_i \frac{\partial}{\partial x} (r^k \rho_i u_i) + H_i \frac{\partial}{\partial y} (r^k \rho_i v_i) + r^k \rho_i u_i \frac{\partial H_i}{\partial x} + r^k \rho_i v_i \frac{\partial H_i}{\partial y} \\
 = \frac{\partial}{\partial y} r^k \left\{ \frac{\mu}{Pr} \frac{\partial H_i}{\partial y} + \mu \left(1 - \frac{1}{Pr}\right) u_i \frac{\partial u_i}{\partial y} \right\} &\quad (6.11a)
 \end{aligned}$$

which can be written as

$$\frac{\partial}{\partial x} (r^k \rho_i u_i)(H_i) + \frac{\partial}{\partial y} (r^k \rho_i v_i)(H_i) = \frac{\partial}{\partial y} r^k \left\{ \frac{\mu}{Pr} \frac{\partial H_i}{\partial y} + \mu \left(1 - \frac{1}{Pr}\right) u_i \frac{\partial u_i}{\partial y} \right\} \quad (6.11b)$$

Introducing the expressions defined by (6.7) into (6.11b), averaging with respect to time, and using (6.8) gives

$$\begin{aligned}
 (\rho u + \overline{\rho'u'}) \frac{\partial H}{\partial x} + (\rho v + \overline{\rho'v'}) \frac{\partial H}{\partial y} &= -\frac{1}{r^k} \frac{\partial}{\partial x} r^k (\rho \overline{u'H'} + u \overline{\rho'H'} + \overline{\rho'u'H}) \\
 + \frac{1}{r^k} \frac{\partial}{\partial y} r^k \left\{ \frac{\mu}{Pr} \frac{\partial H}{\partial y} - \rho \overline{v'H'} + \mu \left(1 - \frac{1}{Pr}\right) u \frac{\partial u}{\partial y} - v \overline{\rho'H'} - \overline{\rho'v'H'} \right\} &\quad (6.12)
 \end{aligned}$$

Since for flows at high Reynolds number the boundary layer is assumed to be thin and the terms such as  $\rho$ ,  $u$ ,  $H$ , and  $x$  are assumed to be of the order of 1 and  $v$ ,  $y$  of the order of  $\delta$ , some of the correlation terms involving  $u'$ ,  $v'$ ,  $\rho'$ , and  $H'$  in (5.8), (6.10), and (6.12) can be neglected. The double correlation terms such as  $\overline{\rho'u'}$ ,  $\overline{u'H'}$ ,  $\overline{\rho'H'}$ , and  $\overline{\rho'v'}$  are of the order of  $\delta$  at most, and the triple correlation terms such as  $\overline{\rho'v'u'}$  and  $\overline{\rho'v'H'}$  are of the order of  $\delta^2$  at most. When these simplifications are introduced into (6.8), (6.10), and (6.12) and the predominant terms of the same order of

magnitude are retained, the resulting equations are of the same form as those of laminar flow except for the terms  $\overline{\rho'v'}$ ,  $-\overline{\rho u'^2}$ ,  $-\rho \overline{v'u'}$ , and  $-\rho \overline{v'H'}$ . In addition, if the pressure fluctuations within the boundary layer are considered, then another term, namely,  $-\frac{\partial}{\partial x} \rho \overline{v'^2}$ , should be included on the left-hand side of (6.10). For flow conditions away from separation, the terms  $-\rho \overline{u'^2}$  and  $-\rho \overline{v'^2}$ , known as Reynolds normal stresses, are small and will be neglected. Hence, with all these simplifications, the governing equations for the compressible turbulent boundary layer become:

CONTINUITY

$$\frac{\partial}{\partial x} (r^k \rho u) + \frac{\partial}{\partial y} \left[ r^k (\rho v + \overline{\rho'v'}) \right] = 0 \quad (6.13)$$

MOMENTUM

$$\rho u \frac{\partial u}{\partial x} + (\rho v + \overline{\rho'v'}) \frac{\partial u}{\partial y} = -\frac{dp}{dx} + \frac{1}{r^k} \frac{\partial}{\partial y} \left[ r^k \mu \left( 1 + \frac{\epsilon}{\mu} \right) \frac{\partial u}{\partial y} \right] \quad (6.14)$$

ENERGY

$$\rho u \frac{\partial H}{\partial x} + (\rho v + \overline{\rho'v'}) \frac{\partial H}{\partial y} = \frac{1}{r^k} \frac{\partial}{\partial y} \left[ r^k \left\{ \frac{\mu}{Pr} \left( 1 + \frac{\epsilon}{\mu} \frac{Pr}{Pr_T} \right) \frac{\partial H}{\partial y} + \mu \left( 1 - \frac{1}{Pr} \right) u \frac{\partial u}{\partial y} \right\} \right] \quad (6.15)$$

where the term  $-\rho \overline{u'v'}$ , known as the Reynolds shear stress, is eliminated through the use of Boussinesq's eddy-viscosity ( $\epsilon$ ) concept and the term  $-\rho \overline{v'H'}$  is eliminated through the use of an eddy-conductivity ( $\lambda_T$ ) concept.

$$-\rho \overline{u'v'} = \epsilon \frac{\partial u}{\partial y} \quad (6.16)$$

$$-\rho \overline{v'H'} = \frac{\lambda_T}{c_p} \frac{\partial H}{\partial y} \quad (6.17)$$

$$Pr_T = \frac{c_p \epsilon}{\lambda_T} \quad (6.18)$$

If ( )<sub>w</sub> denotes wall, the boundary conditions to be considered are:

MOMENTUM

$$u(x, 0) = 0 \quad (6.19a)$$

$$v(x, 0) = 0 \text{ or } v(x, 0) = v_w \text{ (mass transfer)} \quad (6.19b)$$

$$\lim_{y \rightarrow \infty} u(x, y) = u_e(x) \quad (6.19c)$$

ENERGY

$$H(x, 0) = H_w \quad \text{or} \quad \frac{\partial H}{\partial y}(x, 0) = \left( \frac{\partial H}{\partial y} \right)_w \quad (6.20a)$$

$$\lim_{y \rightarrow \infty} H(x, y) = H_e(x) \quad (6.20b)$$

## 6.2 Formulation of Eddy Viscosity and Turbulent Prandtl Number

In order to solve the compressible turbulent boundary-layer equations given in the last section, it is necessary to use expressions for eddy viscosity and turbulent Prandtl number. The eddy-viscosity formulation that will be used in this study is the same as the one used for incompressible flow in a previous study [7]. This formulation has worked well for incompressible flow and hence it was decided to extend it, with small modifications, to compressible flow. In this formulation, the boundary layer is regarded as a composite layer characterized by inner and outer regions. In the inner region, an eddy viscosity based on Prandtl's mixing-length theory is used; in the outer region, a nearly constant eddy viscosity is used. It is exactly constant when the flow is incompressible and without heat transfer. An intermittency factor is applied to this basic "outer viscosity".

### 6.2.1. Viscosity in the inner region.

In the inner region, the eddy viscosity is represented by Prandtl's formula based on the mixing-length theory; that is,

$$\epsilon_i = \rho l^2 \left| \frac{\partial u}{\partial y} \right| \quad (6.21)$$

where  $l$ , the mixing length, is given by  $l = k_1 y$ . However, to account for the viscous sublayer close to the wall, a modified expression for  $l$  is used in (6.21). This modification, suggested by Van Driest [14] and developed by consideration of a Stokes-type flow, is

$$l = k_1 y [1 - \exp(-y/A)] \quad (6.22)$$

Substituting this expression for  $l$  into (6.21) gives

$$\epsilon_i = \rho k_1^2 y^2 [1 - \exp(-y/A)]^2 \left| \frac{\partial u}{\partial y} \right| \quad (6.23)$$

This expression, as it stands, applies to incompressible flows. The quantity  $\rho$  is a constant,  $k_1 = 0.4$ , and  $A$  is a constant for a given streamwise location in the boundary layer, defined as  $26\nu(\rho/\tau_w)^{1/2}$ . Equation (6.23) shows that as  $y$  increases, the exponential term disappears, leaving Prandtl's form, namely, equation (6.21). It also shows that, for  $y \rightarrow 0$ ,  $\epsilon_i$  should vary as  $y^4$ . The latter conclusion is in contrast to the behavior of eddy-viscosity expressions proposed by Townsend [15] and Reichardt [16], which show that  $\epsilon_i$  should vary as  $y^3$ . On the other hand, (6.23) has the same behavior close to the wall as Deissler's eddy-viscosity expression [17]; that is,  $\epsilon_i$  varies as  $y^4$  as  $y \rightarrow 0$ . An analysis given in Appendix A indicates that  $\epsilon_i$  should vary as  $y^4$  as  $y \rightarrow 0$ .

Equation (6.23) can also be applied to compressible flows if  $\rho$  is taken to be a variable and if the exponential term is modified to account for the heat transfer in the sublayer. A logical generalization is to consider a Stokes-type flow in which the fluid has a variable viscosity. An analysis given in Appendix B indicates that the eddy-viscosity formula for the inner region should now be

$$\epsilon_i = \rho k_1^2 y^2 \left[ 1 - \exp\left\{-\left(\frac{v_w}{\bar{v}}\right)^{\frac{1}{2}} \frac{y}{A}\right\}\right]^2 \left| \frac{\partial u}{\partial y} \right| \quad (6.24)$$

where  $A = 26\nu_w(\rho_w/\tau_w)^{1/2}$  and  $\bar{v}$  is the mean value of  $v$  obtained by averaging (6.24) over some arbitrary distance, perhaps the sublayer. As an initial step, the ratio of  $v_w/\bar{v}$  is assumed to be unity. At high wall temperatures, the exponential term will decay much more slowly with  $y$ . For example, on a wall with a temperature of  $60^\circ\text{F}$  at sea level,  $A\sqrt{\tau_w} = 2.25 \times 10^{-4}$ . On a wall with a temperature of  $3000^\circ\text{F}$  at 50,000 feet,  $A\sqrt{\tau_w} = 5.46 \times 10^{-3}$ , or more than 20 times as large.

### 6.2.2 Viscosity in the outer region.

In the work on incompressible flows, the form for eddy viscosity in the outer region suggested by Clauser [5] was used; that is,

$$\epsilon_o = k_2 \rho u_e \delta^* \quad (6.25)$$

where the constant  $k_2$  is taken to be 0.0168, the value given in [18]. The same formula is used for compressible flow, except that  $\rho$  is a variable; that is,  $\rho = \rho(x, y)$ . Equation (6.25) is modified by an intermittency factor  $\gamma$  that was obtained by Klebanoff [19]. It is given by

$$\gamma = \frac{1}{2} [1 - \operatorname{erf} 5 (\frac{y}{\delta} - .78)] \quad (6.26)$$

where  $\delta$  is the thickness of the boundary layer. This formula was deduced from measurements of an incompressible flow, and, for want of anything better, it is also used for compressible flow. With (6.26), the eddy-viscosity formula for the outer region becomes

$$\epsilon_o = \rho k_2 u_e \delta^* \gamma \quad (6.27)$$

### 6.2.3 Definition of inner and outer regions.

The constraint used to define the end of the inner region and the beginning of the outer region is the continuity of the eddy viscosity. It can be seen from (6.24) and (6.27) that, at a given position along the body,  $\epsilon_i$  increases with  $y$  and  $\epsilon_o$  remains constant over practically the whole boundary layer. Hence, from the wall outward, the expression for inner eddy viscosity applies until

$$\epsilon_i = \epsilon_o \quad (6.28)$$

or, in terms of the distance from the wall, inner and outer regions thus can be defined as

$$\epsilon_i = \rho k_1^2 y^2 \left[ 1 - \exp \left\{ - (v_w/\bar{v})^{1/2} \frac{y}{A} \right\} \right]^2 \left| \frac{\partial u}{\partial y} \right| \quad 0 \leq y \leq y_c \quad (6.29)$$

$$\epsilon_o = \rho k_2 u_e \delta^* \gamma \quad y_c \leq y \leq \delta \quad (6.30)$$

where  $y_c$  is determined by (6.28).

#### 6.2.4 Turbulent Prandtl number.

The turbulent Prandtl number is a measure of the ratio of eddy viscosity to eddy conductivity, that is, the ratio of the transport of momentum to the transport of heat. Since the flow in the outer region shows some similarity to a wake flow, one may argue that a more realistic formulation of turbulent Prandtl number requires a separate expression in each region, as in eddy-viscosity formulation. The fact that in boundary layers the ratio of eddy conductivity to eddy viscosity is smaller than in free turbulence permits one to conclude that the lowering of this ratio is due to the influence of the wall [20]. Consequently, if the ratio of eddy conductivity to eddy viscosity is lowered by the effect of the wall, it follows that this ratio decreases with decreasing wall distance and increases with increasing wall distance. It appears that at large wall distance this ratio approaches the value 2, that is, the same value observed for free turbulence. On the other hand, no experimental results have been obtained on the minimum value of this ratio in the immediate neighborhood of the wall. For these reasons, as an initial step the turbulent Prandtl number is assumed to be a constant and equal to unity.

### 6.3 Transformation of Boundary-Layer Equations

Before (6.13), (6.14), and (6.15) can be solved, by a method to be described later, it is convenient to transform them to a coordinate system that removes the singularity at  $x = 0$  and stretches the coordinate normal to the flow direction, as is usually done in laminar flow. First, the equations are placed in an almost two-dimensional form by the Probstein and Elliot transformation [21].

#### PROBSTEIN-ELLIOT TRANSFORMATION

$$d\bar{x} = \left( \frac{r_o^k(x)}{L} \right)^2 dx \quad (6.31)$$

$$d\bar{y} = \frac{r^k(x, y)}{L} dy \quad (6.32)$$

where  $r_o(x)$  is specified by the body shape and  $r(x, y)$  is given by (see figure 4)

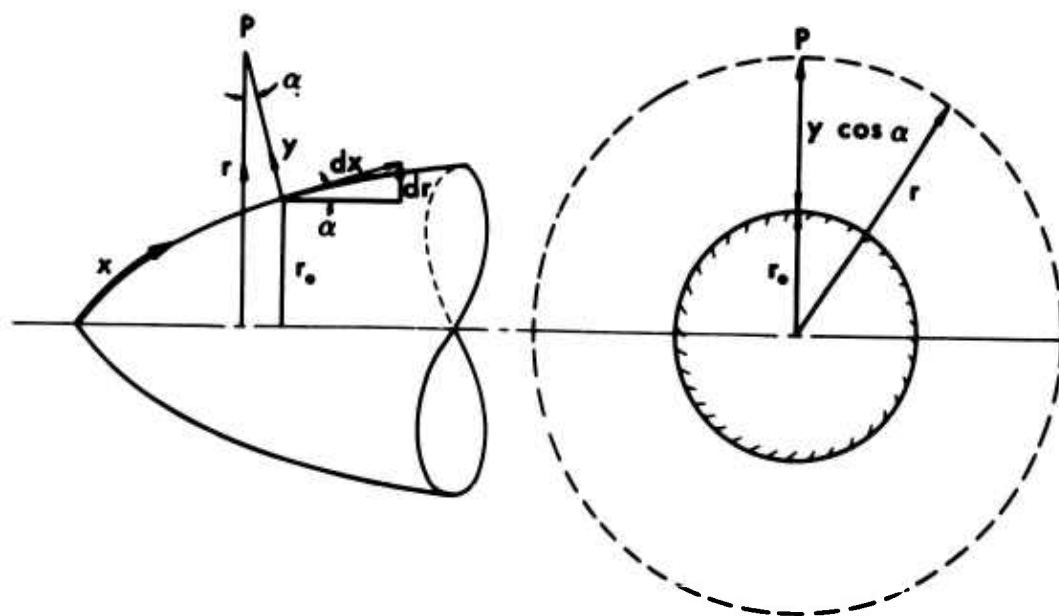


Figure 4.-Coordinates for axially symmetric body.

$$r(x, y) = r_0(x) + y \cos \alpha \quad (6.33)$$

Then from (6.31) and (6.32),

$$\frac{\partial}{\partial x} = \frac{\partial \bar{x}}{\partial x} \frac{\partial}{\partial \bar{x}} + \frac{\partial \bar{y}}{\partial x} \frac{\partial}{\partial \bar{y}} = \left( \frac{r_0^k}{L} \right)^2 \frac{\partial}{\partial \bar{x}} + \frac{\partial \bar{y}}{\partial x} \frac{\partial}{\partial \bar{y}} \quad (6.34)$$

$$\frac{\partial}{\partial y} = \frac{\partial}{\partial \bar{y}} \frac{\partial \bar{y}}{\partial y} = \frac{r^k}{L} \frac{\partial}{\partial \bar{y}} \quad (6.35)$$

Define a stream function  $\psi$  that satisfies the continuity equation (6.13), namely,

$$\frac{\partial \psi}{\partial y} = r^k \rho u \quad (6.36a)$$

$$\frac{\partial \psi}{\partial x} = -r^k (\rho v + \overline{\rho'v'}) \quad (6.36b)$$

Let

$$\begin{aligned} \bar{\psi} &= \frac{\psi}{L} & \bar{u} &= u & \bar{v} &= v \\ \overline{\rho'v'} &= \overline{\rho'v'} & \bar{\epsilon} &= \epsilon & \overline{\text{Pr}_T} &= \text{Pr}_T \end{aligned} \quad (6.37)$$

Now if in the barred plane the continuity equation (6.13) is written as

$$\frac{\partial}{\partial \bar{x}} (\rho \bar{u}) + \frac{\partial}{\partial \bar{y}} (\rho \bar{v} + \overline{\rho'v'}) = 0 \quad (6.38)$$

then the stream function  $\bar{\psi}$  that satisfies this equation is

$$\frac{\partial \bar{\psi}}{\partial \bar{y}} = \rho \bar{u} \quad \frac{\partial \bar{\psi}}{\partial \bar{x}} = -(\rho \bar{v} + \overline{\rho'v'}) \quad (6.39)$$

Therefore, if the relations defined by (6.34), (6.35) (6.37) and (6.39) are used, (6.36a) and (6.36b) become

$$\rho u = \frac{L}{r^k} \frac{\partial \bar{\psi}}{\partial \bar{y}} = \frac{L}{r^k} \left( \frac{r^k}{L} \frac{\partial \bar{\psi}}{\partial \bar{y}} \right) = \frac{\partial \bar{\psi}}{\partial \bar{y}} \quad (6.40a)$$

$$\rho v + \overline{\rho'v'} = -\frac{L}{r^k} \frac{\partial \bar{\psi}}{\partial \bar{x}} = -\frac{L}{r^k} \left( \frac{r_o^{2k}}{L^2} \frac{\partial \bar{\psi}}{\partial \bar{x}} + \frac{\partial \bar{\psi}}{\partial \bar{x}} \frac{\partial \bar{\psi}}{\partial \bar{y}} \right) \quad (6.40b)$$

By substituting from (6.40) into (6.14) and using the relations given by (6.34), (6.35), and (6.39), the following Probstein-Elliott transformed momentum equation is obtained:

$$\frac{\partial \bar{\psi}}{\partial \bar{y}} \frac{\partial}{\partial \bar{x}} \left( \frac{1}{\rho} \frac{\partial \bar{\psi}}{\partial \bar{y}} \right) - \frac{\partial \bar{\psi}}{\partial \bar{x}} \frac{\partial}{\partial \bar{y}} \left( \frac{1}{\rho} \frac{\partial \bar{\psi}}{\partial \bar{y}} \right) = -\frac{dp}{dx} + \frac{\partial}{\partial \bar{y}} \left[ (1+t)^{2k} \mu \left( 1 + \frac{\bar{\epsilon}}{\mu} \right) \frac{\partial}{\partial \bar{y}} \left( \frac{1}{\rho} \frac{\partial \bar{\psi}}{\partial \bar{y}} \right) \right] \quad (6.41)$$

where  $t$  is the transverse-curvature term defined as

$$t = \frac{y}{r_o} \cos \alpha \quad (6.42)$$

by using the relationship between  $r(x, y)$  and  $r_o(x)$  given by (6.33). Note that in (6.41) the eddy-viscosity term has a bar. This is necessary because  $\epsilon$  is not a scalar function (e.g., like  $\mu$ ) and must be transformed by (6.31) and (6.32).

Similarly, the energy equation (6.15) may be transformed into the form

$$\frac{\partial \bar{\psi}}{\partial \bar{y}} \frac{\partial H}{\partial \bar{x}} - \frac{\partial \bar{\psi}}{\partial \bar{x}} \frac{\partial H}{\partial \bar{y}} = \frac{\partial}{\partial \bar{y}} \left[ (1+t)^{2k} \left\{ \frac{\mu}{Pr} \left( 1 + \frac{\bar{\epsilon}}{\mu} \frac{Pr}{Pr_T} \right) \frac{\partial H}{\partial \bar{y}} + \frac{\mu}{\rho} \left( 1 - \frac{1}{Pr} \right) \cdot \right. \right. \\ \left. \left. \cdot \frac{\partial \bar{\psi}}{\partial \bar{y}} \frac{\partial}{\partial \bar{y}} \left( \frac{1}{\rho} \frac{\partial \bar{\psi}}{\partial \bar{y}} \right) \right\} \right] \quad (6.43)$$

by using (6.40), (6.34), (6.35), and (6.39). Equations (6.41) and (6.43) have the desired two-dimensional form.

Next, the Levy-Lees transformation [22] is introduced, in order to put (6.41) and (6.43) into a still more convenient form.

#### LEVY-LEES TRANSFORMATION

$$d\xi = \rho_e \mu_e u_e d\bar{x} \quad (6.44)$$

$$d\eta = \frac{\rho_e u_e}{(2\xi)^{1/2}} d\bar{y} \quad (6.45)$$

A dimensionless stream function  $f$  is related to  $\bar{\psi}$  as follows:

$$\bar{\psi} = (2\xi)^{1/2} f(\xi, \eta) \quad (6.46)$$

With (6.44), (6.45), and (6.46), the partial-derivative operators in the new coordinate system  $(\xi, \eta)$  become

$$\frac{\partial}{\partial \bar{x}} = \rho_e \mu_e u_e \left( \frac{\partial}{\partial \xi} + \frac{\partial \eta}{\partial \xi} \frac{\partial}{\partial \eta} \right) \quad (6.47)$$

$$\frac{\partial}{\partial \bar{y}} = \frac{\rho_e u_e}{(2\xi)^{1/2}} \frac{\partial}{\partial \eta} \quad (6.48)$$

$$\frac{\partial \bar{\psi}}{\partial \xi} = (2\xi)^{1/2} \left( \frac{f}{2\xi} + \frac{\partial f}{\partial \xi} \right) \quad (6.49)$$

$$\frac{\partial \bar{\psi}}{\partial \eta} = (2\xi)^{1/2} f' \quad (6.50)$$

where the prime on  $f$  denotes the derivative with respect to  $\eta$ . Introducing the transformations from (6.47) through (6.50) into (6.41) and (6.43) and using Euler's equation, namely,

$$dp + \rho_e u_e du_e = 0$$

to replace the  $dp/dx$ -term in (6.41) yields the transformed momentum and energy equations for the compressible turbulent boundary layer.

MOMENTUM

$$\left[ (1 + \tilde{t})^{2k} c \left( 1 + \frac{\tilde{\epsilon}}{\mu} \right) f'' \right]' + f f'' + \beta \left[ \frac{\rho_e}{\rho} - (f')^2 \right] = 2\xi \left[ f' \frac{\partial f'}{\partial \xi} - f'' \frac{\partial f}{\partial \xi} \right] \quad (6.51)$$

ENERGY

$$\left[ (1 + \tilde{t})^{2k} c \left\{ \left( 1 + \frac{\tilde{\epsilon}}{\mu} \frac{\text{Pr}}{\text{Pr}_T} \right) \frac{1}{\text{Pr}} g' + \frac{u_e^2}{H_e} \left( 1 - \frac{1}{\text{Pr}} \right) f' f'' \right\} \right]' + f' g' = 2\xi \left[ f' \frac{\partial g}{\partial \xi} - \frac{\partial f}{\partial \xi} g' \right] \quad (6.52)$$

where

$$\beta = \frac{2\xi}{u_e} \frac{du_e}{d\xi} \quad (6.53)$$

$$g = \frac{H}{H_e} \quad (6.54)$$

and

$$c = \frac{\rho \mu}{\rho_e \mu_e}$$

The prime on  $g$  denotes the derivative with respect to  $\eta$ , and the sign  $\sim$  indicates that the quantity is transformed by (6.44) and (6.45). For example, the transformed transverse-curvature term in (6.51) and (6.52) is given by

$$\tilde{t} = \frac{L \cos \alpha (2\xi)^{1/2}}{r_o \rho_e u_e} \int_0^\eta (\rho_e/\rho) \frac{1}{r^k} d\eta \quad (6.55)$$

In (6.51) and (6.52) the relationship between the quantities in the transformed plane and those in the physical plane is given by (6.31), (6.32), (6.44), and (6.45) - what might be called a Probstein-Elliot-Levy-Lees transformation.

PROBSTEIN-ELLIOT-LEVY-LEES TRANSFORMATION

$$d\xi = \rho_e \mu_e u_e (r_0^k/L)^2 dx \quad (6.56)$$

$$d\eta = \frac{\rho_e u_e}{(2\xi)^{1/2}} \frac{r^k}{L} dy \quad (6.57)$$

It can be seen from (6.51) and (6.52) that setting  $k = 0$  reduces them to two-dimensional form. On the other hand, for axisymmetric flow with no transverse-curvature (TVC) effect,  $k = 1$  and  $t = 0$ , which indicates that the ratio of  $r$  to  $r_0$  is unity.

The boundary conditions of (6.51) and (6.52) can now be transformed. From (6.48) and (6.50),

$$u = u_e f' \quad (6.58)$$

and from (6.40b), (6.47), and (6.46),

$$f(\xi, 0) = -\frac{1}{(2\xi)^{1/2}} \int_0^\xi \frac{\rho_w v_w}{\rho_e \mu_e u_e} \frac{L}{r_0^k} d\bar{\xi}$$

since at the wall  $u = 0$ ,  $\overline{\rho'v'} = 0$ , and  $r = r_0$ . The length  $L$  is taken equal to unity for two-dimensional and for axisymmetric flow with no TVC-effect. Then in the  $\xi, \eta$ -plane the boundary conditions given by (6.19) become

$$f(\xi, 0) = f_w = 0 \quad \text{or} \quad f_w = -\frac{1}{(2\xi)^{1/2}} \int_0^\xi \frac{1}{r_0^k} \frac{\rho_w v_w}{\rho_e \mu_e u_e} d\bar{\xi} \quad (\text{mass transfer}) \quad (6.59a)$$

$$f'(\xi, 0) = 0 \quad (6.59b)$$

$$\lim_{\eta \rightarrow \infty} f'(\xi, \eta) = 1 \quad (6.59c)$$

Similarly, from the definition of  $g$ , namely,  $g = H/H_e$ , the boundary conditions given by (6.20) become

$$g(\xi, 0) = \frac{H_w}{H_e} = g_w \quad \text{or} \quad g_w'(\xi, 0) = g_w' \quad (6.60a)$$

$$\lim_{\eta \rightarrow \infty} g(\xi, \eta) = 1 \quad (6.60b)$$

#### 6.4 Transformation of Eddy-Viscosity Equations

The eddy-viscosity term appearing in the momentum equation (6.51) is a function of flow-field quantities and must be transformed. The turbulent Prandtl number, on the other hand, is assumed to be a constant and therefore is not transformed.

Using (6.35), (6.40a), (6.48), (6.50), and the transformation given by (6.57) transforms the expression for the inner eddy viscosity given by (6.24) to

$$\epsilon_i = (\rho/\rho_e)^2 k_1^2 (2\xi)^{1/2} r^k f'' \left( \int_0^\eta \frac{\rho_e}{\rho} \frac{1}{r^k} d\bar{\eta} \right)^2 \left[ 1 - \exp \left\{ - \left( \frac{v_w}{v} \right)^{1/2} \rho_w/\rho_e \frac{1}{26} \cdot \left[ \frac{(2\xi)^{1/2} r_o^k f'' L}{\mu_w} \right]^2 \int_0^\eta \rho_e/\rho \frac{1}{r^k} d\bar{\eta} \right\} \right]^2 \quad (6.61)$$

Using (6.58), the relation given by (6.57), and the definition of displacement thickness, namely,

$$\delta^* = \int_0^\infty \left( 1 - \frac{\rho u}{\rho_e u_e} \right) dy = \frac{(2\xi)^{1/2} L}{u_e \rho_e} \int_0^\infty \frac{1}{r^k} (\rho_e/\rho - f') d\eta \quad (6.62)$$

transforms the expression for the outer eddy-viscosity given by (6.27) to

$$\epsilon_o = 0.0084 \frac{\rho}{\rho_e} (2\xi)^{1/2} L \left[ 1 - \operatorname{erf} 5 \left( \frac{\int_0^\eta \frac{\rho_e}{\rho} \frac{1}{r^k} d\bar{\eta}}{\int_0^\infty \frac{\rho_e}{\rho} \frac{1}{r^k} d\bar{\eta}} - 0.78 \right) \right] \cdot \int_0^\infty \frac{1}{r^k} (\rho_e/\rho - f') d\bar{\eta} \quad (6.63)$$

#### 6.5 Fluid Properties

Fluid properties that appear in the momentum and energy equations are density ( $\rho$ ), viscosity ( $\mu$ ), specific heat at constant pressure ( $c_p$ ), and thermal conductivity ( $\lambda$ ). The latter appears in the energy equation through the laminar Prandtl number,  $Pr$ , defined as

$$\text{Pr} = \frac{\mu c_p}{\lambda} \quad (6.64)$$

These fluid properties, which are assumed to be functions of temperature only, are given by the following formulas [23] for air:

$$c_p(T) = \sum_{i=0}^5 A_{i+1} T^i \quad (6.65)$$

$$\mu(T) = \sum_{i=0}^5 A_{i+1} T^i \quad (6.66)$$

$$\lambda(T) = \mu(c_p + \frac{5}{4} R) \quad (6.67)$$

where  $R = 1716 \text{ lb}_f\text{-ft}/\text{lb}_m\text{-deg R}$  and the A's are different for  $c_p$  and  $\mu$ . By means of (6.65), specific enthalpy can be expressed in the form

$$h(T) = \sum_{i=1}^6 A_i T^i \quad (6.68)$$

This relation is necessary because, once a solution of the energy equation is obtained, the temperatures are required in the calculation of the new fluid properties. The coefficients of these polynomials are given in Table I.

In addition to the relations given by (6.65) through (6.68) it is also necessary to have the relation of density to temperature. This can be obtained from the equation of state and from the assumption that static pressure remains constant within the boundary layer.

$$\rho = \frac{p_e}{R T} \quad (6.69)$$

## 6.6 Overall Method of Solution

In previous studies[7 through 13] the method used to solve the momentum and the energy equations was based on ideas originated by Hartree and Womersley [24]. It consists of replacing the  $\xi$ -derivatives by finite-difference relations

TABLE I. COEFFICIENTS OF FLUID PROPERTIES OF AIR

Fluid Property	Temperature Range, °R	A <sub>1</sub>	A <sub>2</sub>	A <sub>3</sub>	A <sub>4</sub>	A <sub>5</sub>	A <sub>6</sub>	Units
c <sub>p</sub>	0 ≤ T ≤ 2000	6.0351797 x10 <sup>3</sup>	-9.4509125 x10 <sup>-4</sup>	-7.3022675 x10 <sup>-4</sup>	1.7322782 x10 <sup>-6</sup>	-9.7657438 x10 <sup>-10</sup>	1.7465179 x10 <sup>-13</sup>	$\frac{\text{ft}^2}{\text{sec}^2 - \text{deg R}}$
	2000 ≤ T ≤ 6300	6.4371993 x10 <sup>3</sup>	-4.4825613 x10 <sup>-1</sup>	7.1435785 x10 <sup>-4</sup>	-2.4394435 x10 <sup>-7</sup>	3.4477526 x10 <sup>-11</sup>	-1.7810174 x10 <sup>-15</sup>	
μ	90 ≤ T ≤ 6.3 x10 <sup>3</sup>	-1.9336805 x10 <sup>-2</sup>	8.9325935 x10 <sup>-3</sup>	-3.918504 x10 <sup>-6</sup>	1.1728501 x10 <sup>-9</sup>	-1.649344 x10 <sup>-13</sup>	8.751547 x10 <sup>-18</sup>	$\frac{\text{lb}_f - \text{sec}}{\text{ft}^2}$
	0 ≤ T ≤ 2000	6.0351797 x10 <sup>3</sup>	-4.7254562 x10 <sup>-4</sup>	-2.4340867 x10 <sup>-4</sup>	4.3306955 x10 <sup>-7</sup>	-1.9531487 x10 <sup>-10</sup>	2.9108631 x10 <sup>-14</sup>	
h	2000 ≤ T ≤ 6300	6.4371993 x10 <sup>3</sup>	-2.2412806 x10 <sup>-1</sup>	2.3811928 x10 <sup>-4</sup>	-6.098608 x10 <sup>-8</sup>	6.895505 x10 <sup>-12</sup>	-2.968362 x10 <sup>-16</sup>	$\frac{\text{lb}_f}{\text{sec} - \text{deg R}}$
	0 ≤ T ≤ 2000	6.0351797 x10 <sup>3</sup>	-4.7254562 x10 <sup>-4</sup>	-2.4340867 x10 <sup>-4</sup>	4.3306955 x10 <sup>-7</sup>	-1.9531487 x10 <sup>-10</sup>	2.9108631 x10 <sup>-14</sup>	

while retaining the  $\eta$ -derivatives. In this way, a partial differential equation at a given  $\xi$ -location is reduced to an ordinary differential equation that can then be solved by various integration techniques or by finite-difference techniques, in either nonlinear or linear form. In the previous studies, this approach is used quite successfully in the solution of the equations of both incompressible and compressible boundary layers by an integration technique. The momentum equation is solved in its nonlinear form.

When the same method is extended to the solution of the equations of the incompressible turbulent boundary layer, the two chief disadvantages of the method become quite pronounced. First, computation time is too long. This is due to the greater thickness of the turbulent boundary layer and to the much greater variation in the transformed velocity gradient of the turbulent boundary layer. For example, for a laminar boundary layer the transformed boundary-layer thickness,  $\eta_{\delta}$ , is about 6, and the transformed velocity gradient at the wall,  $i_w''$ , varies between 0 and 2. On the other hand, for a turbulent boundary layer the transformed boundary-layer thickness may be 130 or more, and the transformed velocity gradient at the wall may vary between 0 and 30 or more. The old shooting method, which is based on the cut-and-try technique, thus has a much bigger range to search in meeting the boundary conditions. Second, accuracy is reduced when small step sizes are used in the streamwise direction. This is a serious problem, because short steps are essential near separation or in any region in which changes in the outer flow take place rapidly.

To overcome both of these disadvantages, the momentum equation is linearized and the integration method is replaced by an implicit finite-difference method containing a variable grid in the  $\eta$ -direction. The previous technique of replacing the  $\xi$ -derivatives by finite-difference relations is retained. Solution of the resulting algebraic equations in both momentum and energy equations is obtained by the Choleski matrix method [25].

6.6.1 Solution of the momentum equation.

6.6.1.1 Finite-difference representation of  $\xi$ -derivatives. With three-point-finite-difference formulas for the  $\xi$ -derivatives at  $\xi = \xi_n$  (6.51)

becomes

$$\left[ (1 + \tilde{t})^{2k} c \left( 1 + \frac{\tilde{\epsilon}}{\mu} \right) f_n'' \right] + f_n' f_n'' + \beta \left[ \frac{\mu_e}{\rho} - (f_n')^2 \right] = \quad (6.70)$$

$$= 2\xi_n \left[ f_n' \left( A_1 f_n' + A_2 f_{n-1}' + A_3 f_{n-2}' \right) - f_n'' \left( A_1 f_n + A_2 f_{n-1} + A_3 f_{n-2} \right) \right]$$

where the coefficients  $A_1$ ,  $A_2$ , and  $A_3$  are as follows:

For three points:

$$A_1 = \frac{1}{(\xi_n - \xi_{n-1})} + \frac{1}{(\xi_n - \xi_{n-2})} \quad (6.71a)$$

$$A_2 = - \frac{\xi_n - \xi_{n-2}}{(\xi_n - \xi_{n-1})(\xi_{n-1} - \xi_{n-2})} \quad (6.71b)$$

$$A_3 = \frac{\xi_n - \xi_{n-1}}{(\xi_n - \xi_{n-2})(\xi_{n-1} - \xi_{n-2})} \quad (6.71c)$$

At  $\xi = \xi_n$ , the quantities  $A_1$ ,  $A_2$ , and  $A_3$  are known, and the quantities having the subscripts  $n-1$  and  $n-2$  are known functions of  $\eta$  from solutions obtained at the two previous stations. Thus, at  $\xi = \xi_n$ , (6.50) is an ordinary differential equation in  $\eta$ . There is no problem of starting the solution, because the terms with  $\xi$ -derivatives disappear since  $\xi = 0$ . At the next station,  $\xi_1$ , the three-point formulas are replaced by two-point formulas; at all stations farther downstream the three-point formulas are used.

For two points:

$$A_1 = \frac{1}{\xi_n - \xi_{n-1}} \quad A_2 = - \frac{1}{\xi_n - \xi_{n-1}} \quad A_3 = 0 \quad (6.72)$$

6.6.1.2 Linearization of momentum equation. As it stands, (6.70) is an ordinary nonlinear differential equation of third order, and with boundary conditions given by (6.59) it is difficult to solve. In [7 through 13] this equation is solved quite satisfactorily for laminar and incompressible turbulent boundary-layer flows in its nonlinear form; here it is solved in a linear

form in order to speed up the computations and to be able to take smaller step sizes in the streamwise direction.

Two different linearization techniques were used to linearize (6.70). The first one is based on the quasi-linearization technique [26]. If (6.70) is written in the form

$$g(f, f', f'', f''', \eta, \xi) = 0 \quad (6.73)$$

and expanded in a Taylor series around a known solution designated by subscript 0,

$$g = g_0 + (f'''' - f_0'''' ) \left( \frac{\partial g}{\partial f''''} \right)_0 + (f''' - f_0''') \left( \frac{\partial g}{\partial f'''} \right)_0 + (f'' - f_0'') \left( \frac{\partial g}{\partial f''} \right)_0 + (f - f_0) \left( \frac{\partial g}{\partial f} \right)_0 + \text{higher order terms} \quad (6.74)$$

the following quasi-linearized equation is obtained:

$$E_1 \varphi'''' + E_2 \varphi''' + E_3 \varphi'' + E_4 \varphi' = E_5 \quad (6.75)$$

where  $\varphi$ 's are the perturbation quantities defined as

$$\varphi = f - f_0, \quad \varphi' = f' - f_0', \text{ etc.}$$

Note that in previous studies,  $\varphi$ 's are used to denote translated stream function  $f$ 's and should not be confused with the perturbation terms that are denoted by  $\varphi$ 's in this study. The latter are used for what are commonly called  $\epsilon$ 's, because  $\epsilon$ 's have already been used to denote eddy-viscosity terms.

The coefficients  $E_j$  are given by

$$E_1 = (1 + \tilde{t})^{2k} C_0 \left( 1 + \frac{\tilde{\epsilon}}{\mu} \right)_0 \quad (6.76a)$$

$$E_2 = \left[ (1 + \tilde{t})^{2k} C_0 \left( 1 + \frac{\tilde{\epsilon}}{\mu} \right)_0 \right]' + f_0' + 2\{A_1 f_0' + A_2 f_{n-1}' + A_3 f_{n-2}'\} \quad (6.76b)$$

$$E_3 = -2\{f_0' \beta + \{2A_1 f_0' + A_2 f_{n-1}' + A_3 f_{n-2}'\}\} \quad (6.76c)$$

$$E_4 = f_0''' (1 + 2\xi A_1) \quad (6.76d)$$

$$E_5 = - (1 + \tilde{t})^{2k} C_0 (1 + \frac{\tilde{c}}{\mu})_0 f_0'''' - [(1 + \tilde{t})^{2k} C_0 (1 + \frac{\tilde{c}}{\mu})_0]' f_0''' - f_0' f_0'''' \\ - \beta [(\rho_e/\rho)_0 - (f_0')^2] - 2\xi [f_0' (A_1 f_0' + A_2 f_{n-1}' + A_3 f_{n-2}')] \\ - f_0'' (A_1 f_0 + A_2 f_{n-1} + A_3 f_{n-2}) \quad (6.76e)$$

When (6.75) is solved by the finite-difference method to be described later, successive iterations on  $f_w''$  cause oscillations in  $f_w''$  and convergence is not obtained.\* On the other hand, (6.75) shows no oscillations in  $f_w''$  for laminar flow. For the latter case the convergence is fast (quadratic), and the results are very satisfactory. However, unlike the old shooting method used in previous studies, this method gives results that indicate that much finer spacing in the streamwise direction is necessary to obtain results comparable to those of the old shooting method. That is to be expected, since with finer spacing the difference between the calculated and assumed solutions ( $f_0$  and its derivatives) decreases.

The second technique used to linearize (6.70) is in principle similar to the one used in the energy equation in previous studies (see [11], for example). In this case, certain terms that make the equation nonlinear are assumed to be known from previous iterations, that is,

---

\* Since the previous studies have indicated that the greatest error usually appears in  $f_w''$ , again successive values of  $f_w''$  are used for the convergence criterion; that is,

$$\left| f_{w_{Q+1}}'' - f_{w_Q}'' \right| < \gamma$$

where  $\gamma$  is a prescribed value and  $Q$  denotes the iteration number.

$$\left[ (1 + \tilde{t})^{2k} C_o \left(1 + \frac{\tilde{\epsilon}}{\mu}\right)_o f'' \right]' + f_o f''' + \beta \left[ (\rho_e/\rho)_o - f_o' f' \right] = \quad (6.77)$$

$$2\xi \left[ f_o' (A_1 f' + A_2 f'_{n-1} + A_3 f'_{n-2}) - f_o'' (A_1 f + A_2 f_{n-1} + A_3 f_{n-2}) \right]$$

The subscript o denotes that the function is obtained from a previous iteration. For simplicity, the subscript n is dropped. Equation (6.77) can be expressed in the same form as (6.75), where again the  $\varphi$ 's are the perturbation quantities defined as before. However, the coefficients  $E_j$  now are given by

$$E_1 = (1 + \tilde{t})^{2k} C_o \left(1 + \frac{\tilde{\epsilon}}{\mu}\right)_o$$

$$E_2 = \left[ (1 + \tilde{t})^{2k} C_o \left(1 + \frac{\tilde{\epsilon}}{\mu}\right)_o \right]' + f_o$$

$$E_3 = -\beta f_o' - 2\xi f_o' A_1 = -f_o' (\beta + 2\xi A_1) \quad (6.78)$$

$$E_4 = 2\xi f_o'' A_1$$

$$E_5 = -\beta (\rho_e/\rho)_o + 2\xi [f_o' (A_2 f'_{n-1} + A_3 f'_{n-2}) - f_o'' (A_2 f_{n-1} + A_3 f_{n-2})]$$

$$- [E_1 f_o'' + E_2 f_o''' + E_3 f_o' + E_4 f_o'']$$

Again, when (6.75) with the coefficients defined by (6.78) is solved by the same finite-difference method as before, oscillations in  $f_w''$  continue and convergence is not obtained. On the other hand, the results for laminar flow indicate that even though the convergence rate of this linearization method is not as rapid as the other one, this linearization methods shows much less sensitivity to streamwise spacing and the results are as accurate as the other one. Furthermore, when a 3-point mean of the eddy-viscosity expression appearing in (6.78) is taken in the  $\eta$ -direction and a 2-point mean of the coefficients given by (6.78) is taken in the  $\xi$ -direction, oscillations in  $f_w''$  stop and excellent convergence on  $f_w''$  is obtained.

6.6.1.3 Variable-grid spacing in the  $\eta$ -direction. From a computational aspect, a turbulent boundary layer presents a much more difficult problem of calculation than a laminar boundary layer. Consider, for example, an

incompressible turbulent flow. The skin-friction is appreciably greater than it is for laminar flow. This means that  $\partial u/\partial y$  is greater. To maintain computing accuracy when  $\partial u/\partial y$  is large, short steps in  $y$  must be taken; when it is small, longer steps can be taken. Therefore, near the wall the steps in a turbulent boundary layer must be shorter than they are in a laminar layer under similar conditions. In the outer region, the expression for the eddy viscosity can be written as (see 6.27)

$$\frac{\epsilon_0}{\mu_e} = 0.0168 (\rho/\rho_e) R_{\delta^*} \quad (6.79)$$

where  $R_{\delta^*}$  is defined as  $\rho_e u_e \delta^*/\mu_e$  and  $\gamma$  is assumed to be unity. Since  $R_{\delta^*}$  may easily exceed 10,000,  $\epsilon_0/\mu_e$  may easily exceed 100. This part of the boundary layer then behaves like that of a highly viscous flow (oil, for example), and the thickness of this part becomes very great. On the whole, the turbulent boundary layer is something like a cold oil flowing past a heated wall. Thus it can be seen that the turbulent boundary layer is characterized by great thickness; but, in spite of that, the steps near the wall must be shorter than for laminar flow. As a result, if steps of constant  $\eta$ -spacing are used, far more are required than are necessary to solve a laminar layer, nor will ordinary scaling improve the situation.

A possible solution of this problem is to devise a simple variable-step system that has short steps near the wall, which lengthen with distance from the wall. A promising idea, illustrated in figure 5, is a grid whose spacing is such that the ratio of lengths of any two adjacent intervals is a constant; that is,  $h_i = Kh_{i-1}$ . The distance to the  $i$ -th grid line is given by the following formula:

$$\eta_i = h_1 \left( \frac{K^i - 1}{K - 1} \right) \quad i = 0, 1, 2, 3, \dots, N \quad (6.80)$$

There are two parameters:  $h_1$ , the length of the first step, and  $K$ , the ratio of two successive steps. A number of useful relations for this system can be derived, but the following is of particular interest:

$$K = \frac{\eta_i - h_1}{\eta_1 - h_1} \quad (6.81)$$

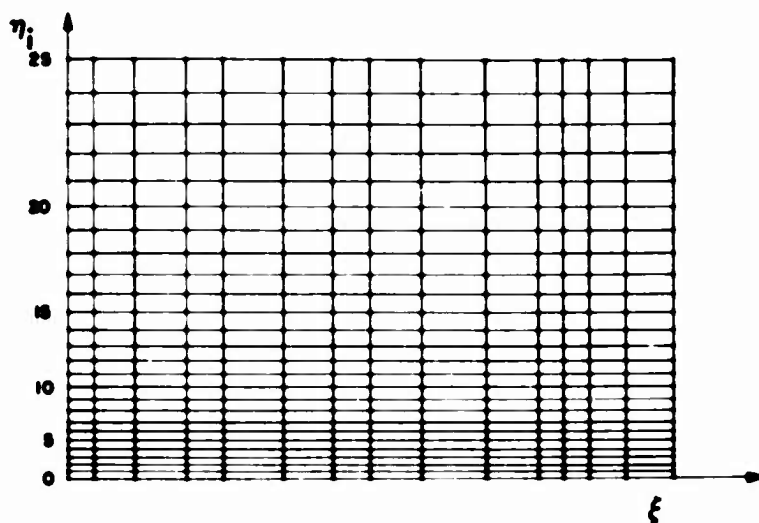


Figure 5.- Finite-difference variable-grid system in the  $\eta$ -direction.

Suppose the boundary layer has a thickness  $\eta_w = 100$ . Assume that an error analysis shows that  $h_1$  must be 0.1, but that it also shows that  $h_1 (= h_w)$  could be 2. What is  $K$ ? It is

$$K = \frac{100 - 0.1}{100 - 2} = \frac{99.9}{98} = 1.0194$$

and 157 steps are required for the traverse. At a constant step length of 0.1, which is based on the wall accuracy requirements, 1000 steps would be required. In the usual problem, the value of  $K$  lies between 1.01 and 1.02. Figure 5 accurately represents the spacing for  $K = 1.07$ , a grossly large value. The spacing in the  $\xi$ -direction is arbitrary.

6.6.1.4 Method of solution. An implicit finite-difference technique is used to solve (6.75). Figure 6 shows the finite-difference molecule selected. The variable-grid differentiation formulas for this molecule, as well as for a 3-point molecule that is used in the energy equation, are derived for the Lagrange interpolation formula and are given in Appendix C (see also [27]). By using the first-, second-, and third-derivative formulas at point  $(n, i)$ , (6.75) can be written as follows:

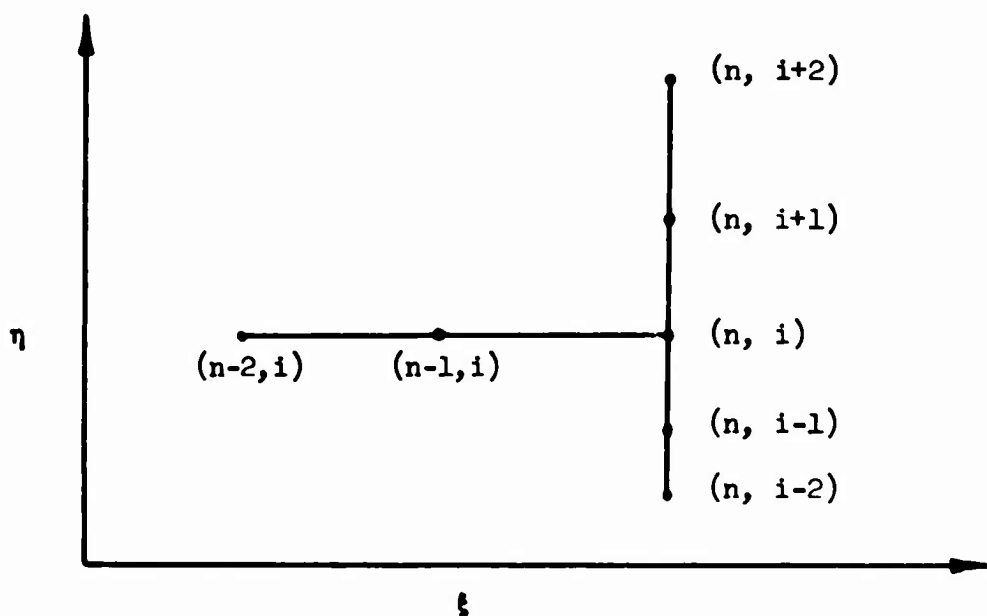


Figure 6.- Finite-difference molecule for the momentum equation at (n, i).

$$\varphi_{i+2} + F_i \varphi_{i+1} + G_i \varphi_i + I_i \varphi_{i-1} + M_i \varphi_{i-2} = N_i \quad i = 2, 3, 4, \dots, N-2 \quad (6.82)$$

where

$$F_i = \frac{B_4}{R} \left[ 6(a_1 + K - K^2 a_1) + 2 \frac{E_2}{E_1} h_{i-2} K a_1 (1 - K a_1 - K^2) - \frac{E_3}{E_1} h_{i-2}^2 K^3 a_1^2 \right] \quad (6.83a)$$

$$G_i = \frac{B_3}{R} \left[ 6(a_1 + K - K^2 - K^2 a_1) + 2 \frac{E_2}{E_1} h_{i-2} K (a_1 - K a_1 - K a_1^2 - K^2 - K^2 a_1 + K^3 a_1) + \frac{E_3}{E_1} h_{i-2}^2 K^3 a_1 (K^2 + K a_1 - a_1 - 1) + \frac{E_4}{E_1 B_3 h_{i-2}} \right] \quad (6.83b)$$

$$I_i = \frac{B_2}{R} \left[ 6(a_1 - K^2 - K^2 a_1) + 2 \frac{E_2}{E_1} h_{i-2} K^2 a_1 (K^2 - a_1 - 1) + \frac{E_3}{E_1} h_{i-2}^2 K^4 a_1^2 \right] \quad (6.83c)$$

$$M_i = \frac{B_1}{R} \left[ 6K(1 - K - K a_1) + 2 \frac{E_2}{E_1} h_{i-2} K^3 (K a_1 - a_1 - 1) + \frac{E_3}{E_1} h_{i-2}^2 K^5 a_1 \right] \quad (6.83d)$$

$$N_i = \frac{E_5}{E_1 R h_{i-2}} \quad (6.83e)$$

$$R_i = B_5 \left[ 6(a_1 + K - K^2) + 2 \frac{E_2}{E_1} h_{i-2} K(a_1 - K a_1 - K^2) - \frac{E_3}{E_1} h_{i-2}^2 K^3 a_1 \right] \quad (6.83f)$$

The eddy-viscosity expressions appearing in the coefficients  $E_5$  and  $E_4$  at  $(n, i)$  are taken as the 3-point means of the eddy-viscosity expressions in the  $\eta$ -direction; that is,

$$(\epsilon_{av})_i = \frac{1}{3} [\epsilon_{i-1} + \epsilon_i + \epsilon_{i+1}] \quad (6.84)$$

This averaging process was introduced in order to stop the oscillations in  $f_w''$  and cause the iterations to converge.

For each point  $(n, i)$  at station  $i$ , an algebraic equation of the form of (6.82) is written, yielding  $N - 3$  algebraic equations with  $N$  unknowns. The other three equations are obtained by considering the following finite-difference molecule at  $(n, N-1)$  (see figure 7) and by the boundary conditions given by (6.59).

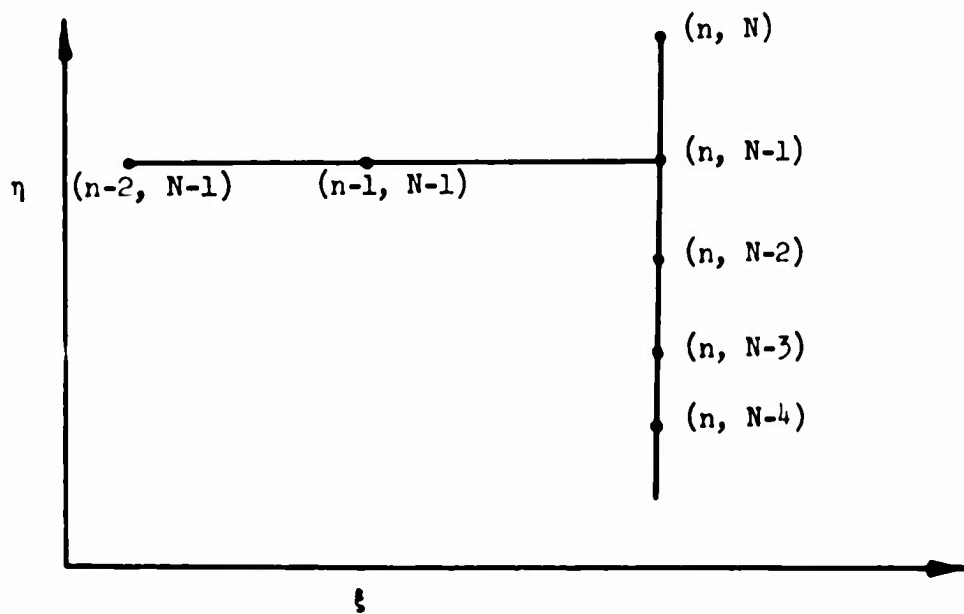


Figure 7.- Finite-difference molecule for the momentum equation at  $(n, N-1)$ .

By using the variable-grid differentiation formulas at point  $(n, N-1)$ , (6.75) can be written as follows:

$$\varphi_N + F_{N-1} \varphi_{N-1} + G_{N-1} \varphi_{N-2} + I_{N-1} \varphi_{N-3} + M_{N-1} \varphi_{N-4} = N_{N-1} \quad (6.85)$$

where

$$F_{N-1} = \frac{B_4}{R_{N-1}} \left[ 6(a_2 + K a_1 + K^2 - K^3) + 2 \frac{E_2}{E_1} h_{N-4} K (a_1 a_2 + K a_2 - K^2 a_2 + K^2 a_1 - K^3 a_1 - K^4) \right. \\ \left. + \frac{E_3}{E_1} h_{N-4}^2 K^3 (a_1 a_2 - K a_1 a_2 - K^2 a_2 - K^3 a_1) + \frac{E_4}{B_4 E_1 h_{N-4}} \right] \quad (6.86a)$$

$$G_{N-1} = \frac{B_3}{R_{N-1}} \left[ 6(a_2 + K a_1 - K^3) + 2 \frac{E_2}{E_1} h_{N-4} K (a_1 a_2 - K^2 a_2 - K^3 a_1) \right. \\ \left. - \frac{E_3}{E_1} h_{N-4}^2 (K^4 a_1 a_2) \right] \quad (6.86b)$$

$$I_{N-1} = \frac{B_2}{R_{N-1}} \left[ 6(a_2 + K^2 - K^3) + 2 \frac{E_2}{E_1} h_{N-4} K^2 (a_2 - K a_2 - K^3) - \frac{E_3}{E_1} h_{N-4}^2 (K^5 a_2) \right] \quad (6.86c)$$

$$M_{N-1} = \frac{B_1}{R_{N-1}} \left[ 6K(a_1 + K - K^2) + 2 \frac{E_2}{E_1} h_{N-4} K^3 (a_1 - K a_1 - K^2) - \frac{E_3}{E_1} h_{N-4}^2 K^6 a_1 \right] \quad (6.86d)$$

$$N_{N-1} = \frac{E_5}{E_1 R_{N-1} h_{N-4}} \quad (6.86e)$$

$$R_{N-1} = B_5 \left[ 6(a_2 + K a_1 + K^2) + 2 \frac{E_2}{E_1} h_{N-2} (K a_1 a_2 + K^2 a_2 + K^3 a_1) + \frac{E_3}{E_1} h_{N-4}^2 K^3 a_1 a_2 \right] \quad (6.86f)$$

By using the first-derivative variable-grid differentiation formula at point (n, 0), the boundary condition given by (6.59b) can be written as follows:

$$\varphi_4 + F_1 \varphi_3 + G_1 \varphi_2 + I_1 \varphi_1 = N_1 \quad (6.87)$$

where

$$F_1 = \frac{B_4}{R_1} a_1 a_3 \quad (6.88a)$$

$$G_1 = \frac{B_3}{R_1} a_2 a_3 \quad (6.88b)$$

$$I_1 = \frac{B_2}{R_1} a_1 a_2 a_3 \quad (6.88c)$$

$$N_1 = -\frac{B_1}{R_1} (a_1 a_2 + a_1 a_3 + a_2 a_3 + a_1 a_2 a_3) f_w - \left[ I_1 (f_0)_1 + G_1 (f_0) + F_1 (f_0)_3 + (f_0)_4 \right] \quad (6.88d)$$

$$R_1 = B_5 a_1 a_2 \quad (6.88e)$$

The term  $f_w$  is given by (6.59a). It is equal to zero when there is no mass transfer.

Similarly, by using the first-derivative variable-grid differentiation formula at point  $(n, N)$ , the boundary condition given by (6.59c) can be written as follows:

$$\varphi_N + F_N \varphi_{N-1} + G_N \varphi_{N-2} + H_N \varphi_{N-3} + I_N \varphi_{N-4} = N_N \quad (6.89)$$

where

$$F_N = \frac{B_4}{R_N} K^3 a_1 a_2 a_3 \quad (6.90a)$$

$$G_N = \frac{B_3}{R_N} K^4 a_2 a_3 \quad (6.90b)$$

$$I_N = \frac{B_2}{R_N} K^5 a_1 a_3 \quad (6.90c)$$

$$M_N = \frac{B_1}{R_N} K^6 a_1 a_2 \quad (6.90d)$$

$$N_N = \frac{1}{h_{N-4}^3 R_N} - (F_N (f_0)_{N-1} + G_N (f_0)_{N-2} + H_N (f_0)_{N-3} + I_N (f_0)_{N-4} + (f_0)_N) \quad (6.90e)$$

$$R_N = B_5 (K^3 a_1 a_2 a_3 + K^4 a_2 a_3 + K^5 a_1 a_3 + K^6 a_1 a_2) \quad (6.90f)$$



so that (6.91) becomes

$$L U \varphi = N \quad (6.93)$$

If (6.93) is written in the form

$$L Y = N \quad (6.94)$$

where

$$U \varphi = Y \quad (6.95)$$

then the method of solution is apparent. The two triangular matrices  $L$  and  $U$  are found from (6.92), the column matrix  $Y$  from (6.94), and the column matrix  $\varphi$  from (6.95).

### 6.6.2 Solution of the energy equation.

6.6.2.1 Finite-difference representation of  $\xi$ -derivatives. The method of solution of the energy equation is similar to that of the momentum equation. Again the  $\xi$ -derivatives are replaced by finite differences that are defined by (6.71). Thus (6.52) is written as

$$[P_1 \xi']_n' + (P_2)_n \xi_n' + (P_3)_n \xi_n = (P_4)_n \quad (6.96)$$

where the coefficients  $P_j$  are given by

$$P_1 = (1 + \tilde{t})^{2k} \frac{C}{Pr} \left( 1 + \frac{\tilde{t}}{\mu} \frac{Pr}{Pr_T} \right) \quad (6.97a)$$

$$P_2 = r' + 2\xi(A_1 f + A_2 f_{n-1} + A_3 f_{n-2}) \quad (6.97b)$$

$$P_3 = -2\xi r' A_1 \quad (6.97c)$$

$$P_4 = 2\xi r' (A_2 \xi_{n-1} + A_3 \xi_{n-2}) - \left[ (1 + \tilde{t})^{2k} C \frac{u_c^2}{H_e} \left( 1 - \frac{1}{Pr} \right) r' r'' \right]' \quad (6.97d)$$

6.6.2.2 Method of solution. Again, an implicit finite-difference method is used to solve the energy equation. Figure 8 shows the finite-difference molecule selected.

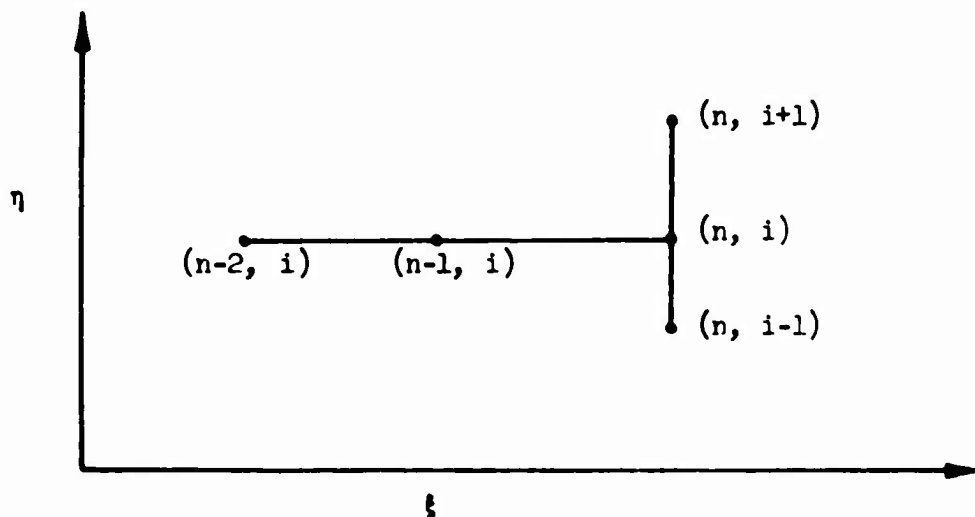


Figure 8.- Finite-difference molecule for the energy equation at (n, i).

By using the first-derivative 3-point variable-grid finite-difference formula at point (n, i), (6.96) can be written as follows:

$$E_{i+1} + S_i E_i + W_i E_{i-1} = Z_i \quad i = 1, 2, 3, \dots, N-1 \quad (6.98)$$

where

$$S_i = \frac{1}{V} \left[ P_3 + P_2 A_2 h_{i-1} (1 - K) + A_2 h_{i-1}^2 \left\{ A_1 K (1 + K) (P_1)_{i-1} + A_2 (1 - K)^2 P_1 + A_3 (1 + K) (P_1)_{i+1} \right\} \right] \quad (6.99a)$$

$$W_i = \frac{A_1 h_{i-1}}{V} \left[ h_{i-1} \left\{ A_1 K (2 + K) (P_1)_{i-1} - A_2 K (1 - K) P_1 + A_3 K (P_1)_{i+1} \right\} - P_2 K \right] \quad (6.99b)$$

$$Z_i = \frac{P_4}{V} \quad (6.99c)$$

$$V_i = A_3 h_{i-1} \left[ h_{i-1} \left\{ A_1 K (P_1)_{i-1} + A_2 (1 - K) P_1 + A_3 (1 + 2K) (P_1)_{i+1} \right\} + P_2 \right] \quad (6.99d)$$

Again, for simplicity, the subscript  $n$  is dropped. In solving (6.98), values of  $f$  and its derivatives determined from the previous solution of the momentum equation and fluid properties determined from the previous solution of the energy equation are used. Details of the iterative procedures for solving both momentum and energy equations are given in Section 6.6.3. With these procedures, (6.98) is linear and  $g$  is the only unknown.

For each point  $(n, i)$ , at station  $i$  an algebraic equation of the form of (6.98) is written, yielding  $N-1$  algebraic equations with  $N-1$  unknowns. The function  $g$  at  $N$  is known from (6.60b), and  $g$  at the wall is known from one form of (6.60a), depending on whether the temperature or the heat transfer is specified at the wall.

Case 1:  $g_w$  is known.

For  $i = 1$ , (6.98) becomes

$$g_2 + S_1 g_1 + W_1 g_w = Z_1 \quad (6.100a)$$

and, since  $g_w$  is known, it can be written as

$$g_2 + S_1 g_1 = Z_1 - W_1 g_w \equiv Z_1^* \quad (6.100b)$$

Case 2:  $g_w'$  is known.

For this case  $g_w$  is unknown, but since  $g_w'$  is known,  $g_w$  can be expressed in terms of  $g_w'$  and  $g_1$ 's by using (6.100a) and the first-derivative variable-grid differentiation formula at point  $(n, 0)$ .

$$g_w' = -h_1 \left[ B_1(2 + K)g_w + B_2(1 + K)g_1 + B_3 g_2 \right] \quad (6.101)$$

Thus, by eliminating  $g_w$  from (6.100a) and (6.101) and rearranging, the following equation is obtained:



$\delta^*$  and  $f''$  are obtained from the final solution at station  $n-1$ , and inner and outer regions are established by (6.28). With this information, the system of equations represented by (6.91) is solved by using the fluid properties from the  $n-1$  station and  $f$  and its derivatives from the  $n-2$ ,  $n-1$  stations. Once (6.91) is solved, new values of  $f$  are obtained from  $\phi$ 's and  $f$ 's. The first derivative of  $f$  is subsequently calculated from the values of  $f$ , the second derivatives from the values of  $f'$ , and the third derivatives from the differential equation, (6.75). A solution at station  $n$  for one iteration is then defined as the averages of the calculated values of  $f$  and its derivatives and previous values of  $f$  and its derivatives; that is, the values of  $f$  and its derivatives are obtained from

$$f = \frac{1}{2} \left[ (f_0)_Q + (f_0)_{Q+1} \right], \quad f' = \frac{1}{2} \left[ (f'_0)_Q + (f'_0)_{Q+1} \right], \quad \text{etc.},$$

where  $Q$  is an iteration number. This is necessary to stop the oscillations in  $f''_w$ .

After a solution of the momentum equation is obtained in this manner, the values of  $f$ 's and their derivatives from this solution are used to solve the energy equation. Again, the fluid properties from station  $n-1$  are used. Once (6.103) is solved, fluid properties are obtained for that particular solution by converting the total enthalpy to static temperature, and inner and outer regions for the next solution of the momentum equation are established. The conversion of enthalpies to temperatures is necessary because the fluid properties given by (6.65), (6.66), (6.67), and (6.69) are expressed as functions of temperature. The procedure of calculating temperatures from the enthalpies is as follows: From the steady-state energy equation, the total enthalpy  $H$  is

$$H = h + \frac{1}{2} u^2 \quad (6.104)$$

By using the definition of  $g$  and the transformation given by (6.58), equation (6.104) can be written as

$$h = g H_e - \frac{1}{2} u_e^2 (f')^2 \quad (6.105)$$

Since  $g$  is known from the solution of the energy equation,  $f'$  is known from the solution of the momentum equation, and  $H_e$  and  $u_e$  are given, the right-hand side of (6.105) is known. Equation (6.105) is effectively a sixth-degree polynomial given by (6.68). Rewriting (6.105) and denoting it by  $F$  gives

$$F = h - g H_e + \frac{1}{2} u_e^2 (f')^2 = F(T) \quad (6.106)$$

The Newton-Raphson method is used to solve (6.106). An initial temperature,  $T_1$ , is obtained from the perfect-gas relationship; that is,

$$T_1 = \frac{1}{c_p} \left[ g H_e - \frac{1}{2} u_e^2 (f')^2 \right] \quad (6.107)$$

where  $c_p$  for air is  $6.035 \times 10^3$  ft<sup>2</sup>/sec-deg R. A new temperature then is calculated by the formula

$$T_2 = T_1 - \frac{F(T_1)}{F'(T_1)} \quad (6.108)$$

where  $F'$  is the derivative of  $F$  with respect to  $T$ . Once  $T_2$  is obtained, the same procedure can be repeated and new values of  $T$  can be obtained until the difference between the consecutive values of  $T$  is less than  $\gamma$ , where  $\gamma$  is a small number.

Once the temperature at each point within the boundary layer is known, the fluid properties are calculated from (6.65), (6.66), (6.67) and (6.69). With these newly calculated fluid properties and with the values of  $\delta^*$  and  $f''$  from the previous solution of momentum equation, inner and outer regions are established and the momentum equation and the energy equation are solved in succession. An iteration procedure based on the convergence of  $f''_w$  is followed. The iteration process continues until either

$$\left| (f''_w)_{Q+1} - (f''_w)_Q \right| < \gamma$$

or

$$Q = Q_{\max}$$

where  $\gamma$  is a prescribed value and  $Q$  denotes the iteration number. A typical value of  $Q$  is 6. Once either of these conditions is satisfied, the program proceeds to the next station. Figure 9 shows the flow diagram at station  $n$ .

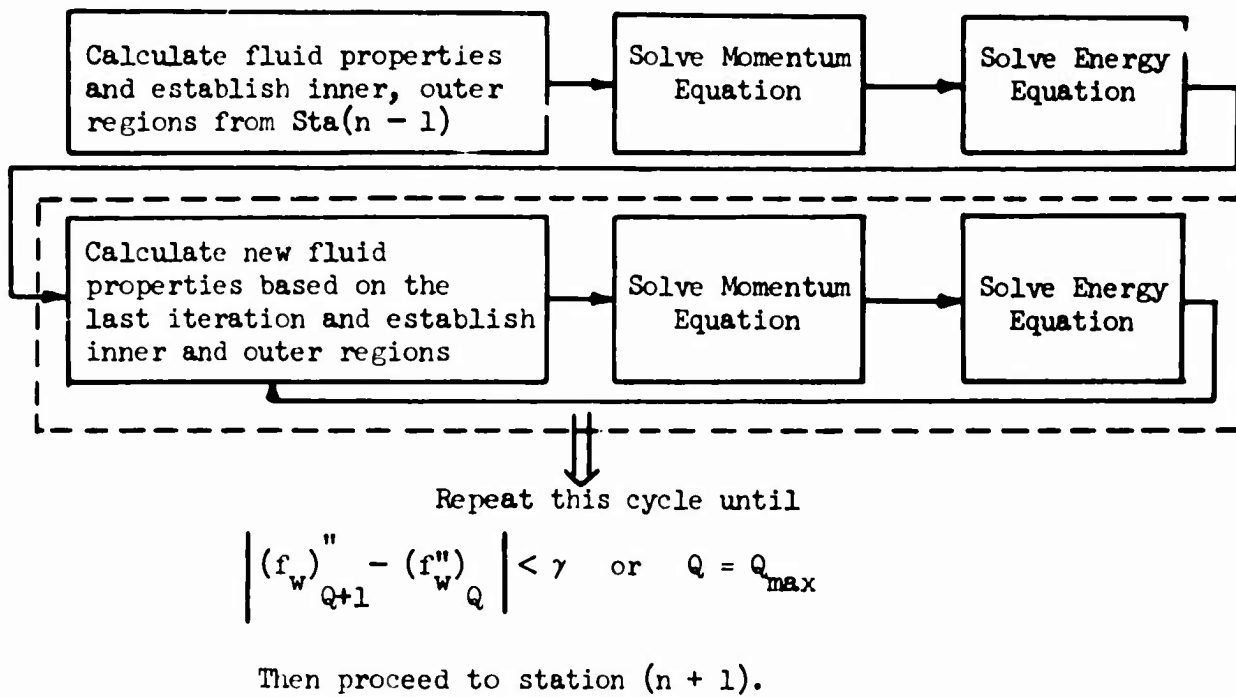


Figure 9.- Flow-diagram for solving the boundary-layer equations at station  $n$ ,  $\xi = \xi_n$ .

As the calculations proceed downstream, the boundary-layer thickness increases. Since at station  $n$  the initial values of  $f$  and its derivatives are obtained from station  $n-1$ , it is necessary to make an assumption for these values for  $\eta > (\eta_{\infty})_{n-1}$ , where  $(\eta_{\infty})_{n-1}$  is the transformed boundary-layer thickness at station  $n-1$ . For this reason, at station  $n$  the values of  $f$  and its derivatives are obtained from station  $n-1$  up to  $\eta = (\eta_{\infty})_{n-1}$ . For  $\eta > (\eta_{\infty})_{n-1}$ ,  $f$  is obtained from  $f = [\eta - (\eta_{\infty})_{n-1} + f_{n-1}(\eta_{\infty})]$ ,  $f'$  is assumed to be unity, and  $f''$  and  $f'''$  are assumed to be zero (see figure 10). The

latter assumption is permissible, since  $f''$  and  $f''''$  approach zero as  $\eta \rightarrow \eta_w$ .

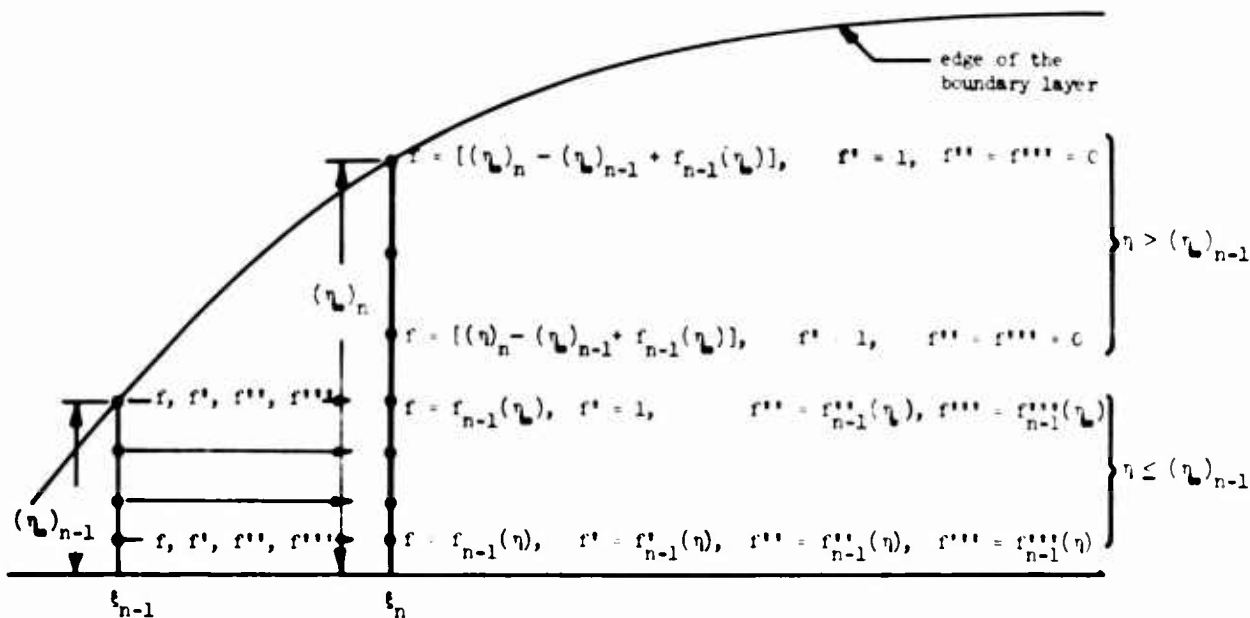


Figure 10.-Diagram showing the method of generating the initial coefficients of the momentum equation at station  $n$ .

6.6.4 Starting the solution at the leading edge or at the stagnation point,  $\xi = 0$ .

At  $\xi = 0$ , the  $\xi$ -dependent terms disappear in both the momentum and energy equations. Hence the coefficients of (6.75) given by (6.78) and the coefficients of (6.96) given by (6.97) do not contain  $\xi$ -dependent terms. In addition, the flow at this zero-station is assumed to be laminar, because the eddy-viscosity and turbulent-Prandtl-number terms are zero.

The procedure of solution requires that the momentum equation be solved first, but to do so requires values of the fluid properties as well as the initial values of  $f$  and its derivatives denoted by the subscript  $o$ . The latter values are obtained by the old shooting method of previous studies [7 through 13]. The fluid properties are obtained by assuming a linear temperature profile of the form

$$T = a + b\eta$$

which becomes

$$T = T_w + (T_e - T_w) \frac{\eta}{\eta_w} \tag{6.109}$$

by assuming  $T(0) = T_w$ ,  $T(\eta_\infty) = T_e$ .

After the first solution of the momentum equation is obtained by (6.91), new values of  $f$  and its derivatives, together with the fluid properties obtained by a linear temperature variation, are used to solve the energy equation. Again, once (6.103) is solved, fluid properties are obtained for that particular solution by converting the total enthalpy to static temperature. These fluid properties are used for the next solution of the momentum equation. Figure 11 shows the flow diagram at  $\xi = 0$ .

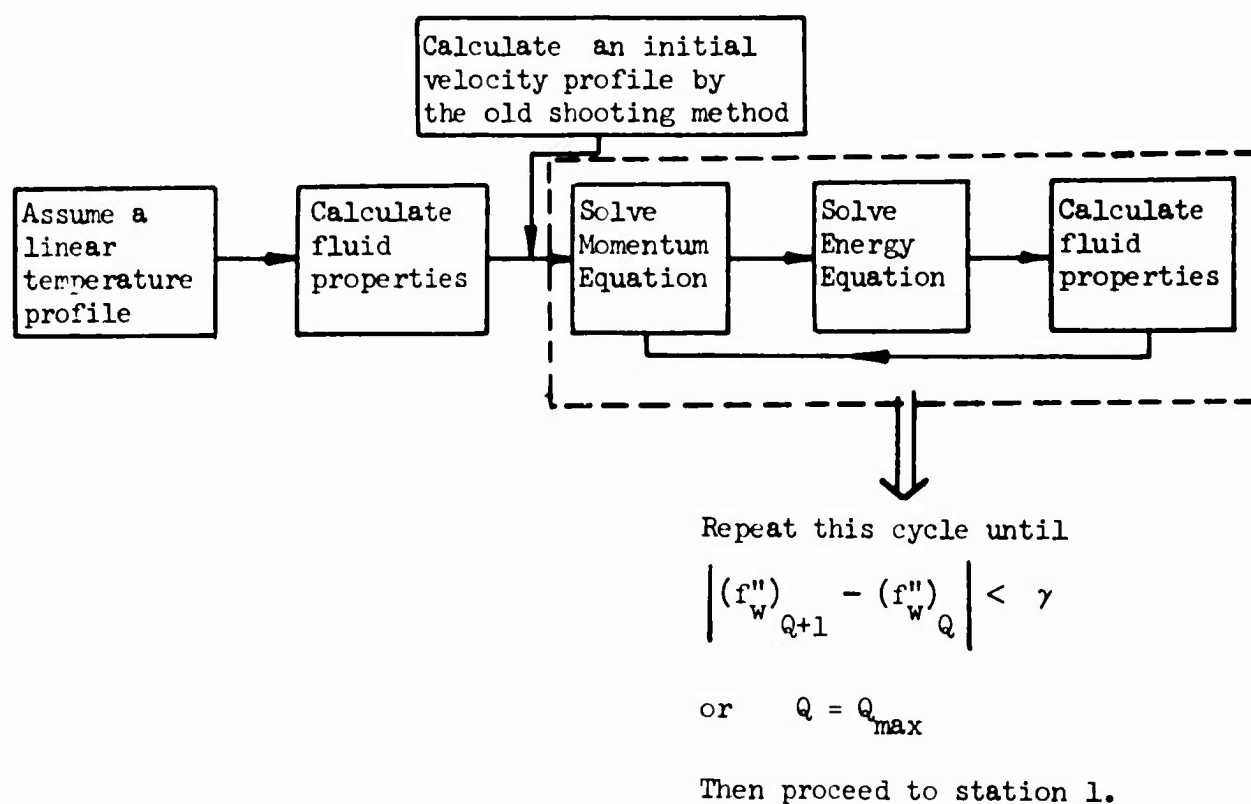


Figure 11.- Flow diagram for solving the boundary-layer equations at  $\xi = 0$ .

### 6.7 Boundary-Layer Parameters

Once the profiles of  $f$  and  $g$  and their derivatives are determined at any  $\xi$ -station, the boundary-layer parameters, such as displacement thickness, momentum thickness, local shear-stress coefficient, local skin-friction coefficient, local heat-transfer rate, Stanton number, as well as the law-of-the-wall coordinates, velocity-defect coordinates, and other parameters of interest, can be calculated. Some of these parameters are given by the following equations.

Displacement thickness:

$$\delta^* = \int_0^{\infty} \left(\frac{r}{r_0}\right)^k \left(1 - \frac{\rho u}{\rho_e u_e}\right) dy \quad (6.110a)$$

or, in terms of  $\xi$ ,  $\eta$ -coordinates,

$$\delta^* = \frac{L}{r_0^k} \frac{(2\xi)^{1/2}}{\rho_e u_e} \int_0^{\infty} \left(\frac{\rho_e}{\rho} - f'\right) d\eta \quad (6.110b)$$

Momentum thickness:

$$\theta = \int_0^{\infty} \left(\frac{r}{r_0}\right)^k \frac{\rho u}{\rho_e u_e} \left(1 - \frac{u}{u_e}\right) dy \quad (6.111a)$$

or, in terms of  $\xi$ ,  $\eta$ -coordinates,

$$\theta = \frac{L}{r_0^k} \frac{(2\xi)^{1/2}}{\rho_e u_e} \int_0^{\infty} f' (1 - f') d\eta \quad (6.111b)$$

Shear stress at the wall:

$$\tau_w = \mu_w \left(\frac{\partial u}{\partial y}\right)_w \quad (6.112a)$$

or, in terms of  $\xi$ ,  $\eta$ -coordinates

$$\tau_w = \frac{\mu_w \rho_w r_0^k u_e^2 f_w''}{L(2\xi)^{1/2}} \quad (6.112b)$$

Local skin-friction coefficient:

$$c_f = \frac{\tau_w}{\frac{1}{2} \rho_e u_e^2} \quad (6.113a)$$

or, in terms of  $\xi$ ,  $\eta$ -coordinates,

$$c_f = (2/\xi)^{1/2} \frac{r_o^k}{L} \frac{\rho_w}{\rho_e} \mu_w f_w'' \quad (6.113b)$$

Local shear-stress coefficient for laminar flow, not necessarily at the wall

$$c_{\tau_L} = \frac{\tau_L}{\frac{1}{2} \rho_e u_e^2} \quad (6.114a)$$

or, in terms of  $\xi$ ,  $\eta$ -coordinates,

$$c_{\tau_L} = (2/\xi)^{1/2} \frac{r^k}{L} \frac{\rho}{\rho_e} \mu f'' \quad (6.114b)$$

Local shear-stress coefficient for turbulent flow:

$$c_{\tau_T} = -\frac{\rho \overline{u'v'}}{\frac{1}{2} \rho_e u_e^2} \quad (6.115a)$$

or, in terms of  $\xi$ ,  $\eta$ -coordinates,

$$c_{\tau_T} = (2/\xi)^{1/2} \frac{r^k}{L} \frac{\rho}{\rho_e} \epsilon f'' \quad (6.115b)$$

Total shear-stress coefficient:

$$c_{\tau_{total}} = c_{\tau_L} + c_{\tau_T} = (2/\xi)^{1/2} \frac{r^k}{L} \frac{\rho}{\rho_e} (\mu + \epsilon) f'' \quad (6.116)$$

Equation (6.116) reduces to (6.113b) at the wall, since  $\epsilon = 0$  at  $y = 0$ .

Heat-transfer rate at the wall:

$$-q_w = \frac{\lambda_w}{c_{p_w}} (\partial h / \partial y)_w \quad (6.117a)$$

or, in terms of  $\xi$ ,  $\eta$ -coordinates,

$$-q_w = \frac{r_o^k}{L} \frac{\rho_w \mu_w u_e H_e}{Pr_w (2\xi)^{1/2}} g_w' \quad (6.117b)$$

Stanton number:

$$St = \frac{-q_w}{\rho_e u_e (H_e - H_w)} \quad (6.118a)$$

or, in terms of  $\xi$ ,  $\eta$ -coordinates,

$$St = \frac{r_o^k \rho_w \mu_w g_w'}{L \rho_e Pr_w (2\xi)^{1/2} (1 - g_w)} \quad (6.118b)$$

The law-of-the-wall coordinates:

$$\frac{u}{u^*} = (2/c_f)^{1/2} f' \quad (6.119a)$$

$$\frac{yu^*}{v} = \frac{(\xi c_f)^{1/2} L}{\rho_e v} \int_0^\eta \frac{1}{r^k} (\rho_e/\rho) d\bar{\eta} \quad (6.119b)$$

The velocity-defect coordinate:

$$\frac{u_e - u}{u^*} = (2/c_f)^{1/2} (1 - f') \quad (6.120)$$

Once  $\delta^*$ ,  $\theta$ , and  $c_f$  are calculated, some of the other boundary-layer parameters such as shape factor  $H$ , defect-shape factor  $G$ , and defect-displacement thickness  $\Delta$  can be calculated from the following relations:

Shape factor:

$$H = \delta^*/\theta \quad (6.121)$$

Defect-shape factor:

$$G = \int_0^\infty \left( \frac{u_e - u}{u^*} \right)^2 dy \Big/ \int_0^\infty \left( \frac{u_e - u}{u^*} \right) dy = \left( \frac{2}{c_f} \right)^{1/2} \left( 1 - \frac{1}{H} \right) \quad (6.122)$$

Defect-displacement thickness:

$$\Delta = \int_0^{\infty} \left( \frac{u_e - u}{u_*} \right) dy = \left( \frac{2}{c_f} \right)^{\frac{1}{2}} \delta_* \quad (6.123)$$

## 7.0 COMPARISON OF CALCULATED AND EXPERIMENTAL RESULTS

The ultimate test of any numerical calculation technique is a comparison of calculations with exact solutions and with experiments. However, when no exact solutions are possible, as, for example, in turbulent flows, all that can be done is to compare the calculations with experiments. For this reason, a variety of both incompressible and compressible turbulent flows are calculated by the present method, and comparisons with experiments are made. The results presented in this report do not represent a finished development, but are only what has been obtained so far by one particular formulation of eddy viscosity and turbulent Prandtl number.

In the present method, the solution begins at the leading edge or at the stagnation point, where  $\xi = 0$ , and proceeds downstream. At station  $\xi = 0$ , the flow is laminar, and it becomes turbulent at any specified station where  $\xi > 0$ . In principle, a calculation can be started in the middle of a flow field, provided that information is available to be used as an input from upstream positions in the flow. In some of the experiments, a specific portion of the flow was instrumented. This is referred to as the test section. Details of the flow field upstream of the test section were not reported, and hence it was necessary to add, in effect, an initial length (usually a flat plate) to the test section. This length was selected to match as well as possible the calculated boundary-layer parameters, such as  $\theta$  and  $H$ , with the experimental values at the beginning of the test section. For each test case, details of the matching procedure are discussed separately.

The computer program of the present method has a capacity of 500 points in the  $\eta$ -direction. There is no restriction of the number of stations in the  $\xi$ -direction. For a turbulent boundary layer, the transformed boundary-layer thickness may be 130 or more, and the transformed velocity gradient at the wall may vary between 0 and 30 or more. Since a variable-grid system is being used in the  $\eta$ -direction and smaller spacing is necessary in the inner region, which occupies approximately 10 to 15 percent of the whole boundary layer, it is convenient to have a table of variable-grid parameters such as Table II. For the cases that have been calculated so far, an initial  $\eta$ -spacing of  $h_1 = 0.01$

TABLE II

VALUES OF VARIABLE-GRID PARAMETERS FOR DIFFERENT  $\eta_w$  VALUES (N = 500 POINTS)

$\eta_w$	$h_1 = 0.001$		$h_1 = 0.01$	
	K	$h_{edge}$	K	$h_{edge}$
30	1.01196	0.355	1.00595	0.187
65	1.01384	0.888	1.00807	0.530
100	1.01487	1.466	1.00920	0.922
130	1.01553	2.019	1.00991	1.305
150	1.01583	2.338	1.01023	1.529
200	1.01650	3.248	1.01096	2.178

was found to be satisfactory for the range of  $f_w''$  between 0 and 10. For values of  $f_w''$  greater than 10, it was found to be necessary to use a much smaller spacing,  $h_1 = 0.001$ , close to the wall.

In calculating the cases for both compressible and incompressible flows, it is necessary to transform the  $x, y$ -coordinates to  $\xi, \eta$ -coordinates. For flows with pressure gradients, it is also necessary to calculate the pressure-gradient term  $\beta$ , defined by (6.53). The  $\xi$ - and  $\eta$ -coordinates are given by (6.56) and (6.57), respectively, and reduce to

$$\xi = \int_0^x \rho_e \mu_e u_e dx \quad (7.1)$$

$$\eta = \frac{\rho_e u_e}{(2\xi)^{1/2}} \int_0^y (\rho/\rho_e) dy \quad (7.2)$$

for two-dimensional flows. The  $du_e/d\xi$ -term in  $\beta$  is calculated from the given velocity distribution  $u_e$  versus  $\xi$  by using a 3-point Lagrange derivative formula

$$(du_e/d\xi)_n = A_{n-1}u_{e_{n-1}} + A_n u_{e_n} + A_{n+1}u_{e_{n+1}} \quad (7.3)$$

where

$$A_{n-1} = \frac{\xi_n - \xi_{n+1}}{(\xi_{n-1} - \xi_n)(\xi_{n-1} - \xi_{n+1})} \quad (7.4a)$$

$$A_n = \frac{2\xi_n - \xi_{n+1} - \xi_{n-1}}{(\xi_n - \xi_{n-1})(\xi_n - \xi_{n+1})} \quad (7.4b)$$

$$A_{n+1} = \frac{\xi_n - \xi_{n-1}}{(\xi_{n+1} - \xi_{n-1})(\xi_{n+1} - \xi_n)} \quad (7.4c)$$

For compressible flows, the fluid properties at the edge of the boundary layer, which are inputs to the computer program, are determined by the test conditions. On the other hand, for incompressible flows, the fluid properties are determined at standard temperature and pressure.

## 7.1 Incompressible Flows

The test cases for which comparisons are calculated by the present method consist of a variety of flows of widely different character: flat-plate, flat-plate with mass transfer (blowing and suction), equilibrium flows in both favorable and adverse pressure gradients, nonequilibrium flows in adverse pressure gradients, separating boundary layers, and recovering boundary layers.

### 7.1.1 Flat-plate flows.

Flat-plate flow offers an excellent opportunity to compare the calculated results with experimental results as well as with well-established correlations such as the law of the wall and the defect law. A flat-plate flow was calculated for a Reynolds number of  $10^7$  per foot, by assuming the following values of the flow parameters:

$$\begin{aligned} \mu &= 0.38 \times 10^{-6} \text{ lb}_f\text{-sec/ft}^2 \\ \rho &= 0.237 \times 10^{-2} \text{ lb}_f\text{-sec}^2/\text{ft}^4 \\ u_e &= 1600 \text{ ft/sec.} \end{aligned}$$

The value of  $u_e$  was selected merely as a matter of convenience. For this case, the relations given by (7.1) and (7.2) reduce to

$$\xi = \mu \rho u_e x \quad (7.5)$$

$$\eta = \frac{\rho u_e}{(2\xi)^{1/2}} y \quad (7.6)$$

respectively. From a previous study, [7], the boundary-layer thickness was estimated, and the approximate value of  $\eta_w$  at each  $\xi$ -station was determined. By calculating  $\xi$  and  $\eta_w$  from (7.5) and (7.6), respectively, a flat-plate flow was calculated up to a Reynolds number of  $1 \times 10^9$ . At station 1, at  $Re_x = 5 \times 10^4$ , the flow was specified to be turbulent. The calculated value of  $R_\theta$  at  $Re_x = 1.05 \times 10^5$  was identical to the corresponding value of  $R_\theta$  in Table II of [28]. The initial spacing,  $h_1$ , was 0.001 and  $K$  was 1.01487. Even though the calculations showed that for  $Re_x > 5 \times 10^8$  the value of  $\eta_w$  should have been about 130, the maximum value of  $\eta_w$  was taken to be 100, because of the computer-capacity limit. Approximately 70 stations in the  $\xi$ -direction were used. The time per station was approximately 10 seconds. The results of the calculations are presented in Figures 12a through 12j.

Figure 12a shows a comparison of local skin-friction coefficients calculated by the present method and those calculated by the Prandtl-Schlichting formula [29],

$$c_f = (2 \log_{10} Re_x - 0.65)^{-2.3} \quad (7.7)$$

as well as experimental values and Coles' line [28]. The experimental values are taken from [28]. The agreement between Coles' line and experiment is very good. At very high Reynolds number, about  $7 \times 10^8$ , the calculated values of  $c_f$  begin to deviate slightly from Coles' line. This is believed to be due to the smaller value of  $\eta_w$ ; rather than 130, a smaller value of  $\eta_w$ , namely 100, was used, in order not to exceed the computer capacity. Figure 12b shows a comparison of calculated shape-factor values with experimental and with those given by Coles' line. In figures 12c and 12d the velocity profiles are plotted in law-of-the-wall coordinates. Figure 12c shows a comparison of calculated

results with experimental and with those given by the universal logarithmic velocity

$$\frac{u}{u^*} = 5.75 \log_{10} \frac{yu^*}{\nu} + 5.10$$

at  $Re_x = 10^6$  and  $10^7$ . Figure 12d shows a comparison of calculated results with those given by Coles' line. In figures 12e and 12f the velocity profiles are plotted in velocity-defect coordinates. Figure 12e shows a comparison of calculated results with experimental and with those given by the logarithmic velocity distribution[28]

$$\frac{u_e - u}{u^*} = 2.80 - 5.75 \log_{10} \left( 4.05 \frac{y}{\delta^*} \frac{u^*}{u_e} \right) \quad (7.9)$$

at  $Re_x = 10^6$  and  $10^7$ . Figure 12f shows a comparison of calculated results with those given by Coles' line. Figure 12g shows a comparison of calculated and experimental sublayer profiles. The experimental data are Klebanoff's data at  $Re_\delta = 77,000$  taken from [28]. The agreement of results in figures 12c, 12e, and 12g with experiment is remarkable, in that the calculated values agree with the experimental values point by point.

The argument of the logarithmic term in (7.9) is sometimes written in terms of  $y/\Delta$ , since from (6.123) and from the definition of  $u^*$

$$\Delta = \frac{u_e}{u^*} \delta^* \quad (7.10)$$

It can also be written in terms of  $y/\delta$ . Use of the latter presents the difficulty of dealing with an ill-defined outer edge of the boundary layer. On the other hand,  $\Delta/\delta = 3.6$  [30] for constant-pressure profiles. For flat-plate flows,  $\delta$  is therefore related to the defect-displacement thickness  $\Delta$  by

$$\delta = \frac{\Delta}{3.6}$$

and can be written in terms of  $c_f$  and  $\delta^*$  as

$$\delta = 0.392837 \sqrt{\frac{\delta^*}{c_f}} \quad (7.11)$$

Figures 12h and 12i show comparisons of calculated and experimental [19] shear-stress distributions and mean-velocity distributions at  $Re_\delta = 7.7 \times 10^4$ ,  $u^*/u_e = 0.037$ . The definition of  $\delta$  given by (7.11) is used for the boundary-layer thickness in plotting the calculated results. The shear-stress coefficients given by (6.114) and (6.115) reduce to

$$c_{\tau_L} = (2/\xi)^{1/2} \mu f'' \quad (7.12a)$$

$$c_{\tau_T} = (2/\xi)^{1/2} \epsilon f'' \quad (7.12b)$$

respectively. The agreement of the velocity profiles is nearly perfect. The shear-stress distribution is also very good except near the edge. This is probably due to the ill-defined definition of  $\delta$  in (6.26), which needs to be reconsidered. For example,  $\delta$  should perhaps be based on the point where  $u = 0.995$ . Figure 12j shows a comparison of calculated eddy-viscosity distributions across a boundary layer with values calculated from both Klebanoff's and Townsend's data. The calculated experimental values are taken from [31]. The results indicate that the calculated eddy-viscosity values are in close agreement in the inner region and are in poor agreement in the outer region.

These results for a flat plate demonstrate that the computing program has the capacity to handle Reynolds numbers greater than those occurring on any existing or contemplated aircraft, as well as on most ships.

### 7.1.2 Flat-plate flow with mass transfer.

The present method is readily applied to flows with surface blowing or suction. Mass transfer at the wall is handled by the boundary condition (6.59a), which reduces to

$$f_w = \begin{cases} 0 & \xi \leq \xi_0 \\ -\frac{v_w(\xi - \xi_0)}{\mu u_e (2\xi)^{1/2}} & \xi > \xi_0 \end{cases} \quad (7.13)$$

for uniform, incompressible, two-dimensional flow. In (7.13),  $\xi_0$  represents the distance from the leading edge without mass transfer.

7.1.2.1 Uniform blowing (Mickley and Davis). The experimental data used for comparison with a calculated flow with uniform blowing were obtained by Mickley and Davis [32]. Two blowing rates,  $v_w/u_e = 0.001$  and  $0.002$ , were studied. A flat-plate flow was calculated for a Reynolds number of  $3.125 \times 10^5$  per ft by using the values of  $\mu$  and  $\rho$  that were used in Section 7.1.1, with  $u_e = 50$  ft/sec. Thus, an effective length that matched the momentum thickness at the station where blowing began was determined. On the basis of this information, (now  $\xi_0$  is known),  $f_w$  was calculated.

The results are shown in figures 13a, 13b, and 13c. Figure 13a shows a comparison of calculated and experimental momentum thickness and local skin-friction coefficient for each blowing rate. The other two figures show comparisons of calculated and experimental velocity profiles. Figure 13b shows the calculated and experimental values for  $v_w/u_e = 0.001$  at  $x = 38.42$  inches and  $83.55$  inches, and figure 13c shows the calculated and experimental values for  $v_w/u_e = 0.002$  at the same stations. The agreement between the calculated results and experimental data as shown by the figures is very good.

7.1.2.2 Uniform suction (Tennekes). Experimental data obtained by Tennekes, [33] and [34], were used for comparison with a calculated flow with uniform suction. Two suction rates,  $v_w/u_e = -0.00312$  and  $-0.00429$ , were studied. A flat plate was calculated for a Reynolds number of  $8.13 \times 10^5$  per ft by using the values of  $\mu$  and  $\rho$  that were used before, with  $u_e = 130$  ft/sec. Again, as with blowing, an effective length was determined that matched the momentum thickness at the point where suction began. On the basis of this information,  $f_w$  was calculated.

Figure 14a shows the calculated values of local skin-friction coefficient and momentum thickness, together with the experimental data deduced from the momentum equation, for both suction rates. Figure 14b shows the velocity-profile comparisons for  $v_w/u_e = -0.00312$  at  $x = 1.25$  feet and  $2.55$  feet, and figure 14c shows the velocity-profile comparisons for  $v_w/u_e = -0.00429$  at  $x = 0.594$  feet and  $2.575$  feet. The agreement between calculations and experiment is very good.

### 7.1.3 Equilibrium flows in both favorable and adverse pressure gradients.

All the previous examples were constant pressure flows. The applicability of any general method depends on the accuracy of the results it gives for a wide variety of flow conditions; hence it must be tested on flows with pressure gradients. Indeed, this is a prerequisite for the important problem of predicting turbulent-boundary-layer separation. Because of the interest in equilibrium flows that are characterized by

$$E = \frac{\delta^*}{\tau_w} \frac{dp}{dx} = \text{constant}$$

calculations were made for several equilibrium flows. Note that for two-dimensional, incompressible flows with pressure gradients the  $\xi$ -coordinate is determined from (7.1), which reduces to

$$\xi = \mu \rho \int_0^x u_e dx'$$

and the  $\eta$ -coordinate is the same as (7.6). The following sections give comparisons of calculated and experimental results for such flows.

7.1.3.1 Equilibrium flow in a favorable pressure gradient (Herring and Norbury). Herring and Norbury [35] experimentally investigated two equilibrium flows characterized by  $E$ 's of  $-0.35$  and  $-0.53$ . The former flow was calculated by the present method. A free-stream velocity at the entrance to the test section of 72 ft/sec and a Reynolds number of  $4.5 \times 10^5$  were the flow conditions used. Figure 15 shows the velocity distribution (obtained by trial and error) used to match the momentum thickness at the initial point of the experimental data, namely, at  $x = 2$  feet. Note that with this effective length added, the experimental lengths are translated 4.37 feet.

Figure 16a shows a comparison of calculated and experimental momentum thickness and shape-factor parameters, together with the experimental velocity distribution, and figures 16b and 16c show comparisons of calculated and experimental velocity profiles at  $x = 2$  and 3 feet and 4 and 5 feet, respectively. The agreement with experiment is very good, and the calculated values of velocity profiles correspond to experimental values point by point.

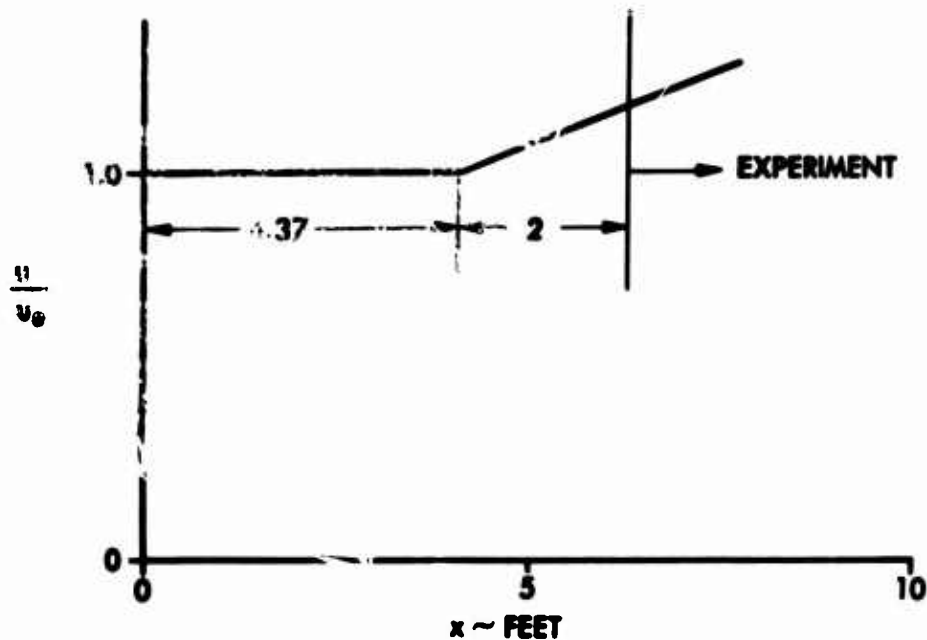


Figure 15.- Velocity distribution used to match the momentum thickness for the experimental data of Herring and Norbury.

7.1.3.2 Equilibrium flow in an adverse pressure gradient (Clauser). In reference [30], Clauser experimentally obtained two equilibrium flows corresponding to two different pressure distributions, sometimes designated as P.D.1 and P.D.2, each having a nearly constant value of  $E$ . The former flow was calculated by the present method. A free-stream velocity of 28.3 ft/sec at the beginning of the flow and a Reynolds number of  $1.8 \times 10^5$  per ft were the flow conditions used. Figure 17 shows the velocity distribution used to match the defect-shape factor,  $G$ , of the experimental data, which is reported to be 10.3. The defect-shape factor was used rather than the momentum thickness,  $\theta$ , because the momentum thickness was not reported explicitly in [30].

Figure 18a shows a comparison of calculated and experimental shape-factor and local skin-friction coefficient parameters, together with the experimental velocity distribution taken from faired velocity distributions given in [30]. Figure 18b shows a comparison of calculated and experimental velocity profiles, and figure 18c shows a comparison of calculated and experimental velocity profiles in the defect-law coordinates, both at  $x = 200$  inches and 375 inches. The agreement is remarkably good.

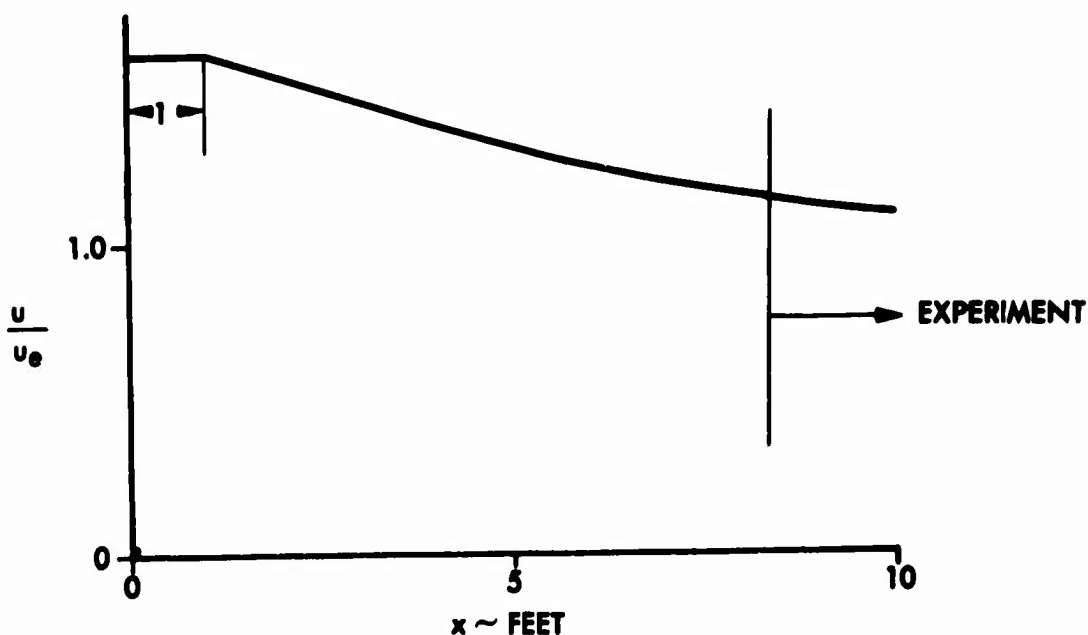


Figure 17.-Velocity distributions used to match the defect-shape factor for the experimental data of Clauser's P.D.1.

7.1.3.3 Equilibrium flow recovering to a constant pressure flow (Bradshaw and Ferriss). An important class of boundary layer flows comprises those that have been perturbed in some manner and are then allowed to recover to some equilibrium condition. As an example of this kind of flow, the boundary layer measured by Bradshaw and Ferriss[36] was considered. A portion of this flow has an external velocity distribution given by  $u_e \propto x^{-0.255}$  from  $x = 0$  to  $x = 47$  inches and is followed by a zero pressure gradient from 60 inches to  $x = 95$  inches. A reference velocity of 110 ft/sec and a Reynolds number of  $6.85 \times 10^5$  per ft were the flow conditions used. Figure 19 shows the velocity distribution used to match the boundary-layer parameters at  $x = 23$  inches. Note that when an effective length is added, the experimental lengths are translated by 2 feet.

Figure 20a shows comparisons of calculated and experimental momentum-thickness, shape-factor, and local skin-friction parameters, together with the experimental velocity distribution. Figure 20b shows a comparison of calculated and experimental velocity profiles at 47, 71 and 95 inches. Even though the agreement in momentum thickness is excellent, except for the first station ( $x = 23$  inches), the results are not as good as in the other flows. This is

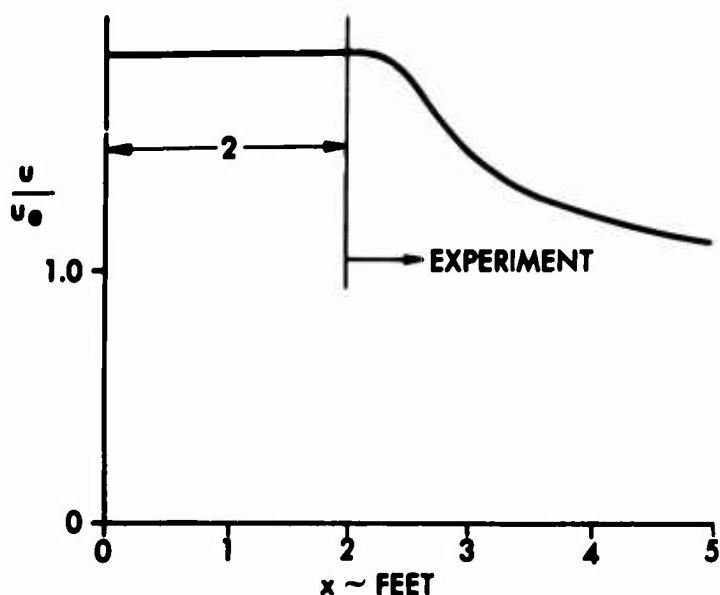


Figure 19.- Velocity distribution used to match the momentum thickness for the experimental data of Bradshaw and Ferriss.

probably due to the inaccuracy of matching the initial boundary-layer parameters at  $x = 23$  inches. Generally, several trial-and-error runs (sometimes considerably more) are necessary to match the initial boundary-layer parameters, which are usually momentum thickness and shape factor. At least one accurate matching of one of these parameters, for example, momentum thickness, is necessary before one can check the calculated results with experiment. This is especially true in an equilibrium boundary layer for which the shape factor is nearly constant and, unlike the shape factor of a nonequilibrium flow, it does not adjust itself. With the velocity distribution shown in figure 19, the calculated and experimental values are

	<u>calculated</u>	<u>experimental</u>
$\theta$ (inches)	0.216	0.200
H	1.637	1.667
$c_f$	$0.96 \times 10^{-3}$	$1.45 \times 10^{-3}$
E	10	5.4

There is also the possibility that the disagreement was caused by the calculation of  $\beta$ , which was computed by the formulas given in Section 7.0. Since  $\beta$  involves the derivatives of velocity, which are inputs to the computer program,

any slight irregularities in velocity distribution cause inaccuracies in the  $\beta$ -values. In general, whereas some small irregularities in the calculations of  $\beta$  do not appreciably alter the results, for flows that are near separation, as this one is, irregularities in  $\beta$  are highly undesirable. For this reason, it is necessary to calculate the values of  $\beta$  and then fair the results. In order to improve the results further calculations should be made.

#### 7.1.4 Nonequilibrium and separating flows.

From a practical standpoint, nonequilibrium and separating flows are perhaps the most important flows, since they are often encountered in the design of diffusers and lifting surfaces. For this reason, three separate flows with turbulent separation were considered. The following sections give comparisons of these flows with experimental flows.

##### 7.1.4.1 Favorable and adverse pressure gradients on an airfoil-like body

(Schubauer and Klebanoff). In reference [37], Schubauer and Klebanoff experimentally obtained a flow characterized by an initial favorable gradient followed by an adverse gradient and separation. The body is two-dimensional and has a sharp nose. It is at a slight angle of attack, which produces a pressure peak at the leading edge that causes transition. Separation is reported to have taken place at 25.7 feet from the leading edge. A reference velocity of 160 ft/sec (velocity at 17.5 ft from the leading edge) and a Reynolds number of  $1 \times 10^6$  per ft were the flow conditions used. A flat-plate flow was used to match the momentum thickness of the experimental data at  $x = 1$  foot.

The results are shown in figures 21a, 21b, and 21c. Figure 21a shows the experimental velocity distribution and comparison of calculated and experimental momentum-thickness, shape-factor and local skin-friction parameters. The other two figures show comparisons of calculated and experimental velocity profiles. Figure 21b shows the calculated and experimental values at  $x = 4$  feet (in favorable pressure gradient) and at  $x = 14.5$  feet (nearly constant-pressure flow). Figure 21c shows the calculated and experimental values at  $x = 20$  and 22 feet (both in adverse-pressure-gradient flow and conditions close to separation). The calculated parameters, with the exception of skin-

friction\*, are in excellent agreement with the experimental data except near separation. The present method predicts separation at  $x = 25$  feet. (Flow is said to be separated at the last station before the one at which  $f_w''$  becomes negative; when  $f_w''$  becomes negative, the calculations are stopped.)

7.1.4.2 Adverse pressure gradient on a body of revolution (Moses). Another example of a nonequilibrium boundary layer with adverse pressure gradient is a flow studied by Moses [38], which was used as a basis of comparison. The pressure distribution designated P.D.2 was considered. The results reported are for the cylindrical section only. Because the body studied is a cylinder of constant diameter, it is not a test of the method for axisymmetric flow, since with the first theory and with the present transformations, the flow is two-dimensional. The experimental separation point was at about 28.8 inches.

A free-stream velocity of 35.3 ft/sec at the beginning of the flow and a Reynolds number of  $2.2 \times 10^5$  per ft were the flow conditions used. Figure 22 shows the velocity distribution (obtained by trial and error) used to match the momentum thickness at the initial point of the experimental data, namely,  $x = 0$ .

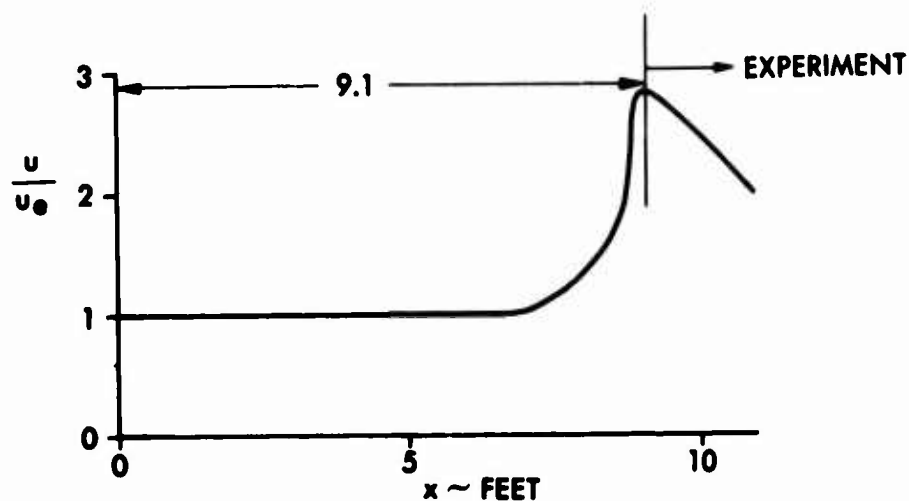


Figure 22.- Velocity distribution used to match the momentum thickness for the experimental data of Moses' P.D.2.

\* Personal communication with Klebanoff indicated the experimental values of these quantities to be in error.

Note that when an effective length is added, the experimental lengths are translated by 9.1 feet.

Figure 23a shows comparisons of calculated and experimental momentum-thickness, shape-factor, and local skin-friction parameters, together with the experimental velocity distribution. Also shown in this figure are the two separation points determined by the present method. The calculated results are based on two values of  $\gamma$  in the convergence criterion for  $f''_w$ , namely,

$$|f''_{Q+1} - f''_Q| < \gamma$$

The results indicated by the solid line in figure 23a are those that are obtained by specifying  $\gamma$  to be 0.01, and the results indicated by the dotted line are those that are obtained by specifying  $\gamma$  to be 0.001. Except near the separation point, the calculated results are identical and are in excellent agreement with the experimental values. According to the present method, separation based on  $\gamma = 0.001$  is indicated at  $x = 27.5$  inches, and separation based on  $\gamma = 0.01$  is indicated at  $x = 29$  inches. Figure 23b shows a comparison of calculated ( $\gamma = 0.001$ ) and experimental velocity profiles at 11, 20, 26, and 29 inches. Again, except near separation, the calculated results are in excellent agreement with experiment. Figure 23c shows a comparison of calculated ( $\gamma = 0.001$ ) and experimental turbulent shear-stress distributions at 11, 20, and 24 inches. The agreement is fair.

#### 7.1.4.3 Adverse pressure gradient on an airfoil (Von Doenhoff and Tetervin).

A further example of a nonequilibrium boundary layer with adverse pressure gradient is the NACA 65(216)-222 airfoil tested by von Doenhoff and Tetervin [39]. The pressure distribution at an angle of attack of  $10.1^\circ$  and a chord Reynolds number of  $2.64 \times 10^6$  was considered. The experimental separation point was at about 55-percent chord. A free-stream velocity of 211 ft/sec at the beginning of the flow and a Reynolds number of  $1.315 \times 10^6$  per ft were the flow conditions used. A flat-plate flow was used to match the momentum thickness of the experimental data at 7.5-percent chord, rather than the leading edge as the origin. This was necessary, since the boundary layer was tripped at 7.5-percent chord.

The results are shown in figures 24a, 24b, 24c, and 24d. Figure 24a shows the experimental velocity distribution and comparisons of calculated and experimental momentum-thickness, shape-factor, and local skin-friction parameters. The other three figures show comparisons of calculated and experimental velocity profiles up to the separation point, namely, at 55-percent chord. In figure 24a, the calculated momentum thickness values are in good agreement with the experimental values. However, the agreement is poor for the shape-factor values. This is somewhat surprising, because the calculated velocity profiles are in good agreement with experiment (for example, at 25-percent chord). Since the shape factor is the ratio of displacement thickness to momentum thickness, a better correlation in H-values would normally be expected. The calculated velocity profiles begin to deviate considerably from the experimental values near separation. Figure 24d shows the calculated velocity profiles at 50- and 54-percent chord with the separation profile at 55-percent chord. The present method predicts separation at 54.5-percent chord, which is in excellent agreement with the experimental separation point.

## 7.2 Compressible Flows

The test cases for which comparisons are calculated by the present method consist of flat-plate flows with and without heat transfer. Only a few test cases were calculated, mostly because of the difficulties experienced in obtaining convergence of the numerical solution of the momentum equation. As a result, most of the time was devoted to attempts to stop the oscillations and obtain convergence. In fact, at present the numerical method for compressible flow still needs to be refined. The calculations for compressible flow use 5-point averages of the coefficients defined by (6.78) in the  $\eta$ -direction. This scheme was initially used to stop the oscillations, and because of the limited time the computer program was not refined. That is, the averaging process in the  $\eta$ -direction was not confined only to the eddy-viscosity terms, as it was in the incompressible flows.

### 7.2.1 Flat-plate flow with adiabatic wall.

Three separate sets of experimental data were used to test the present method for a flat-plate flow with adiabatic wall conditions. The first set of experimental data are those of Spivack [40] at  $M_e = 2.8$ . The measurements

were made on the flat wall of a two-dimensional nozzle. The flow was calculated for a Reynolds number of  $2 \times 10^7$  per ft, by assuming the following values of the flow parameters:

$$\begin{aligned}\mu_e &= 0.376 \times 10^{-6} \text{ lb}_f\text{-sec/ft}^2 \\ \rho_e &= 0.234 \times 10^{-2} \text{ lb}_f\text{-sec}^2/\text{ft}^4 \\ u_e &= 3170 \text{ ft/sec} \\ T_e &= 530 \text{ deg R} \\ H_e &= 8.2 \times 10^6 \text{ ft}^2/\text{sec}^2\end{aligned}$$

The value of  $u_e$  was calculated from the definition of  $M_e$ ,

$$u_e = 49.1 M_e \sqrt{T_e}$$

and the total enthalpy,  $H_e$ , was calculated from

$$H_e = h_e + \frac{1}{2} u_e^2$$

For this case, the transformed  $x$ - and  $y$ -coordinates are given by the relations (7.1) and (7.2), respectively.

Figures 25a and 25b show the calculated local skin-friction parameters and experimental values that were obtained from the momentum equation, namely,

$$\frac{d\theta}{dx} = \frac{c_f}{2}$$

The parameters are plotted against Reynolds number based on length,  $Re_x$ , in figure 25a and on Reynolds number based on momentum thickness,  $Re_\theta$ , in figure 25b. The agreement is very good in both cases.

The second set of experimental data are those of Chapman and Kester [41] at  $M_e = 0.81, 2.5, \text{ and } 3.6$ . The experimental setup consisted of a cylindrical model with air flowing axially at the outer surface of the model. The experimental skin-friction values were obtained by a direct measurement of total

force on the cylinder. The flow was calculated by assuming the following values of the flow parameters:

$$\begin{aligned}\mu_e &= 0.376 \times 10^{-6} \text{ lb}_f\text{-sec/ft}^2 \\ \rho_e &= 0.234 \times 10^{-2} \text{ lb}_f\text{-sec}^2/\text{ft}^4 \\ T_e &= 530 \text{ deg R}\end{aligned}$$

The values of  $u_e$  and  $H_e$  for each Mach number were calculated in the same way as in the preceding case.

Figure 26 shows a comparison of calculated and experimental average skin-friction coefficients at the three Mach numbers. The agreement is excellent for  $M_e = 0.81$ , but only fair at  $M_e = 2.5$  and  $3.6$ .

The third set of experimental data are those of Matting et al [42] at  $M_e = 0.20, 2.95, \text{ and } 4.2$ . The measurements were made on the flat wall of a two-dimensional nozzle. The calculations used the values of the flow parameters tabulated below.

$M_e$	$\mu_e \times 10^6$ $\frac{\text{lb}_f\text{-sec}}{\text{ft}^2}$	$\rho_e \times 10^2$ $\frac{\text{lb}_f\text{-sec}^2}{\text{ft}^4}$	$T_e$ deg R
0.20	0.376	0.234	530
2.95	0.179	0.55	219
4.2	0.110	0.93	132

The values of  $u_e$  and  $H_e$  for each Mach number were calculated in the same way as in the preceding cases.

Figure 27 shows comparisons of calculated and experimental local skin-friction coefficients at the three Mach numbers. The agreement for  $M_e = 0.20$  is excellent, but for the other two Mach numbers is only fair. Comparisons of calculated and experimental boundary-layer Mach number profiles and velocity profiles for  $M_e = 2.95$  and  $Re_x = 31 \times 10^6$  are shown in figure 28a and for

$M_e = 4.2$  and  $Re_x = 69 \times 10^6$  in Figure 28b. The agreement in velocity profiles is better than the agreement in Mach number profiles. However, in both cases the agreement is only fair.

### 7.2.2 Flat-plate flow with heat transfer.

Only one set of experimental data, those of Pappas [43], was used for a flat-plate flow with heat transfer. The test Mach number used in the comparison is 1.69. The experimental skin-friction values were obtained from the momentum equation. Two different ratios of wall temperature to edge temperature, namely  $T_w/T_e$  or  $g_w$ , were considered. The calculations used the following values of the flow parameters:

$$\begin{aligned}\mu_e &= 0.376 \times 10^{-6} \text{ lb}_f\text{-sec/ft}^2 \\ \rho_e &= 0.234 \times 10^{-2} \text{ lb}_f\text{-sec}^2/\text{ft}^4 \\ T_e &= 530 \text{ deg R}\end{aligned}$$

The values of  $u_e$  and  $H_e$  were calculated in the same way as in Section 7.2.1.

Figure 29 shows comparisons of calculated and experimental average skin-friction coefficients for  $g_w = 1.70$  and 1.61. Figure 30 shows comparisons of calculated and experimental local Stanton numbers for the same  $g_w$ -values. The agreement in both cases is fair. Figure 31 shows a comparison of skin-friction variation with Mach number. The ratios of local compressible skin-friction values to incompressible values, namely  $c_f/c_{f_1}$ , were calculated at several Mach numbers and compared to some experimental results. The agreement seems to be satisfactory.

## 8.0 CONCLUDING STATEMENTS

A numerical solution of the turbulent-boundary layer equations based on an eddy-viscosity concept and an eddy-conductivity concept are presented. The numerical method used to solve the boundary layer equations differs from the one used in a previous study [7] under contract NOW 64-0352c. In reference [7], the validity of using an eddy-viscosity concept in solving the equations of the incompressible turbulent boundary layer was explored. The momentum equation was solved in its nonlinear form by the old shooting method of previous studies of laminar flows [8 through 13]. The shooting method had proved itself in accuracy and reliability for laminar flows, and it was therefore preferred to other numerical methods, which are usually based on linearized solutions. The previous study [7] indicated that the eddy-viscosity concept, when used with an accurate technique for solving the boundary-layer equations, was capable of predicting results that were in good agreement with experiment and many of the characteristic features of the turbulent boundary layer. The main objections to that method were long computing times and restrictions on the step sizes in the streamwise direction. In the former case, for example, a typical test case consisting of about 25 stations in the x-direction took approximately one hour on the IBM 709<sup>4</sup> computer. That amounted to about 2 minutes per station. The numerical method used in that study also had the disadvantage that very short steps in the streamwise direction - which are essential near separation - could not be taken.

For these reasons, when the efforts were extended to the solution of the equations of the compressible turbulent boundary layer, it was necessary to use a different numerical method. Almost the same eddy-viscosity formulation as in [7] was used, except for small modifications to account for the compressibility effects. The results indicate that the present method is very fast. A typical computation time for incompressible flows on the IBM 709<sup>4</sup> computer is approximately 10 seconds per station, which means that the present method is at least 10 times as fast as the old method. A typical computation time for compressible flows, on the other hand, is about 15 seconds per station. In addition to having very short computing times, the present method has no restrictions on the step sizes in the streamwise direction; that is, step sizes can

be as small as necessary.

Various incompressible and compressible turbulent flows are calculated by the present method, and comparisons with experiments are made. The results for incompressible flows are, in general, very good, and so far the results for compressible flow are encouraging. More test cases need to be run for both flows, especially for compressible turbulent flows. The results presented do not represent a finished development, but are only what has been obtained by one particular formulation of eddy viscosity and turbulent Prandtl number.

## 9.0 TECHNOLOGICAL FORECAST\*

### 9.1 Problem

A method of calculating velocity and temperature profiles, skin friction, displacement thickness, momentum thickness, heat transfer, and the separation point of the turbulent boundary layers is presented. Accurate calculation of these quantities can be extremely beneficial to the design of ships, turbo-machinery, heat exchangers, lifting surfaces, and all types of aerospace vehicles.

### 9.2 State of the Art, Solution, and Forecast

[See Section 5.0 of this report].

### 9.3 Suggestions and Implications

The present method uses eddy-viscosity and eddy-conductivity concepts in obtaining a numerical solution of the turbulent-boundary-layer equations. The method of solution has the advantage of being applicable to both laminar and turbulent flows. Since most flows have a laminar portion in the vicinity of a stagnation point or leading edge (for example, on an airfoil at high Reynolds numbers), such an advantage is particularly useful. The present method utilizes the upstream history as the calculations proceed downstream. At any station, a laminar profile can be obtained by merely setting the eddy-viscosity term in (6.51) equal to zero.

The present method also has the advantage that various formulations of eddy viscosity or turbulent Prandtl number can be used with very little change in the basic method. Since the results presented in this report are obtained by one particular formulation of eddy viscosity and turbulent Prandtl number, such an advantage may be very useful in improving the results for both incompressible - where the results are very good except near separation - and com-

---

\* This section of the report is included in response to the requirements of the contract.

pressible flows. For example, in the outer region, the present method uses an eddy-viscosity relation modified by an intermittency factor  $\gamma$  to describe the turbulent shear transport. This relation, suggested by Clauser [5] for equilibrium boundary layers, is given by (6.27)

$$\epsilon_0 = \rho k_2 u_e \delta^* \gamma$$

where  $k_2$  is a constant of proportionality. For equilibrium boundary layers this constant is 0.018 [5]. In both incompressible and compressible studies here, however, this constant was taken to be 0.0168, the value given in [18]. In this way, (6.27) was also extended to nonequilibrium boundary layers. In order to improve the results near separation, it is quite possible that the velocity and length scales, namely  $u_e$  and  $\delta^*$ , in (6.27) may need to be changed. According to a recent study [44], it appears that when different length and velocity scales are used in normalizing the eddy-viscosity formula for the outer region, somewhat less variation in eddy viscosity from station to station is obtained than when (6.27) is used. The results of these calculations for the experimental data in [44] are summarized in Table III, which presents the maximum and minimum values for four different normalizations of eddy viscosity. The first is used in this report and evidently is the worst of the lot.

TABLE III. EDDY VISCOSITY VARIATIONS

	$\frac{\epsilon}{u_e \delta^*}$	$\frac{\epsilon}{u^* \delta^*}$	$\frac{\epsilon}{u_e \theta}$	$\frac{\epsilon}{u^* \theta}$
Maximum value	0.028	0.79	0.039	1.4
Minimum value	0.0048	0.26	0.014	0.57
Max/Min	5.83	3.04	2.78	2.75

Another modification of the outer eddy-viscosity relation, which may improve the results, is the use of a mixing length concept, as in the inner region. Escudier and Spalding [45] have recently studied the distribution of mixing length in the turbulent boundary layers. The results indicate that for the outer region of the boundary layer the mixing length is constant and is equal to  $0.075 \delta$ .

The results for compressible flows indicate that it is also necessary to make improvements in the formulation of the turbulent Prandtl number. Even though the velocity profiles agree quite well with experiment, the temperature profiles show considerable deviation from experimental values for compressible flows, especially close to the wall. These results suggest that it is necessary to use a separate expression for turbulent Prandtl number in each region and that the initial assumption of a constant turbulent Prandtl number is not very satisfactory, since the variation of turbulent Prandtl number, especially close to the wall, is considerable. Figure 32 shows turbulent Prandtl numbers of boundary layers on a cooled plate [46]. This figure supports the necessity of expressing turbulent Prandtl number separately in each region.

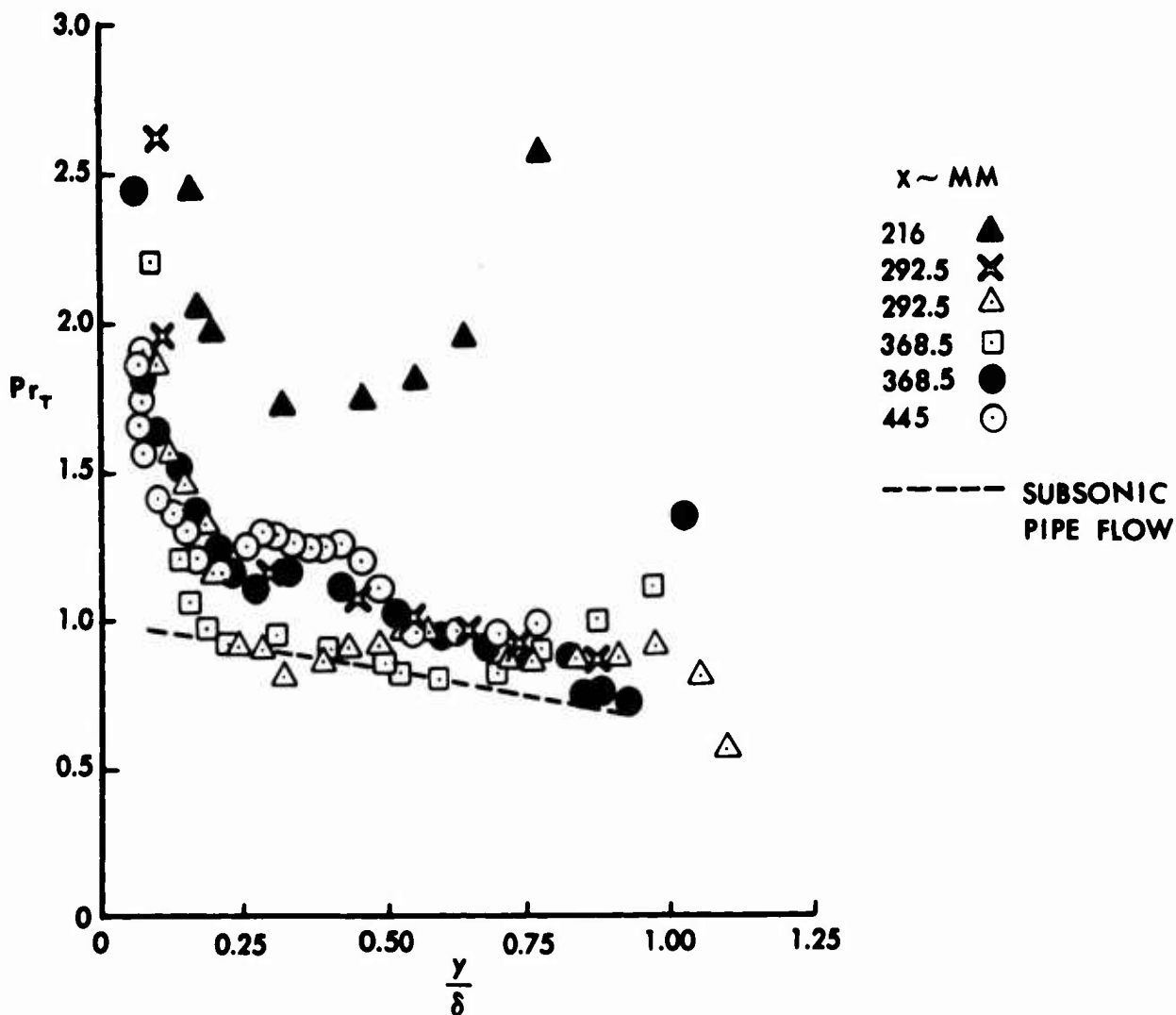


Figure 32.- Turbulent Prandtl numbers of boundary layers on a cooled flat plate,  $Ma_\infty \approx 5.1$ ,  $(T_e - T_w) / T_e \approx 0.35$ .

In summary, it can be said that because the results have been so encouraging, the work should be continued along these lines.

#### 10.0 ACKNOWLEDGMENTS

The authors express their gratitude to Miss Lie Ching Wang for her excellent programming of the boundary-layer equations and for her many helpful suggestions in obtaining the solution of these equations. The importance of her efforts cannot be overemphasized.

The authors also express their gratitude to Miss Sue Faulkner and Mr. David Callin for checking many of the numerical results and preparing the figures in this report.

11.0 REFERENCES

1. Head, M. R.: -Entrainment in the Turbulent Boundary Layer. R. and M. 3152, British A. R. C., 1960.
2. Truckenbrodt, E.: -A Method of Quadratures for the Calculation of the Laminar and Turbulent Boundary Layer in Case of Plane and Rotationally Symmetrical Flow. NACA TM 1379, 1955.
3. Thompson, B. G. J.: -A Critical Review of Existing Methods of Calculating the Turbulent Boundary Layer. F.M. 3492, British A.R.C. 26109, 1964.
4. Prandtl, L.: -Recent Results of Turbulence Research NACA TM 720, 1933.
5. Clauser, F. H.: -The Turbulent Boundary Layer. Advances in Applied Mechanics, Vol. IV, Academic Press Inc., 1956.
6. Mellor, G. L.: -Turbulent Boundary Layers with Arbitrary Pressure Gradients and Divergent or Convergent Cross Flows. Report No. 775, Princeton University, March 1966.
7. Smith, A.M.O., Jaffe, N.A., and Lind, R.C.: -Study of a General Method of Solution of the Incompressible Turbulent Boundary Layer Equations. Douglas Aircraft Company Report No. LB 52949, November 1965.
8. Smith, A.M.O., and Clutter, D.W.: -Solution of the Incompressible Laminar Boundary Layer Equations. AIAA Journal, Vol. 1, No. 9, September 1963, pp. 2002-2071.
9. Smith, A.M.O., and Clutter, D.W.: -Machine Calculation of Compressible Boundary Layers. AIAA Journal, Vol. 3, No.4, April 1965, pp.639-647.
10. Smith, A.M.O., and Clutter, D.W.: -Solution of the Incompressible Laminar Boundary Layer Equations. Douglas Aircraft Company Report No. ES 40446, July 1961.
11. Clutter, D.W., and Smith, A.M.O.: -Solution of the General Boundary Layer Equations for Compressible Laminar Flow, Including Transverse Curvature. Douglas Aircraft Company Report No. LB 31088, February 1963, revised October 1964.
12. Clutter, D.W., Smith, A.M.O., and Jaffe, N.A.: -General Method for Solving the Nonequilibrium Laminar Boundary Layer Equations of a Binary Gas. Douglas Aircraft Company Report No. LB 31616, October 1964.

13. Smith, A.M.O. and Jaffe, N.A.: -General Method for Solving the Nonequilibrium Boundary Layer Equations of a Dissociating Gas. AIAA Journal, Vol. 4, No.4, April 1966.
14. Van Driest, E.R.: -On Turbulent Flow Near a Wall., J.A.S., Vol. 23, No. 11, November 1956, p.1007.
15. Townsend, A.A.: -The Structure of Turbulent Shear Flow. Cambridge University Press, 1956, p.220.
16. Reichardt, H.: -Die Waermeuebertragung in turbulenten Reibungsschichten. ZAMM 20, 1940, p.297.
17. Deissler, R.G.: -Analysis of Turbulent Heat Transfer, Mass Transfer and Friction in Smooth Tubes at High Prandtl and Schmidt Numbers. NACA Report 1210, 1955.
18. Matsui, T.: -Mean Velocity Distribution In The Outer Layer of A Turbulent Boundary Layer. Research Report 42, Aerophysics Department, Mississippi State, Conducted Under Contract Nonr.978(03), January 1963.
19. Klebanoff, P.S.: -Characteristics of Turbulence in a Boundary Layer with Zero Pressure Gradient. NACA TN 3178, July 1954.
20. Reichardt, H.: -The Principles of Turbulent Heat Transfer, Recent Advances in Heat and Mass Transfer. McGraw Hill, Company, 1961.
21. Probst, R.F., and Elliott, D.: -The Transverse Curvature Effect in Compressible Axially Symmetric Laminar Boundary Layer Flow. J. Aeron. Sci., March 1956.
22. Hayes, W.D., and Probst, R.F.: -Hypersonic Flow Theory. Academic Press, New York and London, 1959, p.290.
23. Jaffe, N.A., Lind, R.C., and Smith, A.M.O.: -Solution of the Binary Diffusion Laminar Boundary Layer Equations, Including the Effect of Second-Order Transverse Curvature, Douglas Aircraft Company Report No. LB 32613, January 1966.
24. Hartree, D.R., and Womersley, J.R.: -A Method For the Numerical or Mechanical Solution of Certain Types of Partial Differential Equations. Proc. Royal Soc. Series A, Vol. 161, No.906, August 1937, p.353.
25. Hartree, D.R.: -Numerical Analysis, Oxford, Clarendon Press, 1952.
26. Sylvester, R.J., and Meyer, F.: -Two-Point Boundary Problems by Quasi-linearization. SIAM Journal, Vol. 13, No.2, June 1965, pp.586-602.

27. Lind, R.C., and Keltner, G.L.: -Formulas for Numerical Interpolation, Differentiation, and Integration with a Variable-Grid System. Douglas Aircraft Company Report No. DAC 33741, May 1967.
28. Coles, D.: -Measurements in the Boundary Layer on a Smooth Flat Plate in Supersonic Flow. I. The Problem of the Turbulent Boundary Layer. Jet Propulsion Laboratory Report No. 20-69, June 1953.
29. Schlichting, H.: -Boundary Layer Theory, McGraw-Hill Company, 1960.
30. Clauser, F.H.: -Turbulent Boundary Layers In Adverse Pressure Gradient. J. Aerospace Sci., Vol. 21, 1954, pp.91-108.
31. Hinze, J.O.: -Turbulence. McGraw-Hill Company, 1959.
32. Mickley, H.S., and Davis, R.S.: -Momentum Transfer for Flow Over a Flat Plate with Blowing. NACA TN 4017, November 1957.
33. Tennekes, H.: -Similarity Laws for Turbulent Boundary Layers with Suction or Injection. Report VTH-119 Technological University Delft, December 1964.
34. Tennekes, H.: -Personal communication from author - Tables of experimental measurements used in "Similarity Laws for Turbulent Boundary Layers with Suction or Injection." (Ref.33), July 1965.
35. Herring, H.J., and Norbury, J.F.: -Some Experiments on Equilibrium Turbulent Boundary Layers in Favorable Pressure Gradients. Mech. Eng'g. Report, FLD. No. 15, Princeton University, November 1963.
36. Bradshaw, P., and Ferriss, D.H.: -The Response of a Retarded Equilibrium Turbulent Boundary Layer to the Sudden Removal of Pressure Gradient. FM 3577, British A.R.C.26758, March 1965.
37. Schubauer, G.B., and Klebanoff, P.S.: -Investigation of Separation of the Turbulent Boundary Layer. NACA TN 2133, August 1950.
38. Moses, H.L.: -The Behavior of Turbulent Boundary Layers in Adverse Pressure Gradients. Gas Turbine Laboratory Report No. 73, M.I.T., January 1964.
39. Von Doenhoff, A.E., and Tetervin, N.: -Determination of General Relations for the Behavior of Turbulent Boundary Layers. NACA Report 772, 1943.
40. Spivack, H.M.: -Experiments in the Turbulent Boundary Layer of a Supersonic Flow, North American Aviation Rep. AL-1052, January 1950.
41. Chapman, D.R., and Kester, R.H.: -Turbulent Boundary-Layer and Skin-Friction Measurements in Axial Flow along Cylinders at Mach Numbers Between 0.5 and 3.6. NACA TN 3097, March 1954.

42. Matting, F.W., Chapman, D.R., Nyholm, J.R., Thomas, A.G.:-Turbulent Skin-Friction at High Mach Numbers and Reynolds Numbers in Air and Helium. NASA TR R-82, 1961.
43. Pappas, C.C.: -Measurement of Heat Transfer in the Turbulent Boundary Layer on a Flat Plate in Supersonic Flow and Comparison with Skin-Friction Results. NACA TN 3222, 1954.
44. Goldberg, P.: -Upstream History and Apparent Stress in Turbulent Boundary Layers. MIT Report, May 1966.
45. Escudier, M.P. and Spalding, D.B.: -A Note on the Turbulent Uniform-Hydrodynamic Boundary Layer on a Smooth Impermeable wall; Comparison of Theory with Experiment. M.E.Dept., Imperial College, London, 1965.
46. Rotta, J.C.: -Recent Developments in Calculation Methods for Turbulent Boundary Layers with Pressure Gradients and Heat Transfer. J. of Applied Mechanics, Paper No. 66 - APM-F.

APPENDIX A

BEHAVIOR OF THE EDDY VISCOSITY VERY CLOSE TO THE WALL

The inner region of a turbulent boundary layer contains a layer, commonly called the sublayer, adjacent to the wall, where the flow is primarily viscous, since all velocities, including turbulence fluctuations, become zero at the wall. This region is not uniform either with respect to time or with respect to distance along the wall. In the region  $y > \delta_\ell$ , where  $\delta_\ell$  is the sublayer thickness, the effect of viscosity in the flow decreases gradually with increasing distance from the wall until it finally becomes negligibly small. Beyond this point the flow is completely turbulent. The intermediate region, where the flow is neither completely viscous nor completely turbulent, is called the transition region [31].

In describing the behavior of the eddy viscosity very close to the wall, one can use the above model and can show that  $\epsilon$  should vary as  $y^4$  as  $y \rightarrow 0$  provided disturbances in the boundary layer are two-dimensional and periodic. Since

$$-\overline{u'v'} = \frac{\epsilon}{\rho} \frac{\partial u}{\partial y} \quad (A1)$$

and if  $\partial u/\partial y$  is assumed to be constant in the viscous sublayer (this corresponds to a linear velocity distribution), it is only necessary to show that  $-\overline{u'v'}$ , which is proportional to  $\epsilon$ , should vary as  $y^4$  as  $y \rightarrow 0$ .

Consider a two-dimensional incompressible mean flow and a likewise two-dimensional disturbance. Assume that the mean velocity  $U$  depends only on  $y$ , that is,  $U = U(y)$ , as in parallel flows.\* It is also necessary to assume that the pressure in the main flow depends on  $x$  as well as on  $y$ , because the pressure gradient  $\partial P/\partial x$  maintains the flow. It can be shown that under these

---

\* The flow in the boundary layer can also be regarded as a good approximation of parallel flow, because the dependence of the velocity  $U$  in the main flow on the  $x$ -coordinate is very much smaller than the dependence on  $y$  [29].

conditions the Navier-Stokes equations and the continuity equation can be written as [29]

$$\frac{\partial u'}{\partial t} + U \frac{\partial u'}{\partial x} + v' \frac{dU}{dy} + \frac{1}{\rho} \frac{\partial p'}{\partial x} = \nu \nabla^2 u' \quad (A2)$$

$$\frac{\partial v'}{\partial t} + U \frac{\partial v'}{\partial x} + \frac{1}{\rho} \frac{\partial p'}{\partial y} = \nu \nabla^2 v' \quad (A3)$$

$$\frac{\partial u'}{\partial x} + \frac{\partial v'}{\partial y} = 0 \quad (A4)$$

where the primes denote the fluctuations. By differentiating (A2) with respect to  $y$  and (A3) with respect to  $x$  and subtracting the two equations, the fluctuating pressure term,  $p'$ , can be eliminated. The resulting expression can be written as

$$\frac{\partial \omega_z}{\partial t} + U \frac{\partial \omega_z}{\partial x} - \nu \frac{d^2 U}{dy^2} = \nu \nabla^2 \omega_z \quad (A5)$$

where  $\omega_z$  is the vorticity component perpendicular to the plane of motion. It is defined by

$$\omega_z = \frac{\partial v'}{\partial x} - \frac{\partial u'}{\partial y} \quad (A6)$$

Next introduce a stream function representing a disturbance of the form

$$\psi(x, y, t) = \phi(y) e^{i\alpha(x - ct)} \quad (A7)$$

where  $\phi$  is the amplitude,  $\alpha$  is a real quantity defined by  $\frac{2\pi}{\lambda} L$ ,  $\lambda$  is the wavelength,  $L$  is a characteristic length, and  $c$  is a complex number defined by a propagation velocity  $c_r$  and an amplification factor  $c_i$ , that is,

$$c = c_r + i c_i$$

Now, very close to the wall ( $y \rightarrow 0$ ), where  $U$  and  $v'$  are very small, eq.(A5) may be written as:

$$\frac{\partial \omega_z}{\partial t} \approx \nu \nabla^2 \omega_z \approx \nu \frac{\partial^2 \omega_z}{\partial y^2} \quad (A8)$$

Since

$$u' = \frac{\partial \psi}{\partial y} = \varphi'(y) e^{i\alpha(x-ct)} \quad (A9)$$

$$v' = -\frac{\partial \psi}{\partial x} = -i\alpha \varphi(y) e^{i\alpha(x-ct)} \quad (A10)$$

the vorticity component  $\omega_z$  can be written as

$$\omega_z = -(\varphi'' - \alpha^2 \varphi) e^{i\alpha(x-ct)} = -T(y) e^{i\alpha(x-ct)} \quad (A11)$$

by using (A6). Substituting the expression for  $\omega_z$  in (A11) into (A8) and simplifying gives

$$\frac{d^2 T}{dy^2} + \frac{i\alpha c_r}{v} T = 0 \quad (A12)$$

The solution of (A12) is

$$T = c_1 e^{i \sqrt{i\alpha c_r/v} y} + c_2 e^{-i \sqrt{i\alpha c_r/v} y}$$

which reduces to

$$T = c_1 e^{i \sqrt{i\alpha c_r/v} y} \quad (A13)$$

if  $T$  is assumed to be finite when  $y \rightarrow \infty$ . Equation (A13) can be expanded in the form

$$T = c_1 \left[ 1 - (1-i) \sqrt{\frac{\alpha c_r}{2v}} y - i \frac{\alpha c_r}{2v} y^2 + \dots \right] \quad (A14)$$

Substituting the expression (A14) into (A11) and neglecting the terms higher than  $y^2$  in (A14) gives

$$\varphi'' - \alpha^2 \varphi \approx c_1 \left[ 1 - (1-i) \sqrt{\frac{\alpha c_r}{2v}} y - i \frac{\alpha c_r}{2v} y^2 \right] \quad (A15)$$

The solution of (A15) is, using the method of variation of parameters,

$$\varphi = A e^{\alpha y} + B e^{-\alpha y} - \frac{c_1}{\alpha^2} \left[ 1 - (1-i) \sqrt{\frac{\alpha c_r}{2v}} y - i \frac{\alpha c_r}{2v} \left( y^2 + \frac{2}{\alpha^2} \right) \right] \quad (A16)$$

The constants A and B can be evaluated from the boundary conditions, namely,  $v' = u' = 0$  at the wall. Therefore it follows from (A9) and (A10) that  $\phi'(y)$  and  $\phi(y)$  are equal to zero at the wall. If the constants A and B are evaluated in this way, (A16) now becomes

$$\phi = \frac{c_1}{2} \left[ y^2 - \frac{1}{3} (1 - i) \sqrt{\frac{\alpha c_r}{2\nu}} y^3 + \frac{1}{12} (\alpha^2 - 2i \frac{\alpha c_r}{2\nu}) y^4 \right] \quad (A17)$$

The fluctuating velocities  $u'$  and  $v'$  can now be obtained by using (A9) and (A10) and by considering the real part of the resulting expressions, that is,

$$u' = \text{Re} (\partial\psi/\partial y), \quad v' = -\text{Re} (\partial\psi/\partial x)$$

Then

$$u' = c_1 \left[ \left( y - \frac{1}{2} \sqrt{\frac{\alpha c_r}{2\nu}} y^2 \right) \cos \alpha(x - c_r t) - \frac{1}{2} \sqrt{\frac{\alpha c_r}{2\nu}} y^2 \sin \alpha(x - c_r t) \right] \quad (A18)$$

$$v' = c_1 \left[ \frac{\alpha}{6} \sqrt{\frac{\alpha c_r}{2\nu}} y^3 \cos \alpha(x - c_r t) + \left( \frac{\alpha}{2} y^2 - \frac{\alpha}{6} \sqrt{\frac{\alpha c_r}{2\nu}} y^3 \right) \sin \alpha(x - c_r t) \right] \quad (A19)$$

Therefore, by using (A18) and (A19) it can be shown that

$$-\overline{u'v'} = -\frac{\alpha c_r}{2\pi} \int_0^{2\pi} \overline{u'v'} dt = \frac{1}{24} c_1^2 \sqrt{\frac{\alpha c_r}{2\nu}} y^4$$

and that  $c_1$  should vary as  $y^n$  as  $y \rightarrow 0$ , where  $n \geq 4$ .

APPENDIX B

MODIFICATION OF THE INNER EDDY-VISCOSITY EQUATION FOR COMPRESSIBLE FLOW

The expression for the inner eddy viscosity given by (6.23) can also be used for compressible flows if  $\rho$  is taken to be a variable and if the exponential term is modified to account for the heat transfer in the sublayer. A logical generalization is to consider a Stokes-type flow with the following conditions:

1. Sinusoidally oscillating infinite wall.
2. Variable  $\mu$ ,  $T$ ,  $\rho$ .
3. Oscillations small enough so that any compressibility effects they cause can be neglected.

Because of the last condition, the energy equation does not enter into the problem. For a nonsteady parallel flow, the Navier-Stokes equation reduces to (see eq.(5.17) of [29])

$$\rho \frac{\partial u}{\partial t} = \frac{\partial}{\partial y} \left( \mu \frac{\partial u}{\partial y} \right) \quad (B1)$$

Introducing the transformation

$$dy = \mu dz \quad (B2)$$

into (B1) yields

$$\rho \mu \frac{\partial u}{\partial t} = \frac{\partial^2 u}{\partial z^2} \quad (B3)$$

To solve (B3), let

$$u = f(z) e^{i(\sigma t + \epsilon)} \quad (B4)$$

Then

$$\frac{\partial u}{\partial t} = i \sigma f e^{i(\sigma t + \epsilon)} \quad (B5)$$

$$\frac{\partial^2 u}{\partial z^2} = e^{i(\sigma t + \epsilon)} \frac{\partial^2 f}{\partial z^2} \quad (B6)$$

Substituting the expressions given by (B5) and (B6) into (B3) and rearranging

gives

$$\frac{d^2 f}{dz^2} - \rho \mu i \sigma f = 0 \quad (\text{B7})$$

Assume that  $\rho \mu$  is averaged over a certain distance, and write the average as  $\overline{\rho \mu}$ . Then the solution of (B7) can be written

$$f = A \exp (1 + i) \sqrt{\frac{\overline{\rho \mu} \sigma}{2}} z + B \exp -(1 + i) \sqrt{\frac{\overline{\rho \mu} \sigma}{2}} z \quad (\text{B8})$$

since  $\sqrt{i} = \frac{1 + i}{\sqrt{2}}$ .

Assume that  $f$  remains finite as  $z \rightarrow \infty$  so that  $A = 0$ . Then substituting the resulting expression in (B8) into (B4) yields

$$u = B \exp \left\{ -\sqrt{\frac{\overline{\rho \mu} \sigma}{2}} z + i(\sigma t + \epsilon - \sqrt{\frac{\overline{\rho \mu} \sigma}{2}} z) \right\} \quad (\text{B9a})$$

Then (B9a) can be written as

$$u = B \exp(-\sqrt{\frac{\overline{\rho \mu} \sigma}{2}} z) \cos \left[ \sigma t + \epsilon - \sqrt{\frac{\overline{\rho \mu} \sigma}{2}} z \right] \quad (\text{B9b})$$

or by using the transformation given by (B2), eq.(B9b) becomes

$$u = B \exp \left( -\sqrt{\frac{\overline{\rho \mu} \sigma}{2}} \int_0^y \frac{dy}{\mu} \right) \cos \left[ \sigma t + \epsilon - \sqrt{\frac{\overline{\rho \mu} \sigma}{2}} \int_0^y \frac{dy}{\mu} \right] \quad (\text{B9c})$$

The expression given by (B9c) can be approximated by expanding  $\mu$  by a Taylor series around an average value of  $\mu$ , that is,

$$\mu = \bar{\mu} + y(\overline{d\mu/dy}) + \dots \quad (\text{B10})$$

If the viscosity in (B10) is introduced into (B9c) and if the second-order and higher order terms of  $y$  are neglected, (B9c) can be written as

$$u = B \exp(-\sqrt{\frac{\sigma}{2\nu}} y) \cos \left[ \sigma t + \epsilon - \sqrt{\frac{\sigma}{2\nu}} y \right] \quad (\text{B11})$$

Equation (B11) is the same as the incompressible solution except that mean values of  $\mu$  and  $\rho$  are used. A mean value looks more accurate than the wall value. The mean value of  $\nu$  should be that corresponding to the sublayer thickness.

Since the cosine term is bounded, (B11) can be written as

$$u \propto B \exp\left(-\sqrt{\frac{\sigma}{2\nu}} y\right) \quad (\text{B12})$$

The purpose of modifying the mixing length and consequently the expression for eddy viscosity given by Prandtl's formula, (6.21), is to account for the sublayer and to account for the transition region between the sublayer and the fully turbulent part of the inner region. For this reason, Van Driest [14] defines the mixing length as

$$l = k_1 y [1 - \exp(-y/A)]$$

Because the Stokes effect is localized to a region very close to the wall,  $\nu$  and  $\rho$  should assume values appropriate to this region. A convenient expression can be formed by introducing wall values, but corrected by a factor  $(\nu_w/\nu)^{1/2}$  to account for the small deviation from wall values, as follows:

$$\exp\left(-\sqrt{\frac{\sigma}{2\nu}} y\right) = \exp\left(-\sqrt{\frac{\sigma}{2\nu_w}} \sqrt{\frac{\nu_w}{\nu}} y\right) = \exp\left(-\sqrt{\frac{\nu_w}{\nu}} \frac{y}{A}\right) \quad (\text{B13})$$

The mixing length now becomes

$$l = k_1 y \left[ 1 - \exp\left(-\sqrt{\frac{\nu_w}{\nu}} \frac{y}{A}\right) \right]$$

APPENDIX C  
VARIABLE-GRID DIFFERENTIATION FORMULAS

The first-, second-, and third-derivative formulas for the variable-grid system discussed in Section 6.6.1.3 can be obtained in the following way: Consider the Lagrange interpolation formula

$$f(x) = \sum_{i=0}^n l_i(x) f(x_i) + E(x) \quad (C1)$$

where

$$l_i(x) = \frac{\pi(x)}{(x - x_i) \pi'(x_i)}$$

$$= \frac{(x - x_0) \dots (x - x_{i-1})(x - x_{i+1}) \dots (x - x_n)}{(x_i - x_0) \dots (x_i - x_{i-1})(x_i - x_{i+1}) \dots (x_i - x_n)}$$

and

$$E(x) = \frac{\pi(x)}{(n+1)!} f^{(n+1)}(\xi)$$

Differentiating (C1) gives

$$f^r(x) = \sum_{i=0}^n l_i^r(x) f(x_i) + E^r(x) \quad (C2)$$

The equations (C1) and (C2) are now evaluated for three- and five-point systems to obtain the first-derivative formulas for the variable-grid system with three points and the first-, second- and third derivative formulas for the variable-grid system with five points. Figures C1 and C2 show the variable-grid systems for three and for five points, respectively.

First-Derivative Formulas for Three Points

$$f'_{i-1}(x) = h_i [-B_1(2+K)f_{i-1} - B_2(1+K)f_i - B_3f_{i+1}] + \frac{(1+K)}{6} h_i^2 f^3(\xi) \quad (C3)$$

$$f'_i(x) = h_i [-B_1K f_{i-1} + B_2(1-K) f_i + B_3f_{i+1}] - \frac{K h_i^2}{6} f^3(\xi) \quad (C4)$$

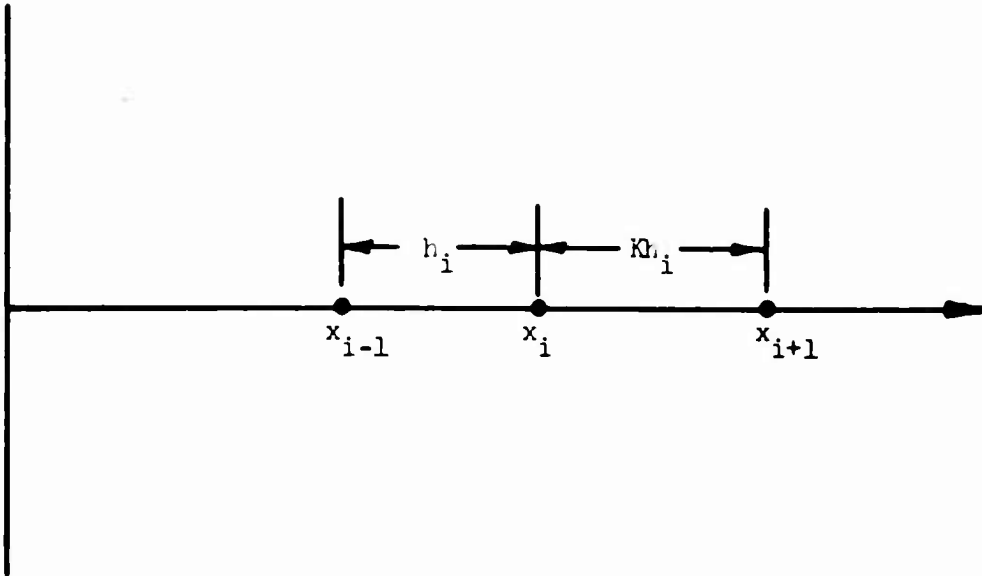


Figure C1.- Variable-grid system for three points.

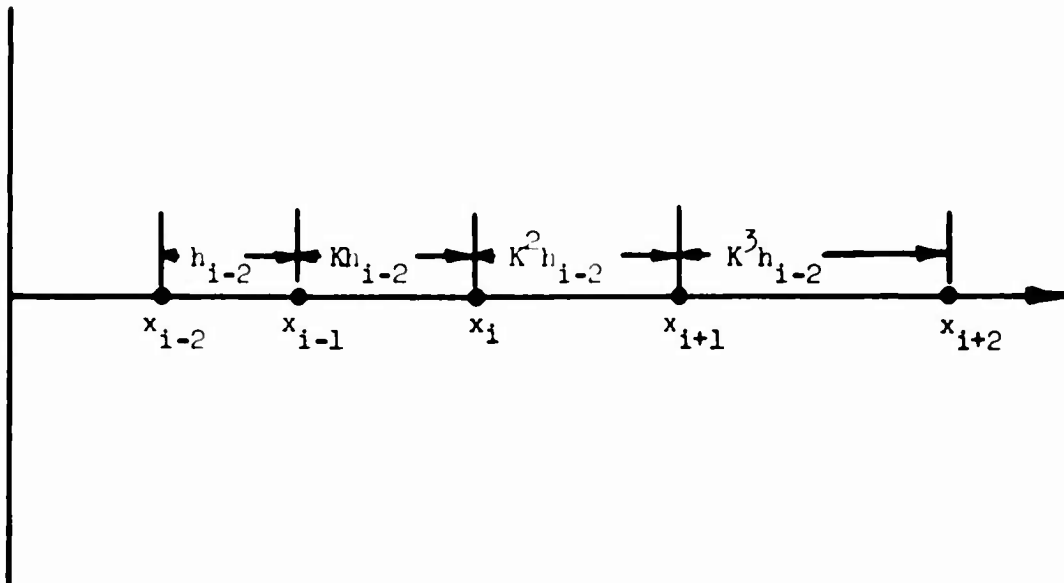


Figure C2.- Variable-grid system for five points.

$$f'_{i+1}(x) = h_i [B_1 K f_{i-1} + B_2 (1 + K) f_i + B_3 (1 + 2K) f_{i+1}] + \frac{K(1 + K)}{6} h_i^2 f^3(\xi) \quad (C5)$$

where

$$B_1 = \frac{1}{h_i^2 (1 + K)} \quad (C6a)$$

$$B_2 = -\frac{1}{h_i^2 K} \quad (C6b)$$

$$B_3 = \frac{1}{h_i^2 K(1 + K)} \quad (C6c)$$

### First Derivative Formulas for Five Points

Definitions of new terms follow the formulas

$$f'_{i-2}(x) = -h_{i-2}^3 [B_1 (a_1 a_2 + a_1 a_3 + a_2 a_3 + a_1 a_2 a_3) f_{i-2} + B_2 a_1 a_2 a_3 f_{i-1} + B_3 a_2 a_3 f_i + B_4 a_1 a_3 f_{i+1} + B_5 a_1 a_2 f_{i+2}] + \frac{a_1 a_2 a_3}{120} h_{i-2}^4 f^5(\xi) \quad (C7)$$

$$f'_{i-1}(x) = h_{i-2}^3 [-B_1 K^3 a_1 a_2 f_{i-2} + B_2 K^2 (a_1 + a_2 + a_1 a_2 - K a_1 a_2) f_{i-1} + B_3 K^2 a_1 a_2 f_i + B_4 K^2 a_2 f_{i+1} + B_5 K^2 a_1 f_{i+2}] - \frac{K^3 a_1 a_2}{120} h_{i-2}^4 f^5(\xi) \quad (C8)$$

$$f'_i(x) = h_{i-2}^3 K^3 a_1 [B_1 K^2 f_{i-2} + B_2 K a_1 f_{i-1} + B_3 (K^2 + K a_1 - a_1 - 1) f_i - B_4 a_1 f_{i+1} - B_5 f_{i+2}] + \frac{K^5 a_1^2}{120} h_{i-2}^4 f^5(\xi) \quad (C9)$$

$$f'_{i+1}(x) = h_{i-2}^3 K^3 [-B_1 K^3 a_1 f_{i-2} - B_2 K^2 a_2 f_{i-1} - B_3 K a_1 a_2 f_i + B_4 (a_1 a_2 - a_1 a_2 K - a_2 K^2 - a_1 K^3) f_{i+1} + B_5 a_1 a_2 f_{i+2}] - \frac{K^6 a_1 a_2}{120} h_{i-2}^4 f^5(\xi) \quad (C10)$$

$$f_{i+2}'(x) = h_{i-2}^3 K^3 [B_1 a_1 a_2 K^3 f_{i-2} + B_2 a_1 a_3 K^2 f_{i-1} + B_3 a_2 a_3 K f_i + B_4 a_1 a_2 a_3 f_{i+1} + B_5 (a_1 a_2 K^3 + a_1 a_3 K^2 + a_2 a_3 K + a_1 a_2 a_3) f_{i+2}] + \frac{K^6 a_1 a_2 a_3}{120} h_{i-2}^4 f^5(\xi) \quad (C11)$$

Second-Derivative Formulas for Five Points

$$f_{i-2}''(x) = 2h_{i-2}^2 [B_1 (a_1 + a_2 + a_3 + a_1 a_2 + a_1 a_3 + a_2 a_3) f_{i-2} + B_2 (a_1 a_2 + a_1 a_3 + a_2 a_3) f_{i-1} + B_3 (a_2 + a_3 + a_2 a_3) f_i + B_4 (a_1 + a_3 + a_1 a_3) f_{i+1} + B_5 (a_1 + a_2 + a_1 a_2) f_{i+2}] - \frac{1}{60} (a_1 a_2 + a_1 a_3 + a_2 a_3 + a_1 a_2 a_3) h_{i-2}^3 f^5(\xi) \quad (C12)$$

$$f_{i-1}''(x) = 2h_{i-2}^2 K [B_1 K (a_1 + a_2 + a_1 a_2) f_{i-2} + B_2 (a_1 a_2 K + a_2 K + a_1 K + a_2 + a_1) f_{i-1} + B_3 (K a_1 a_2 - a_2 - a_1) f_i + B_4 (K a_2 - a_2 - 1) f_{i+1} + B_5 (K a_1 - a_1 - 1) f_{i+2}] + \frac{1}{60} K^2 (a_1 + a_2 + a_1 a_2 - K a_1 a_2) h_{i-2}^3 f^5(\xi) \quad (C13)$$

$$f_i''(x) = 2h_{i-2}^2 K [B_1 K^2 (K a_1 - a_1 - 1) f_{i-2} + B_2 K a_1 (K^2 - a_1 - 1) f_{i-1} + B_3 (a_1 - K a_1 - K a_1^2 - K^2 - K^2 a_1 + K^3 a_1) f_i + B_4 a_1 (1 - K a_1 - K^2) f_{i+1} + B_5 (a_1 - K a_1 - K^2) f_{i+2}] - \frac{1}{60} K^3 a_1 (1 - a_1 - K a_1 + K^2) h_{i-2}^3 f^5(\xi) \quad (C14)$$

$$f_{i+1}''(x) = 2h_{i-2}^2 K [B_1 K^2 (a_1 - K a_1 - K^2) f_{i-2} + B_2 K (a_2 - K a_2 - K^3) f_{i-1} + B_3 (a_1 a_2 - K^2 a_2 - K^3 a_1) f_i + B_4 (a_1 a_2 + K a_2 - K^2 a_2 + K^2 a_1 - K^3 a_1 - K^4) f_{i+1} + B_5 (a_1 a_2 + K a_2 + K^2 a_1) f_{i+2} + \frac{1}{60} K^3 (a_1 a_2 - a_1 a_2 K - a_2 K^2 - a_1 K^3) h_{i-2}^3 f^5(\xi) \quad (C15)$$

$$\begin{aligned}
 f''_{i+2}(x) = & 2h_{i-2}^2 K [B_1 K^2 (a_1 a_2 + K a_2 + K^2 a_1) f_{i+2} + B_2 K (a_1 a_3 + K a_3 + K^3 a_1) f_{i+1} \\
 & + B_3 (a_2 a_3 + K^2 a_3 + K^3 a_2) f_i + B_4 (a_2 a_3 + K a_1 a_3 + K^2 a_1 a_2) f_{i+1} \\
 & + B_5 (a_2 a_3 + K a_1 a_3 + K^2 a_3 + K^2 a_1 a_2 + K^3 a_2 + K^4 a_1) f_{i+2}] \\
 & + \frac{1}{60} K^3 (a_1 a_2 K^3 + a_1 a_3 K^2 + a_2 a_3 K + a_1 a_2 a_3) h_{i-2}^3 f^5(\xi) \quad (C16)
 \end{aligned}$$

Third-Derivative Formulas for Five Points

$$\begin{aligned}
 f'''_{i-2}(x) = & -6h_{i-2} [B_1 (1 + a_1 + a_2 + a_3) f_{i-2} + B_2 (a_1 + a_2 + a_3) f_{i-1} \\
 & + B_3 (1 + a_2 + a_3) f_i + B_4 (1 + a_1 + a_3) f_{i+1} + B_5 (1 + a_1 + a_2) f_{i+2}] \\
 & + \frac{1}{10} (a_1 + a_2 + a_3 + a_1 a_2 + a_1 a_3 + a_2 a_3) h_{i-2}^2 f^5(\xi) \quad (C17)
 \end{aligned}$$

$$\begin{aligned}
 f'''_{i-1}(x) = & -6h_{i-2} [B_1 K (1 + a_1 + a_2) f_{i-2} + B_2 (K a_2 + K a_1 + K - 1) f_{i-1} \\
 & + B_3 (K a_2 + K a_1 - 1) f_i + B_4 (K a_2 + K - 1) f_{i+1} + B_5 (K a_1 + K - 1) f_{i+2}] \\
 & + \frac{1}{10} K (K a_1 a_2 + K a_2 + K a_1 + a_2 + a_1) h_{i-2}^2 f^5(\xi) \quad (C18)
 \end{aligned}$$

$$\begin{aligned}
 f'''_i(x) = & 6h_{i-2} [B_1 K (1 - K - K a_1) f_{i-2} + B_2 (a_1 - K^2 - K^2 a_1) f_{i-1} \\
 & + B_3 (a_1 + K - K^2 - K^2 a_1) f_i + B_4 (a_1 + K - K^2 a_1) f_{i+1} + B_5 (a_1 + K - K^2) f_{i+2}] \\
 & + \frac{1}{10} K (a_1 - K a_1 - K a_1^2 - K^2 - K^2 a_1 + K^3 a_1) h_{i-2}^2 f^5(\xi) \quad (C19)
 \end{aligned}$$

$$\begin{aligned}
 f_{i+1}^{(4)}(x) = & 6h_{i-2} [B_1 K(a_1 + K - K^2)f_{i-2} + B_2(a_2 + K^2 - K^3)f_{i-1} + B_3(a_2 + Ka_1 - K^3)f_i \\
 & + B_4(a_2 + Ka_1 + K^2 - K^3)f_{i+1} + B_5(a_2 + Ka_1 + K^2)f_{i+2}] \\
 & + \frac{1}{10} K(a_1 a_2 + Ka_2 - K^2 a_2 + K^2 a_1 - K^3 a_1 - K^4) h_{i-2}^2 f^5(\xi) \quad (C20)
 \end{aligned}$$

$$\begin{aligned}
 f_{i+2}^{(4)}(x) = & 6h_{i-2} [B_1 K(a_2 + Ka_1 + K^2)f_{i-2} + B_2(a_3 + K^2 a_1 + K^3)f_{i-1} + B_3(a_3 + Ka_2 + K^3)f_i \\
 & + B_4(a_3 + Ka_2 + K^2 a_1)f_{i+1} + B_5(a_3 + Ka_2 + K^2 a_1 + K^3)f_{i+2}] \\
 & + \frac{1}{10} K(a_2 a_3 + Ka_1 a_3 + K^2 a_3 + K^2 a_1 a_2 + K^3 a_2 + K^4 a_1) h_{i-2}^2 f^5(\xi) \quad (C21)
 \end{aligned}$$

The constants  $B_1, B_2, B_3, B_4, B_5$ , and  $a_1, a_2, a_3$ , are given by

$$B_1 = \frac{1}{h_{i-2}^4 a_1 a_2 a_3} \quad (C22a)$$

$$B_2 = -\frac{1}{h_{i-2}^4 K^3 a_1 a_2} \quad (C22b)$$

$$B_3 = \frac{1}{h_{i-2}^4 K^5 a_1^2} \quad (C22c)$$

$$B_4 = -\frac{1}{h_{i-2}^4 K^6 a_1 a_2} \quad (C22d)$$

$$B_5 = \frac{1}{h_{i-2}^4 K^6 a_1 a_2 a_3} \quad (C22e)$$

$$a_1 = 1 + K, \quad a_2 = 1 + K + K^2, \quad a_3 = 1 + K + K^2 + K^3 \quad (C22f)$$

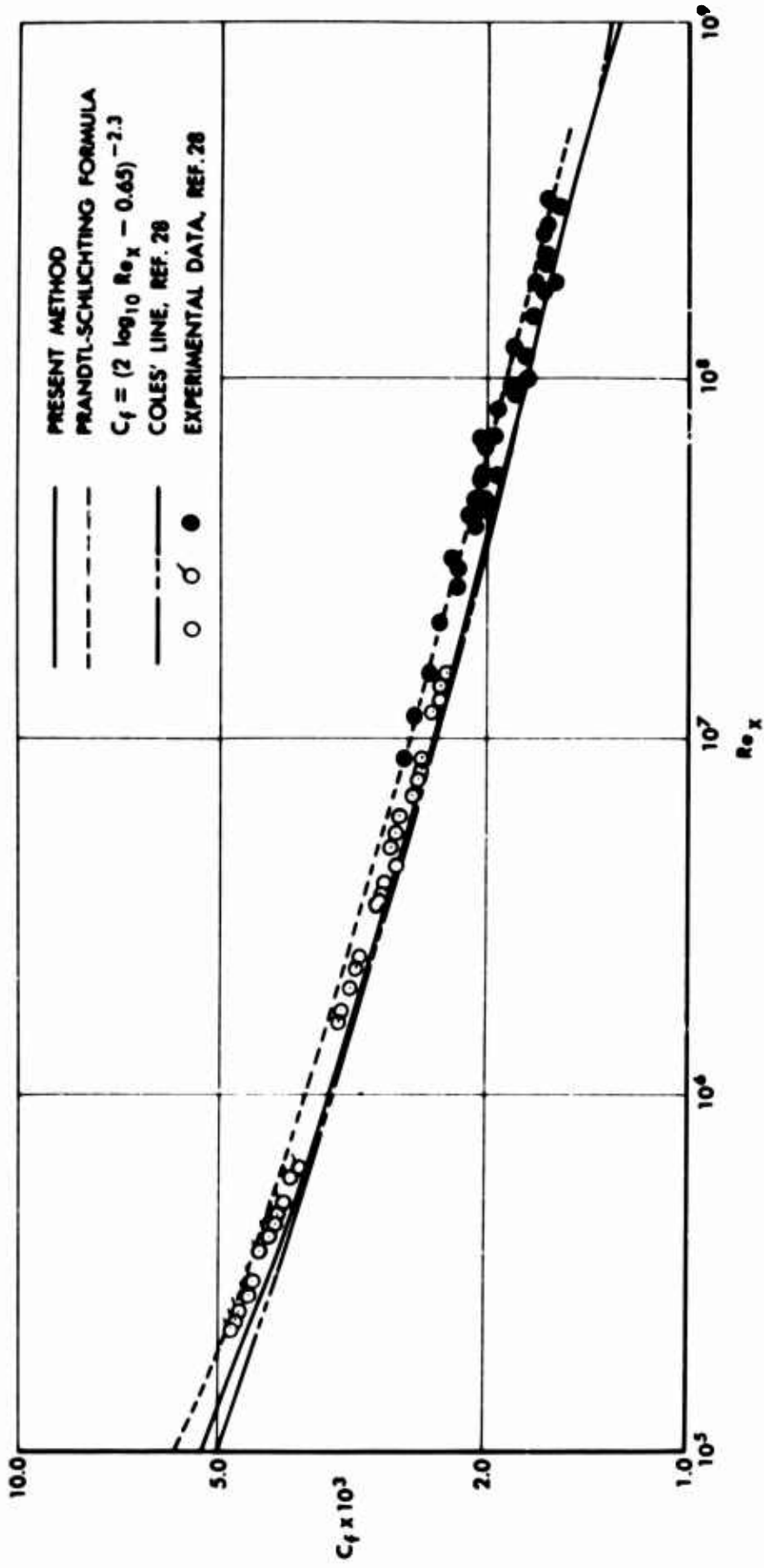


Figure 12.- Results of calculations for a flat-plate flow.  
(a) Comparison of calculated local skin-friction coefficient with experiment, Prandtl-Schlichting formula, and Coles' line.

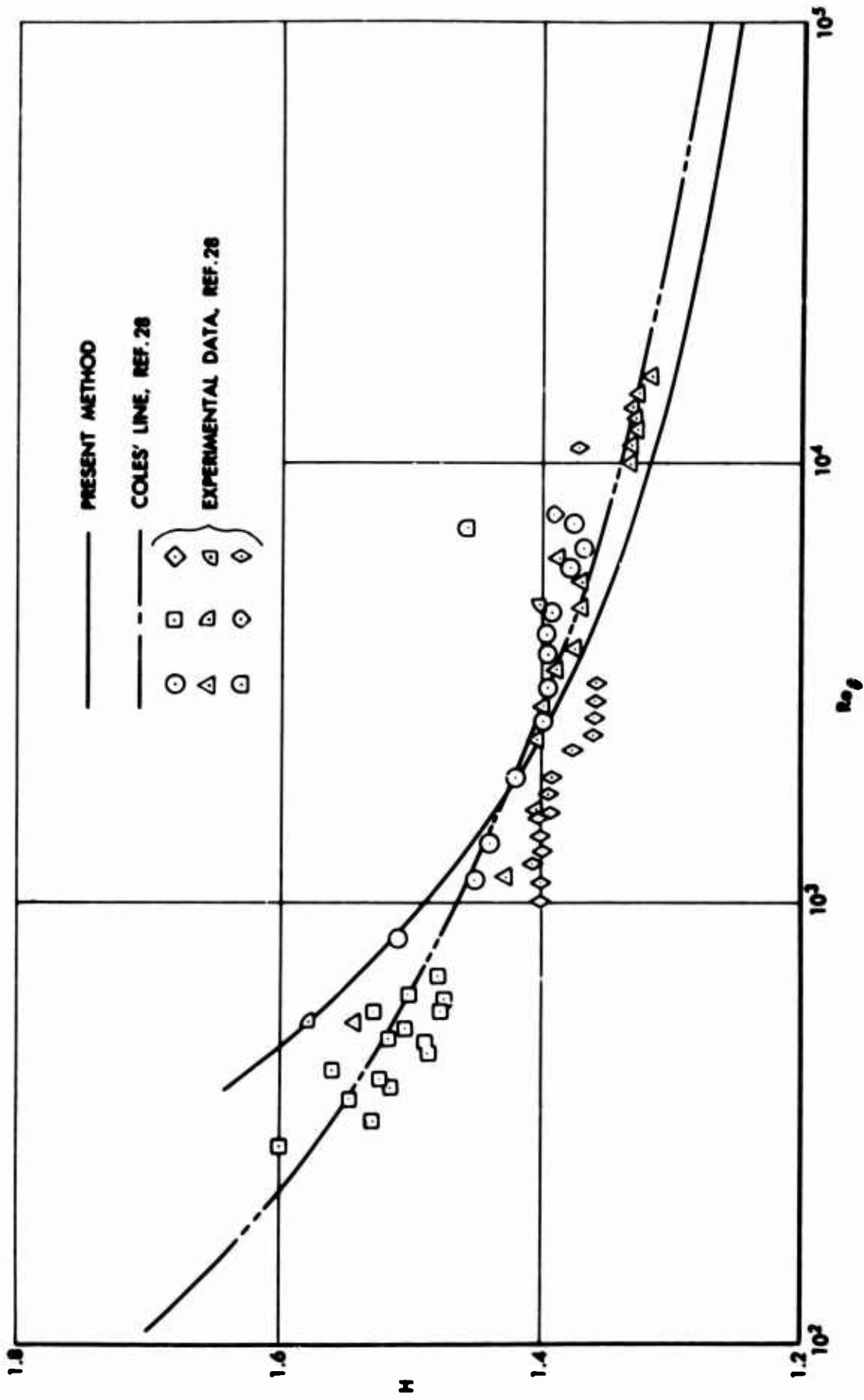


Figure 12.-Continued. (b) Comparison of calculated shape factor with experiment and Coles' line.

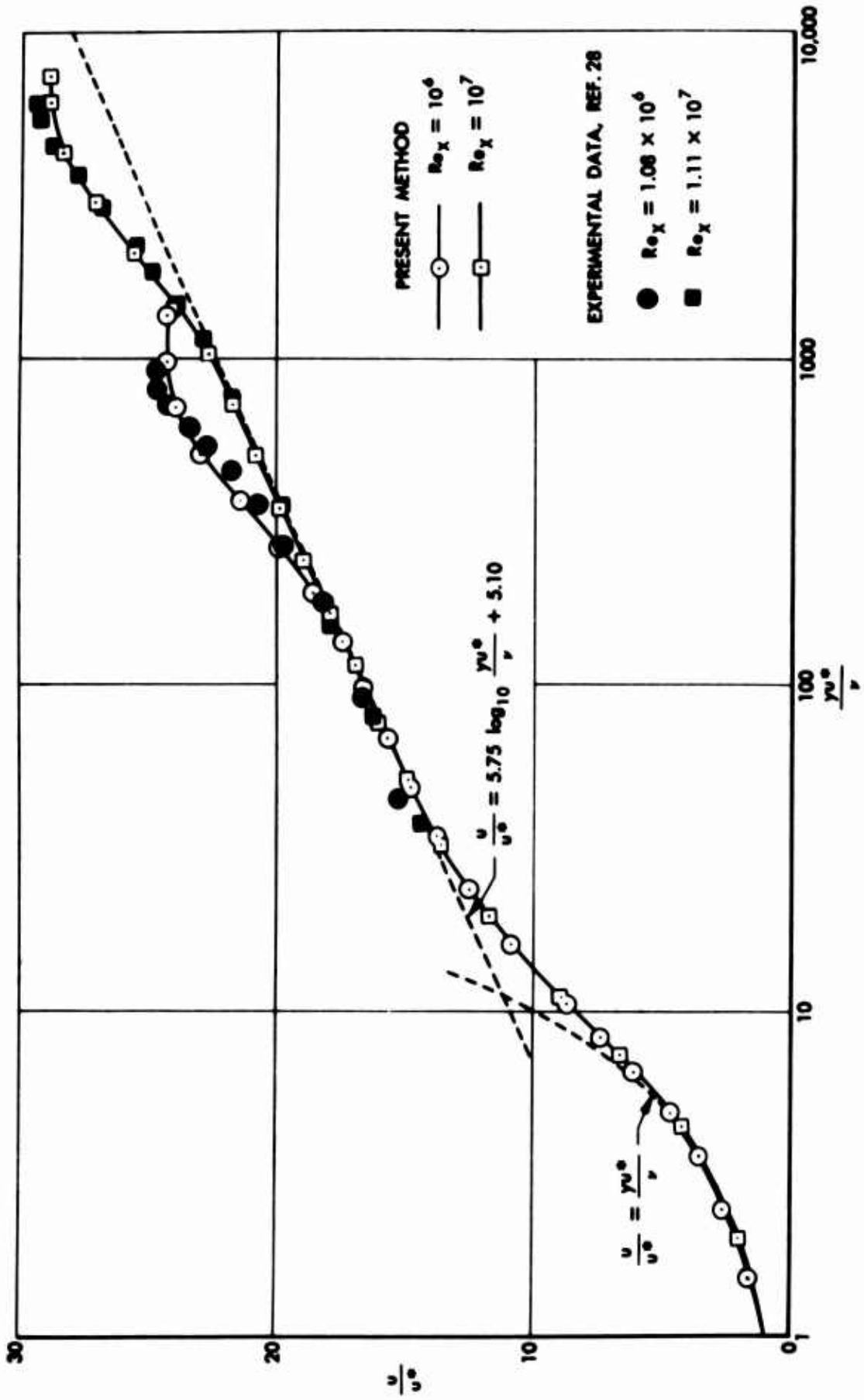


Figure 12.- Continued . (c) Comparison of calculated and experimental law-of-the-wall profiles .

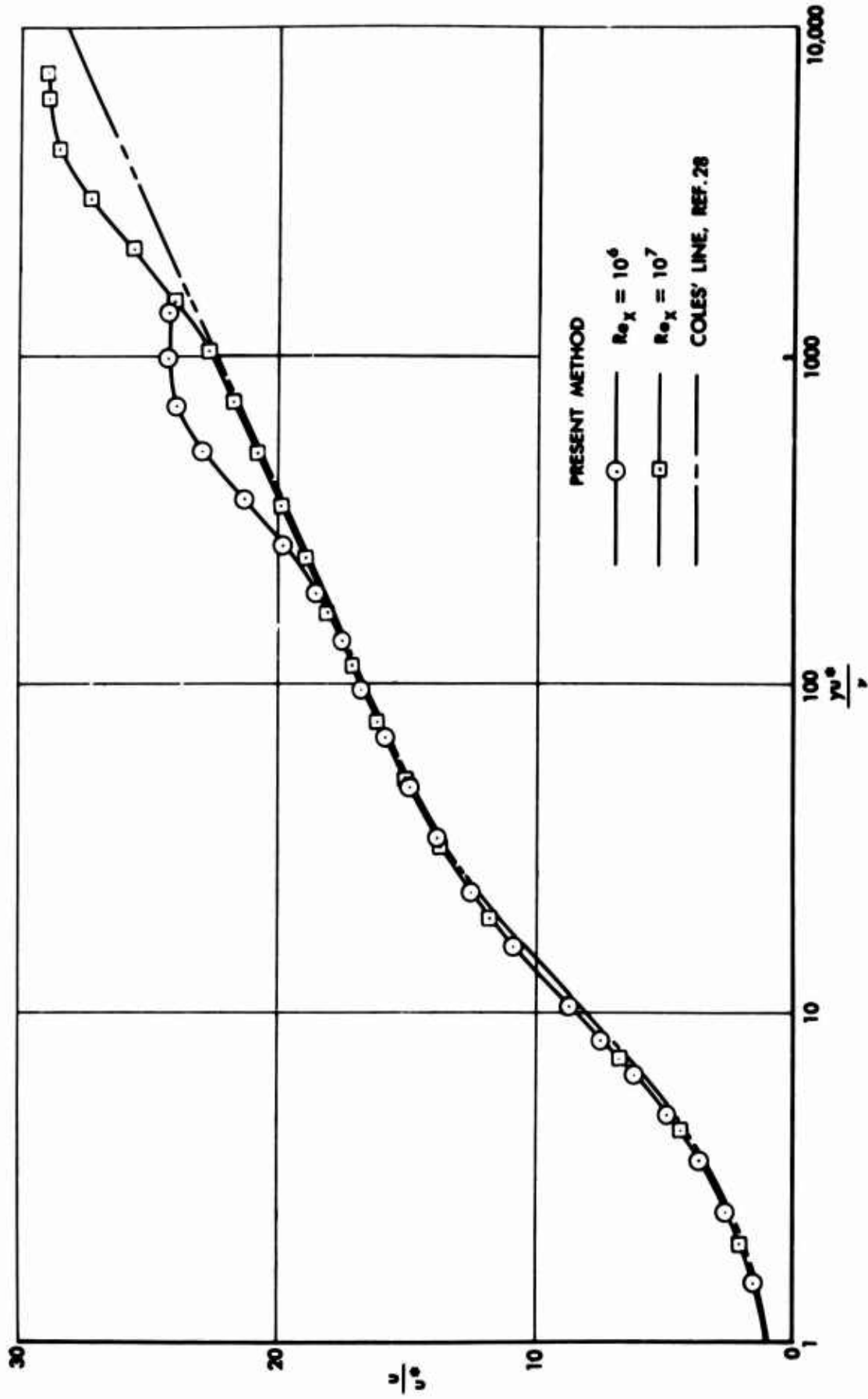


Figure 12.- Continued. (d) Comparison of calculated law-of-the-wall profiles with Coles' line.

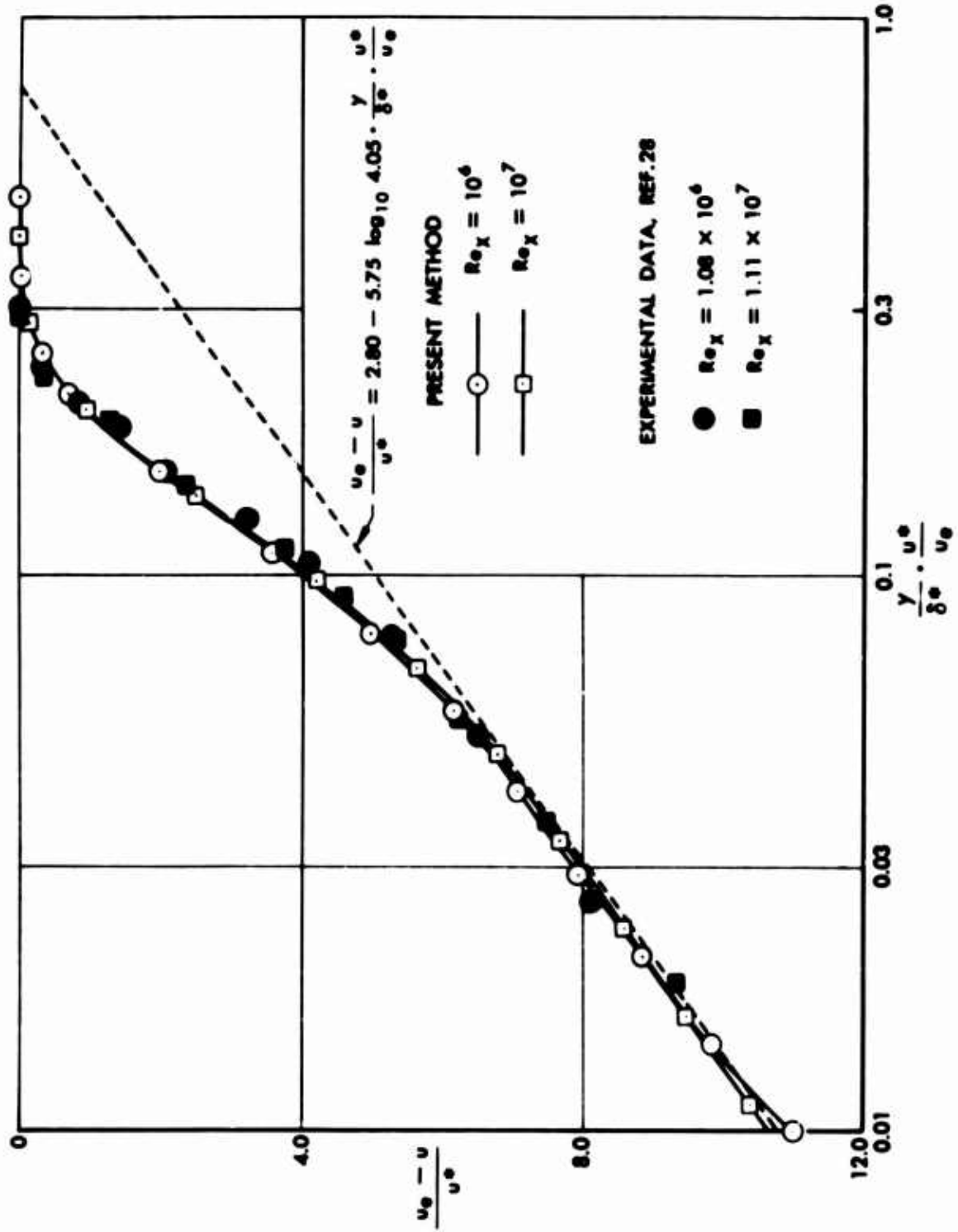


Figure 12 - Continued. (e) Comparison of calculated and experimental velocity-defect-law profiles.

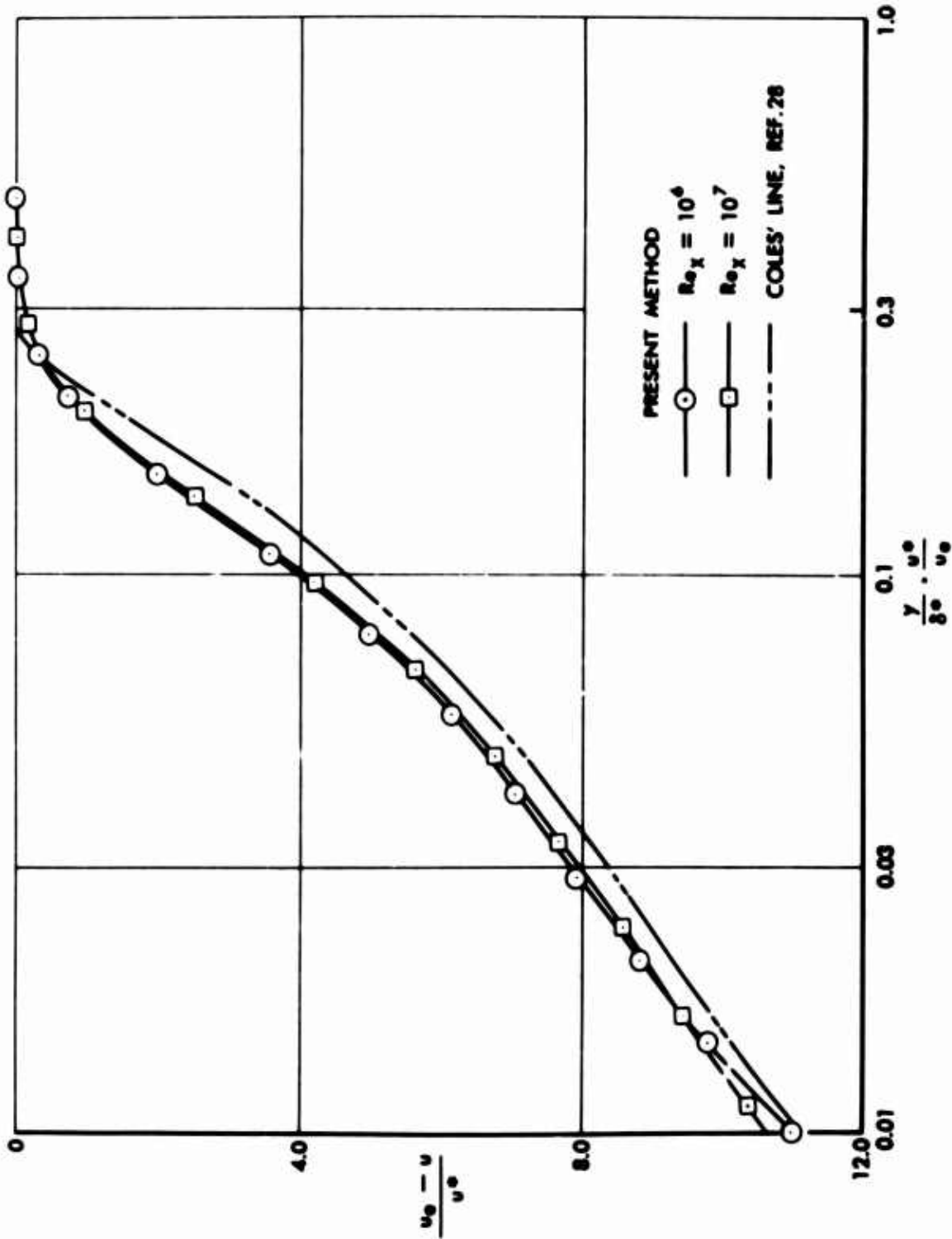


Figure 12.- Continued. (f) Comparison of calculated velocity-defect-law profiles with Coles' line.

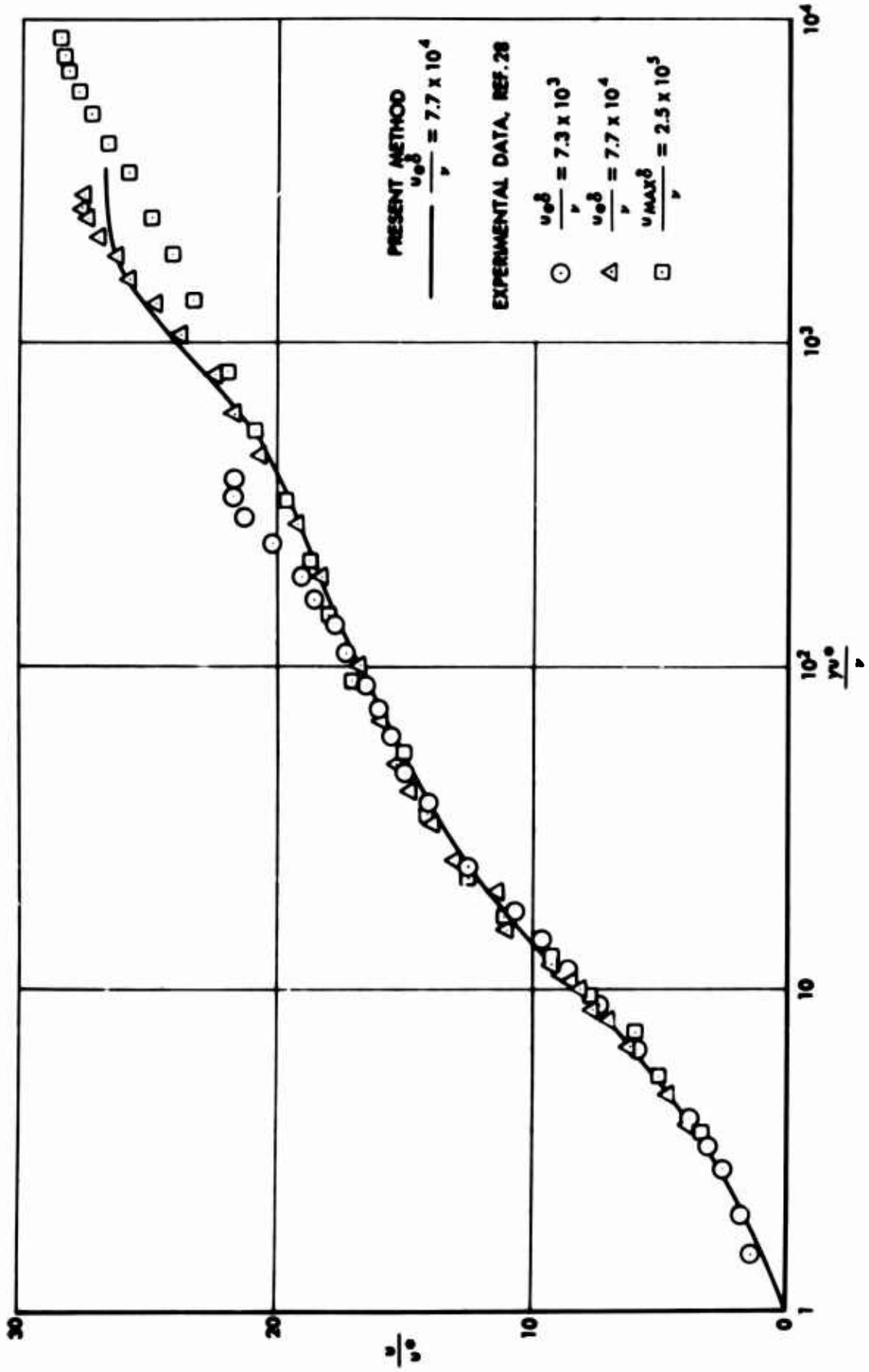


Figure 12.- Continued. (g) Comparison of calculated and experimental sub-layer profile according to Klebanoff.

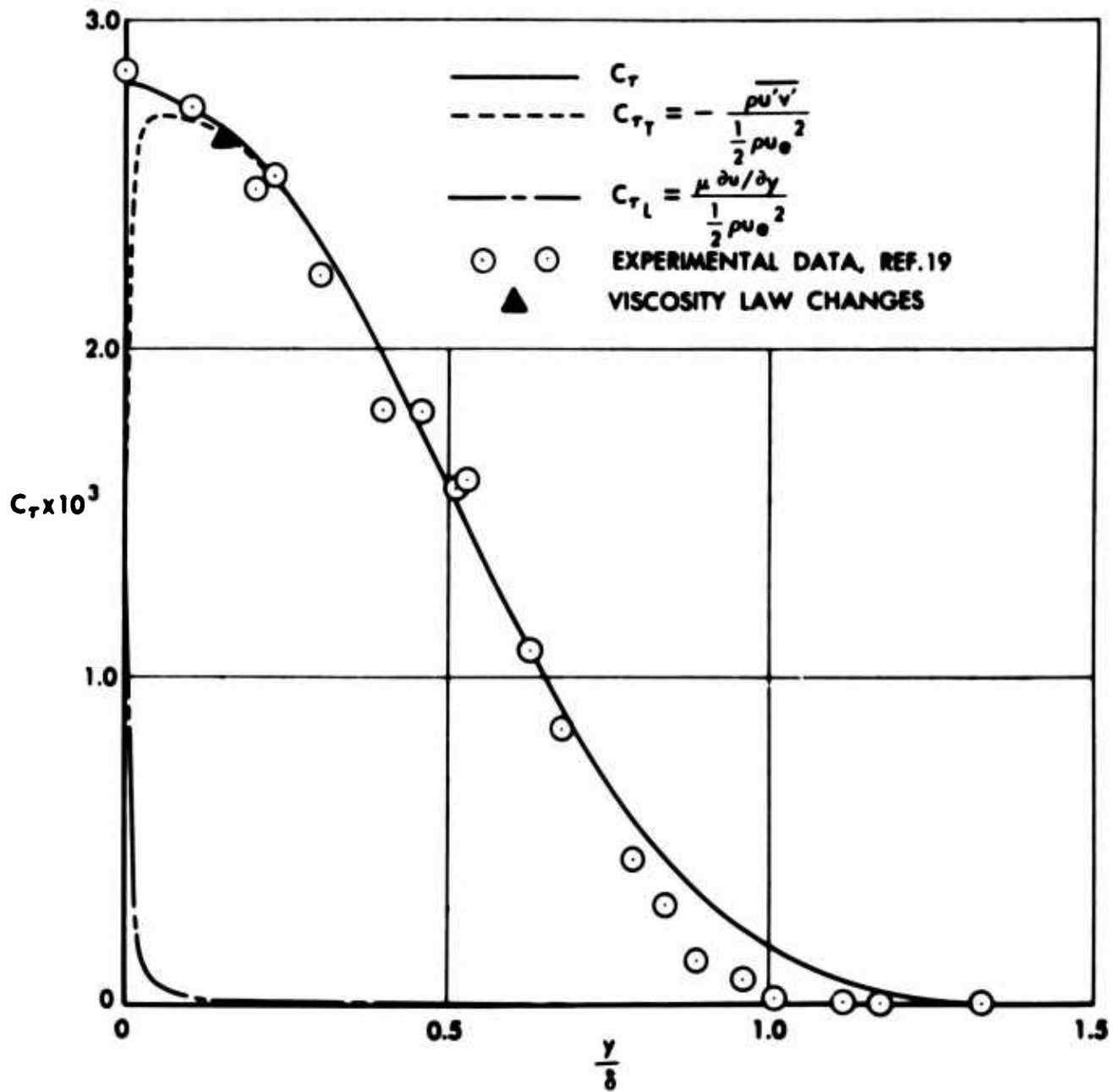


Figure 12.- Continued. (h) Comparison of calculated and experimental shear-stress coefficient according to Klebanoff.  $Re_\delta = 7.7 \times 10^4$ ,  $u'/u_e = 0.037$ .

PRESENT METHOD      EXPERIMENTAL DATA, REF.19

—      ○ ○ ○ ○

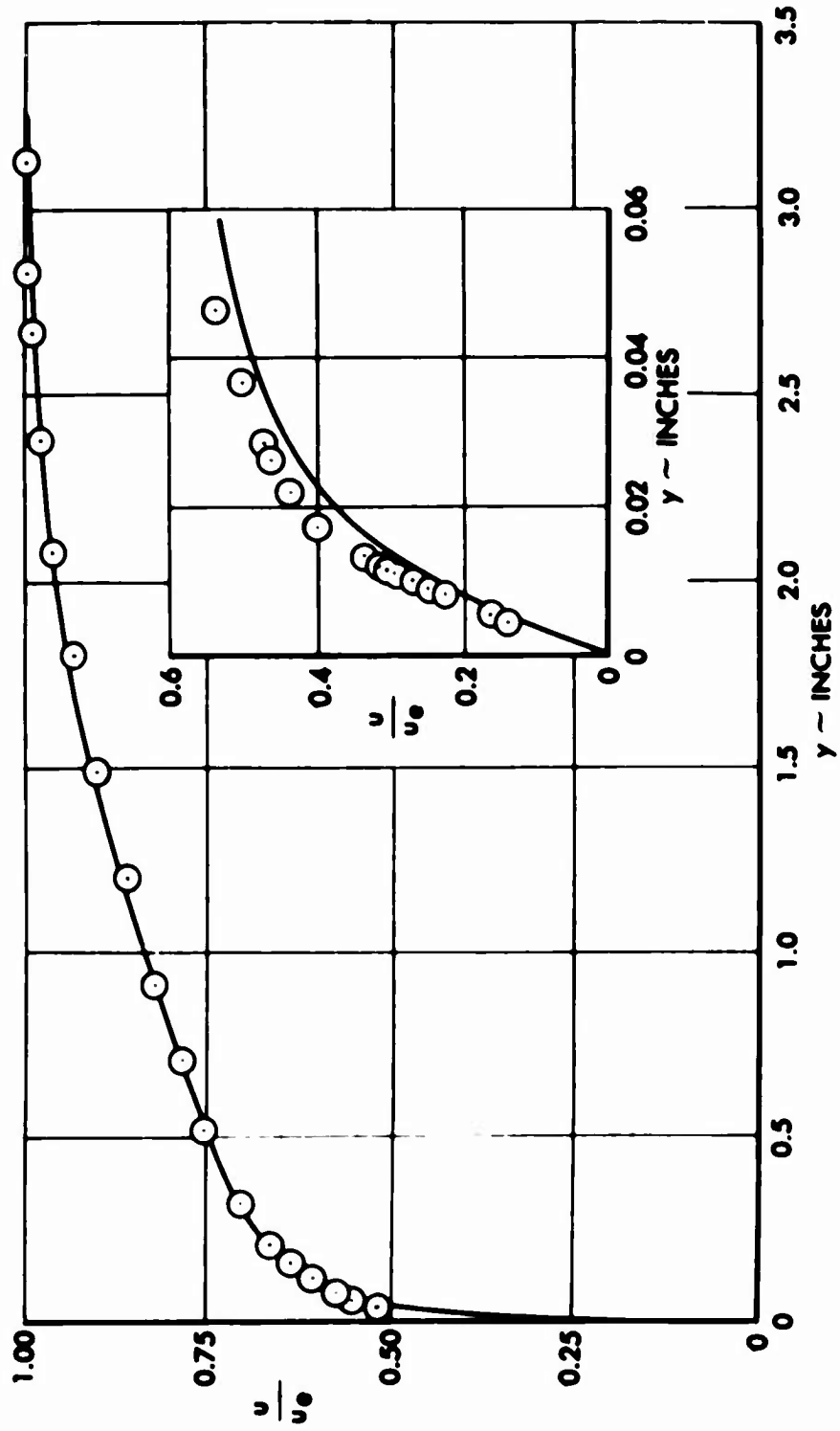


Figure 12.-Continued. (1) Comparison of calculated and experimental mean-velocity distributions according to Klebanoff.  $Re_k = 7.7 \times 10^4$ ,  $u^*/u_e = 0.037$ .

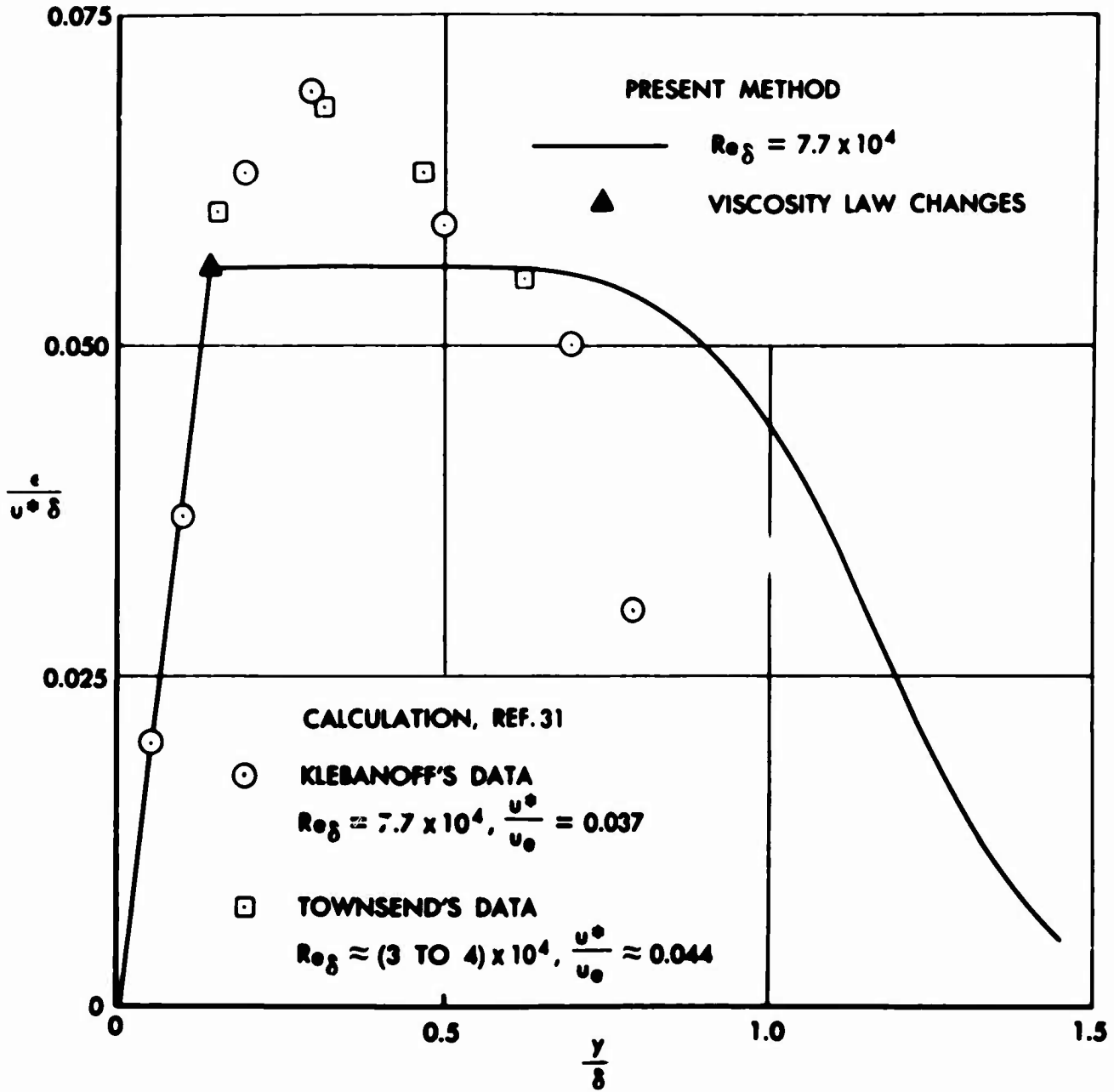


Figure 12.- Continued. (j) Comparison of calculated eddy-viscosity distributions across a boundary layer with values calculated from Klebanoff's and Townsend's data.

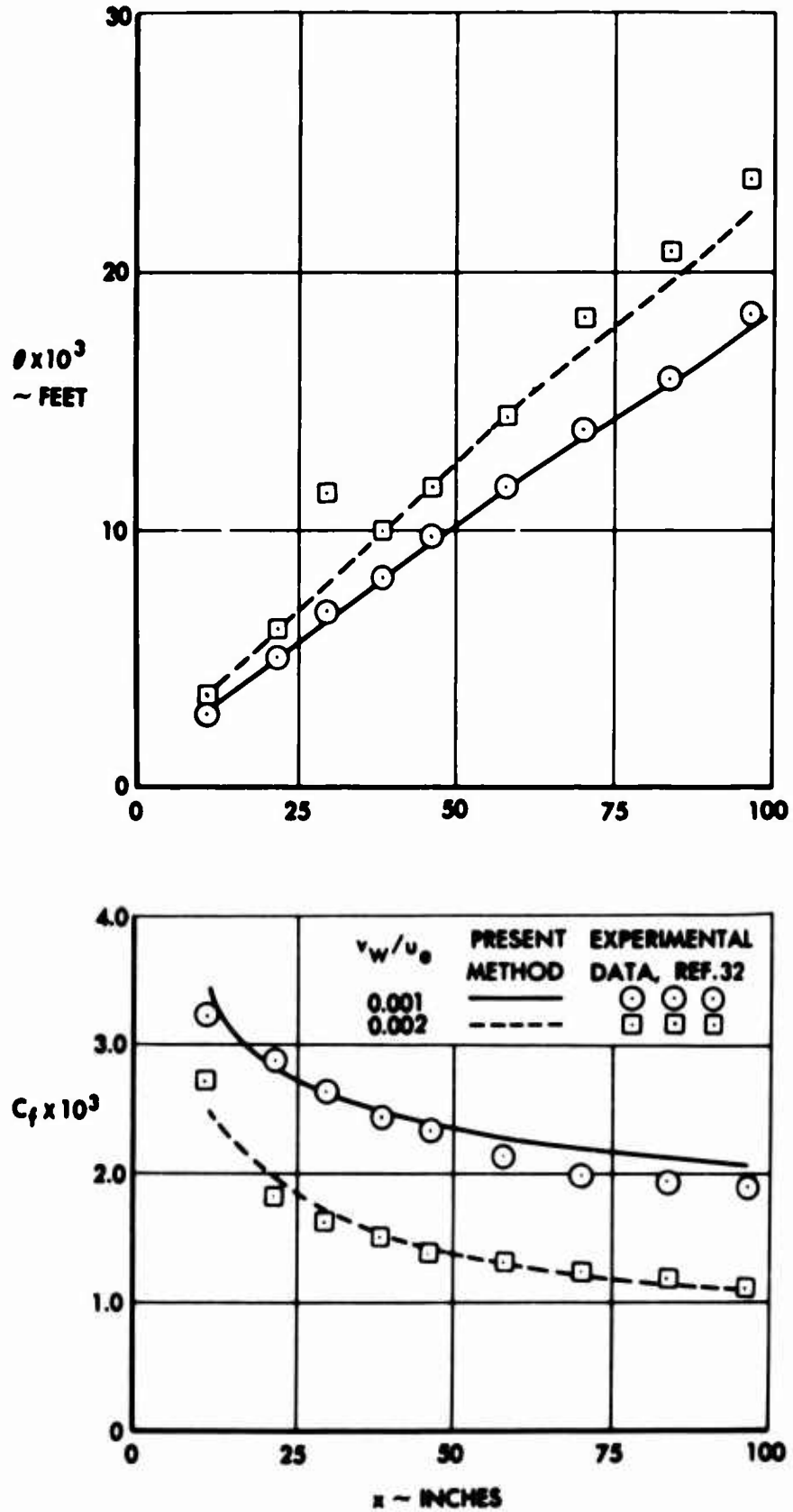


Figure 13.- Results of calculations for the flat plate with two uniform blowing rates,  $v_w/u_e = 0.001$  and  $0.002$ . (Experimental data of Mickley and Davis)  
 (a) Comparison of calculated and experimental momentum thickness and local skin-friction coefficient for the two blowing rates.

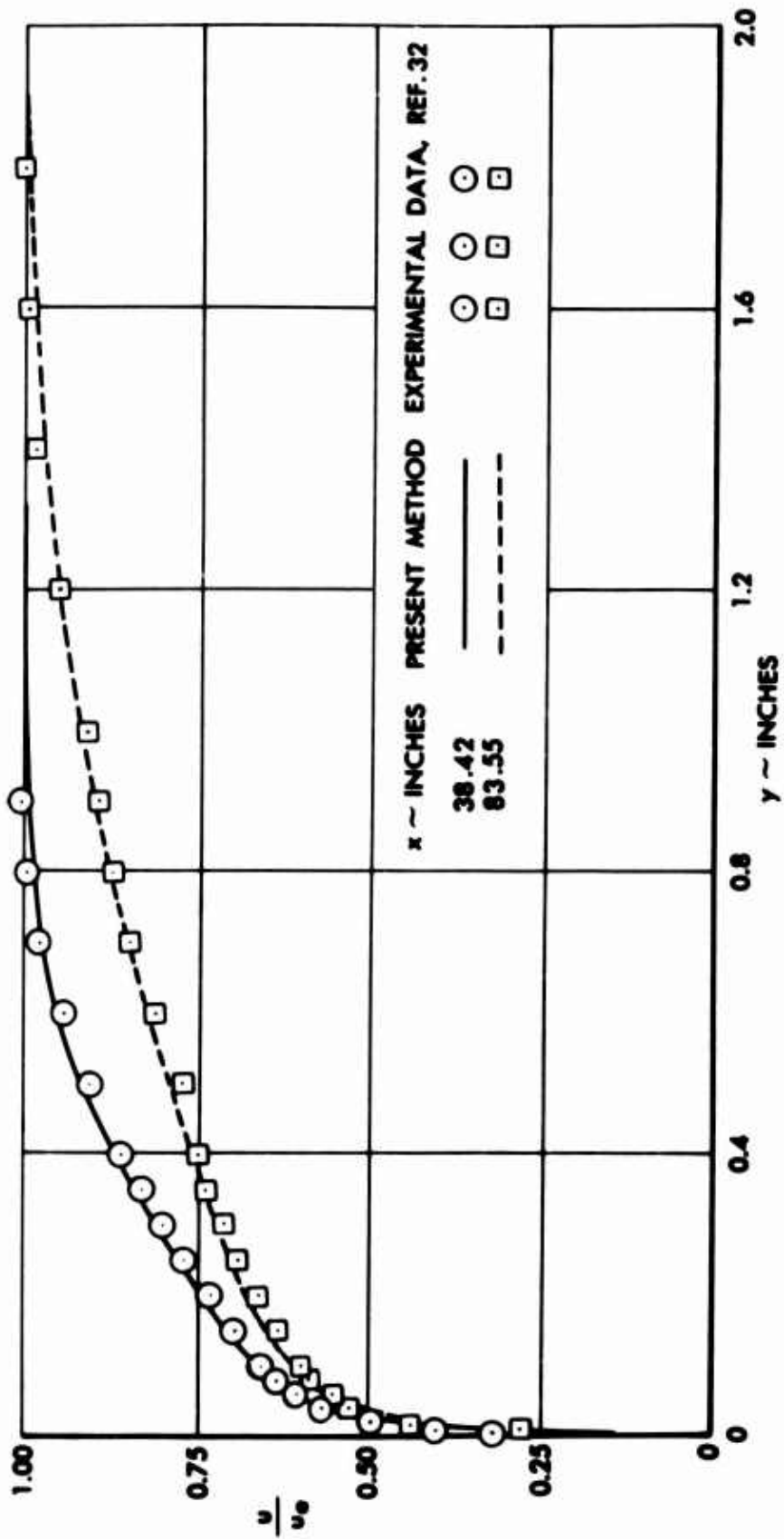


Figure 13.-Continued. (b) Comparison of calculated and experimental velocity profiles for  $v_w/u_e = 0.001$  at stations  $x = 38.42$  and  $83.55$  inches.

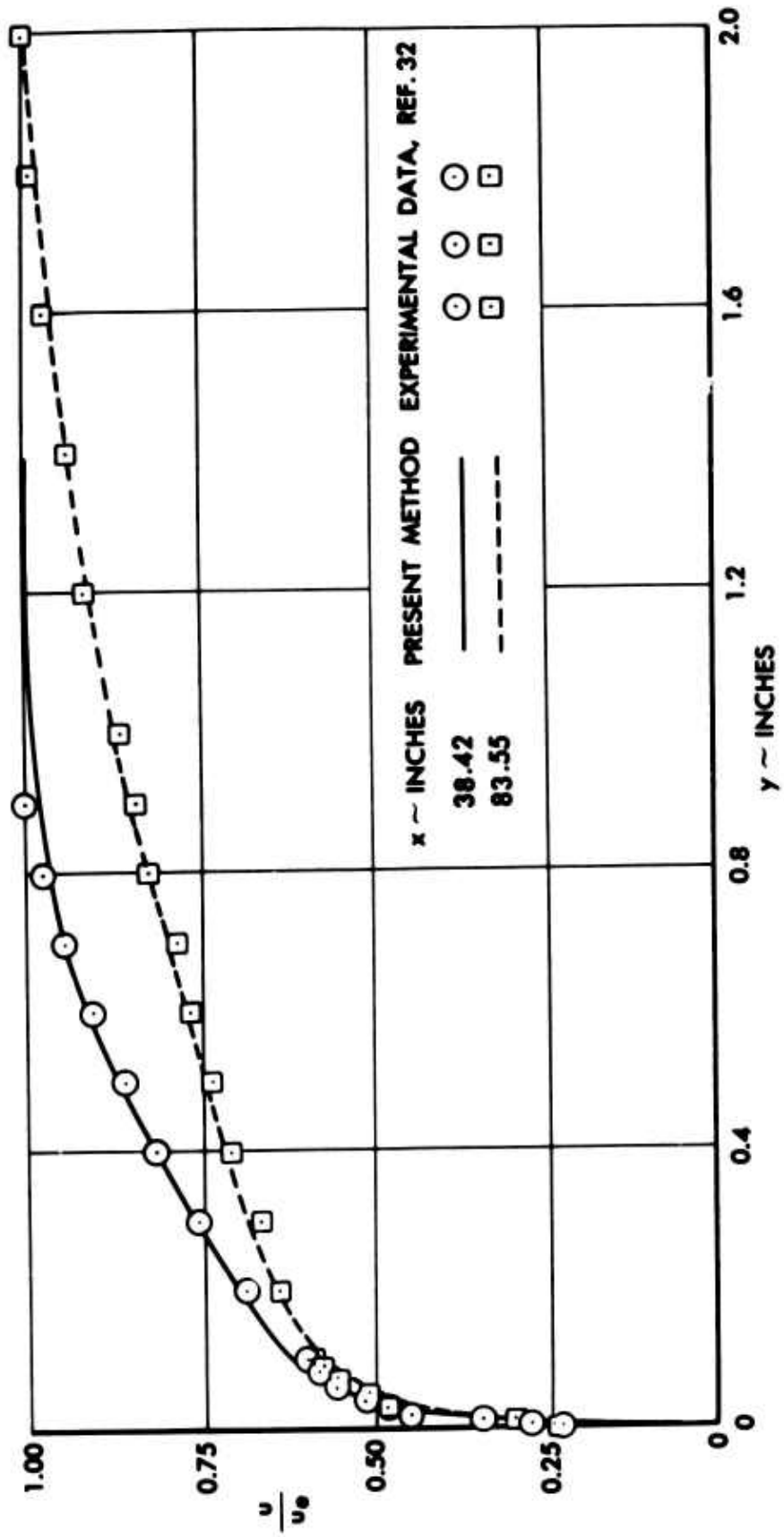


Figure 13.- Continued. (c) Comparison of calculated and experimental velocity profiles for  $v_w/u_e = 0.002$  at stations  $x = 38.42$  and  $83.55$  inches.

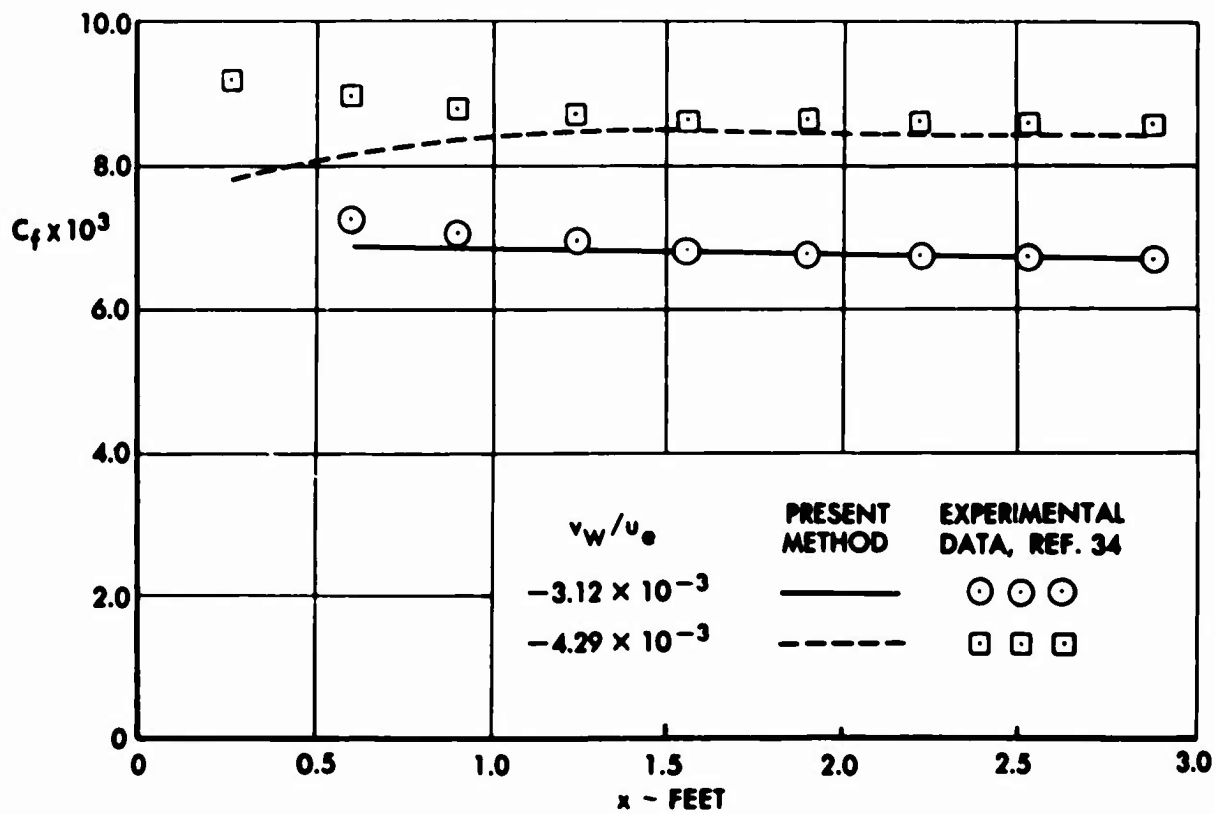
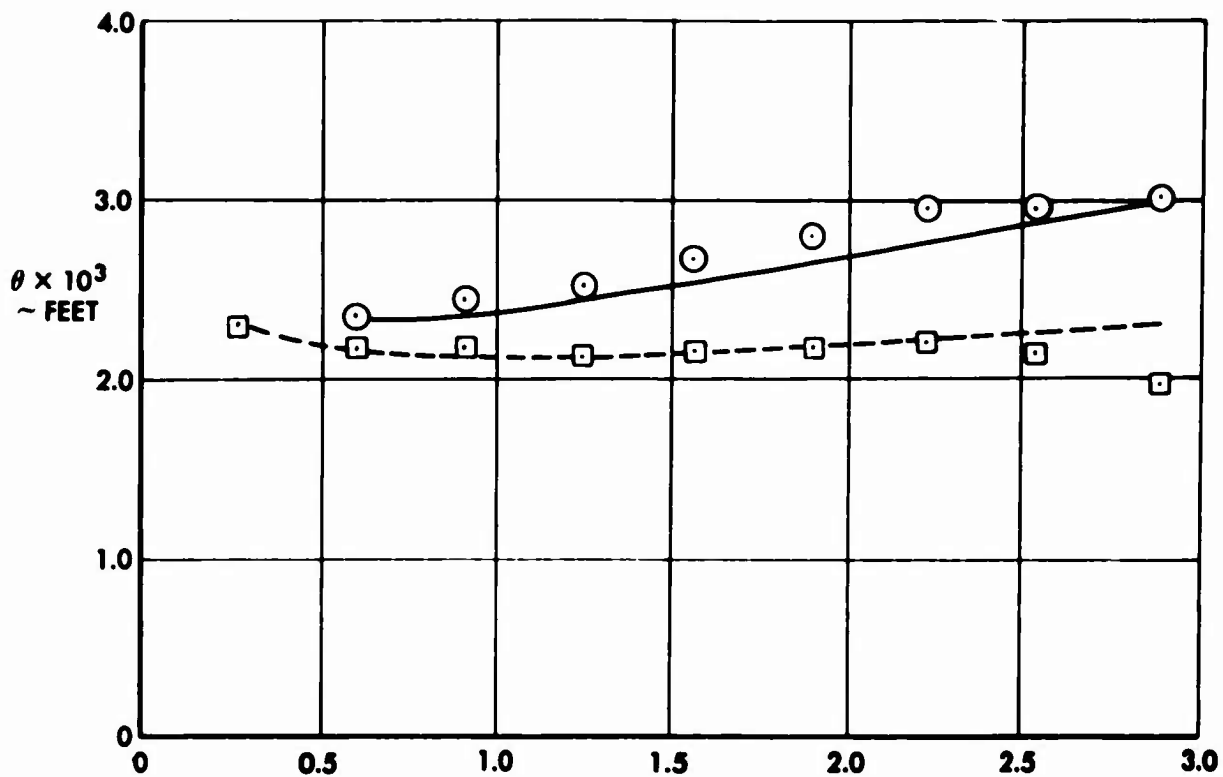


Figure 14.- Results of calculations for the flat plate with two uniform suction rates,  $v_w/u_e = -0.00312$  and  $-0.00429$  (Experimental data of Tennekes).  
 (a) Comparison of calculated and experimental momentum thickness and local skin friction coefficient for the two suction rates.

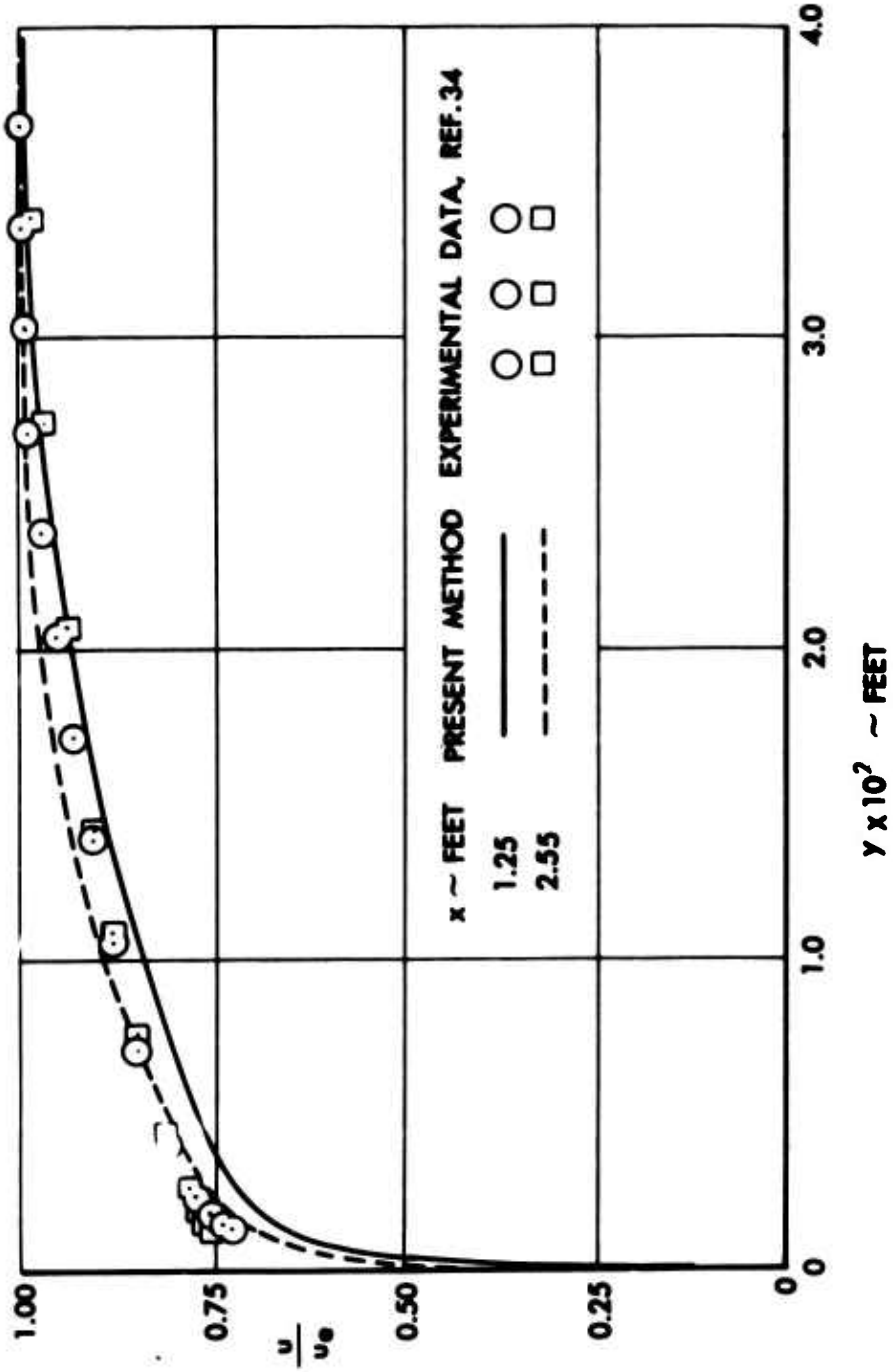


Figure 14.- Continued. (b) Comparison of calculated and experimental velocity profiles for  $v_w/u_e = -0.00312$  at stations  $x = 1.25$  and  $2.55$  feet.

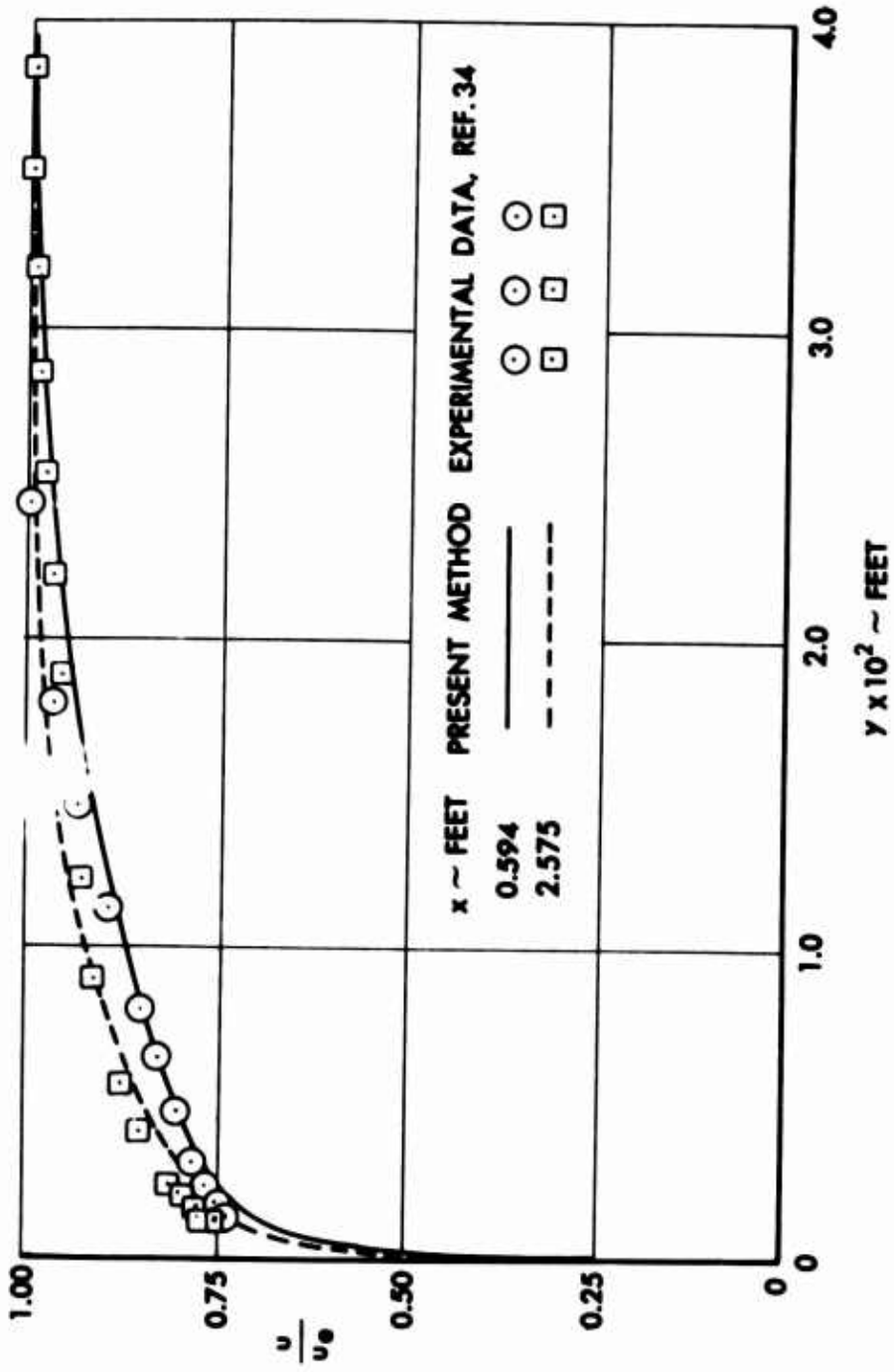


Figure 14.- Continued. (c) Comparison of calculated and experimental velocity profiles for  $v_w/u_e = -0.00429$  at stations  $x = 0.594$  and  $2.575$  feet.

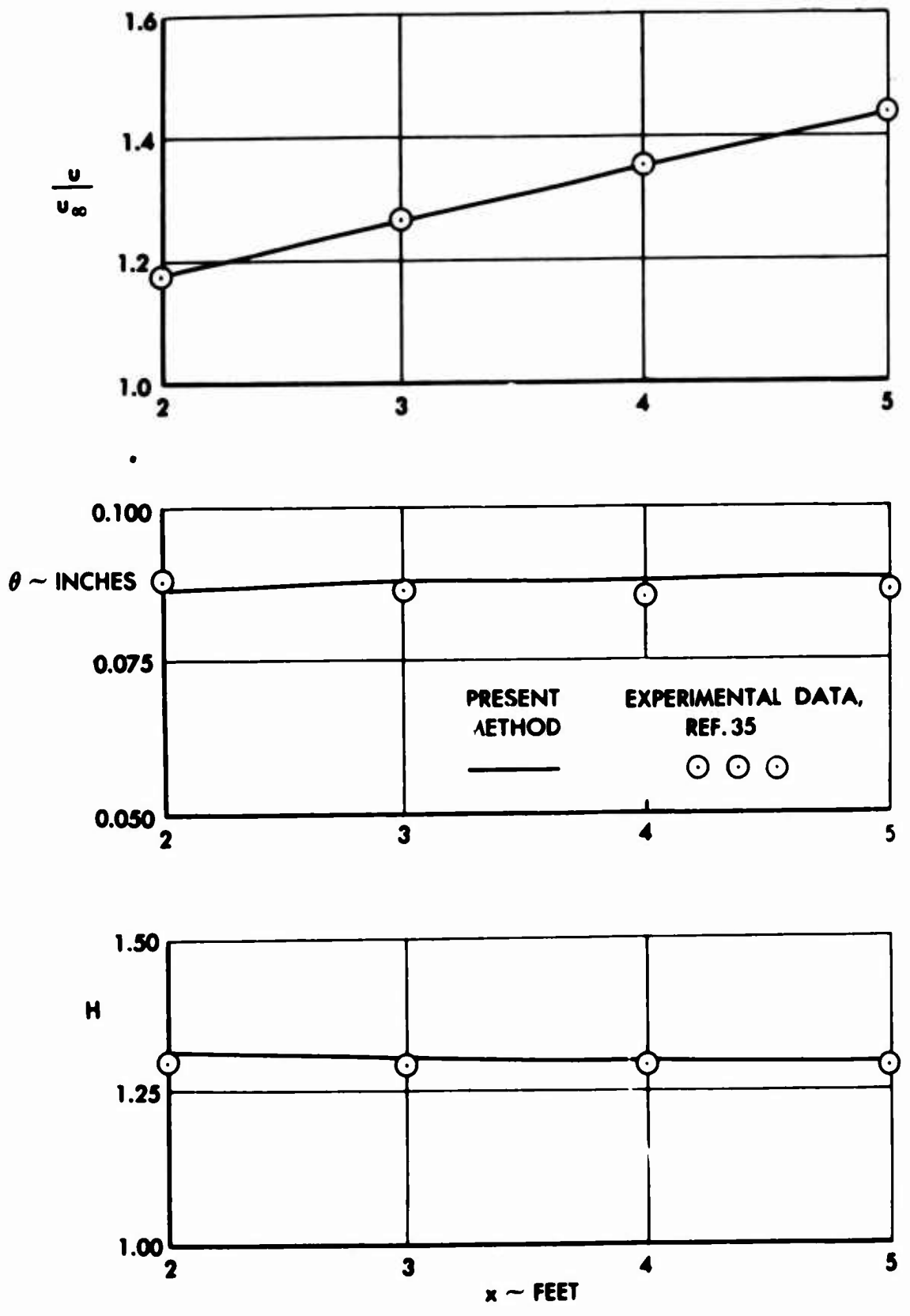


Figure 16.- Results of calculations for an equilibrium flow in a favorable pressure gradient with  $E = -0.35$  (Experimental data of Herring and Norbury).  
(a) Experimental velocity distribution and comparison of calculated and experimental momentum thickness and shape-factor parameters.

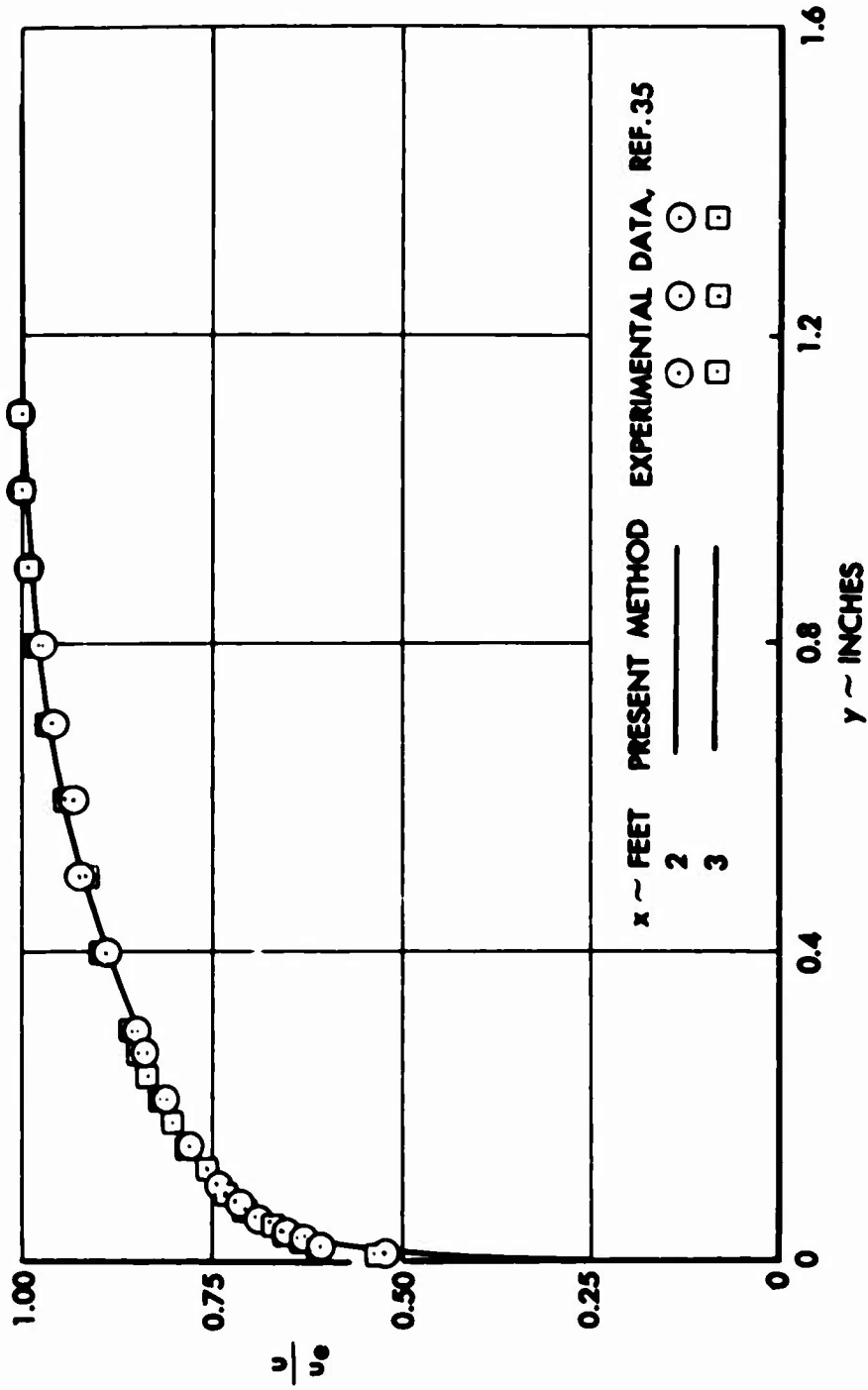


Figure 16.-Continued. (b) Comparison of calculated and experimental velocity profiles at stations x = 2 and 3 feet.

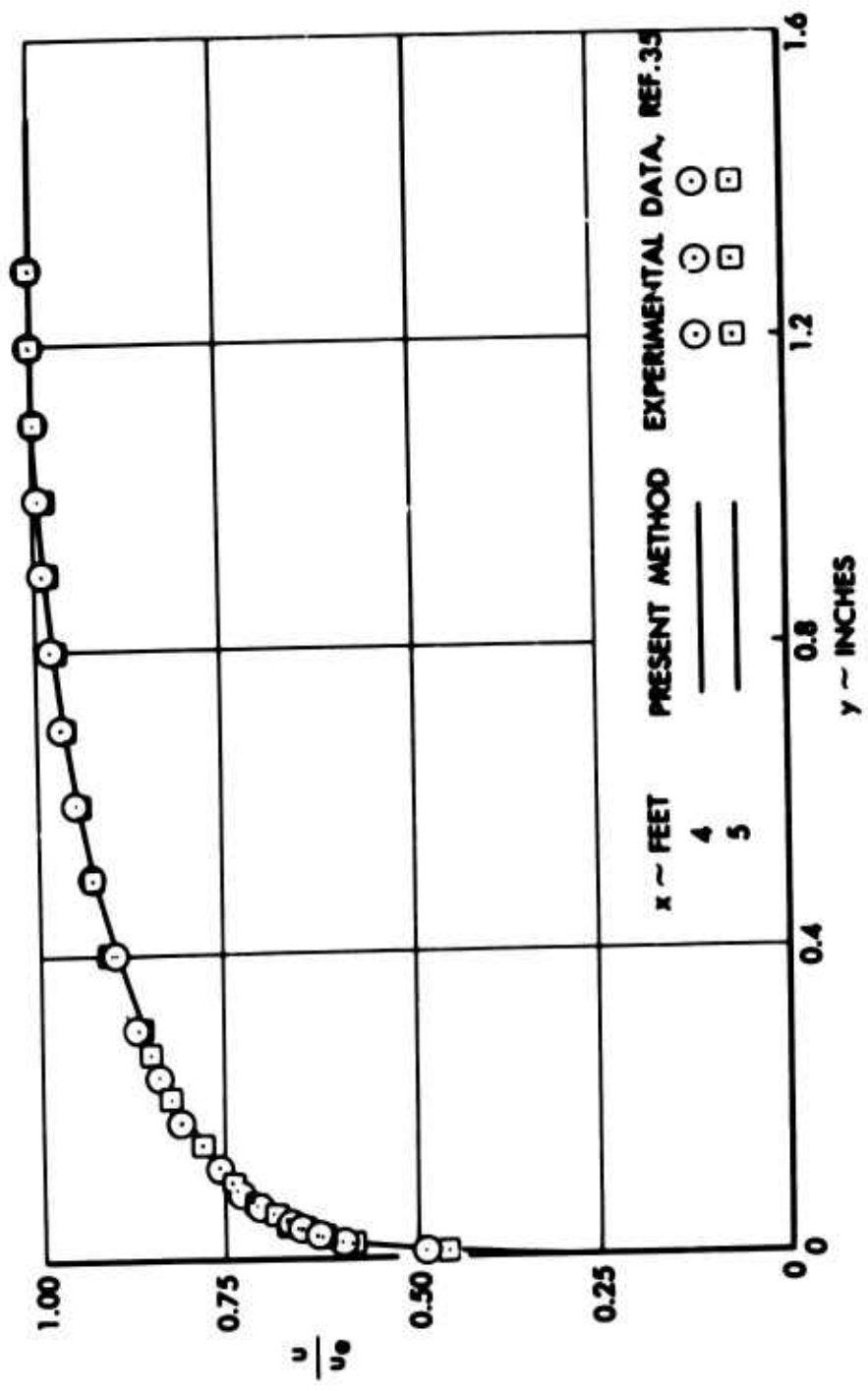


Figure 16.-Continued. (c) Comparison of calculated and experimental velocity profiles at stations x = 4 feet and 5 feet.

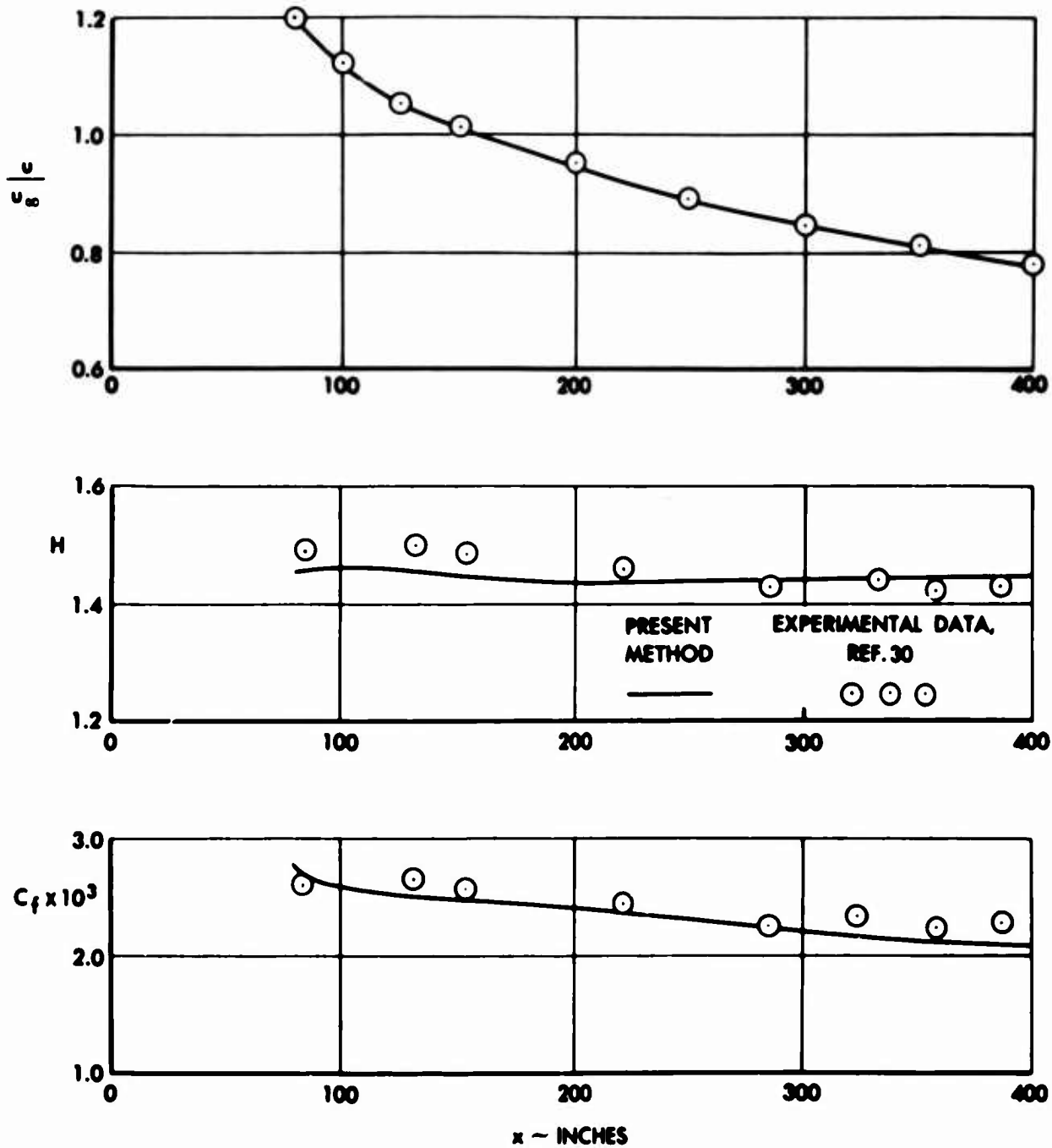


Figure 18.- Results of calculations of an equilibrium flow in an adverse pressure gradient (Experimental data of Clauser's P.D.1).

(a) Experimental velocity distribution and comparisons of calculated and experimental shape-factor and local skin-friction parameters.



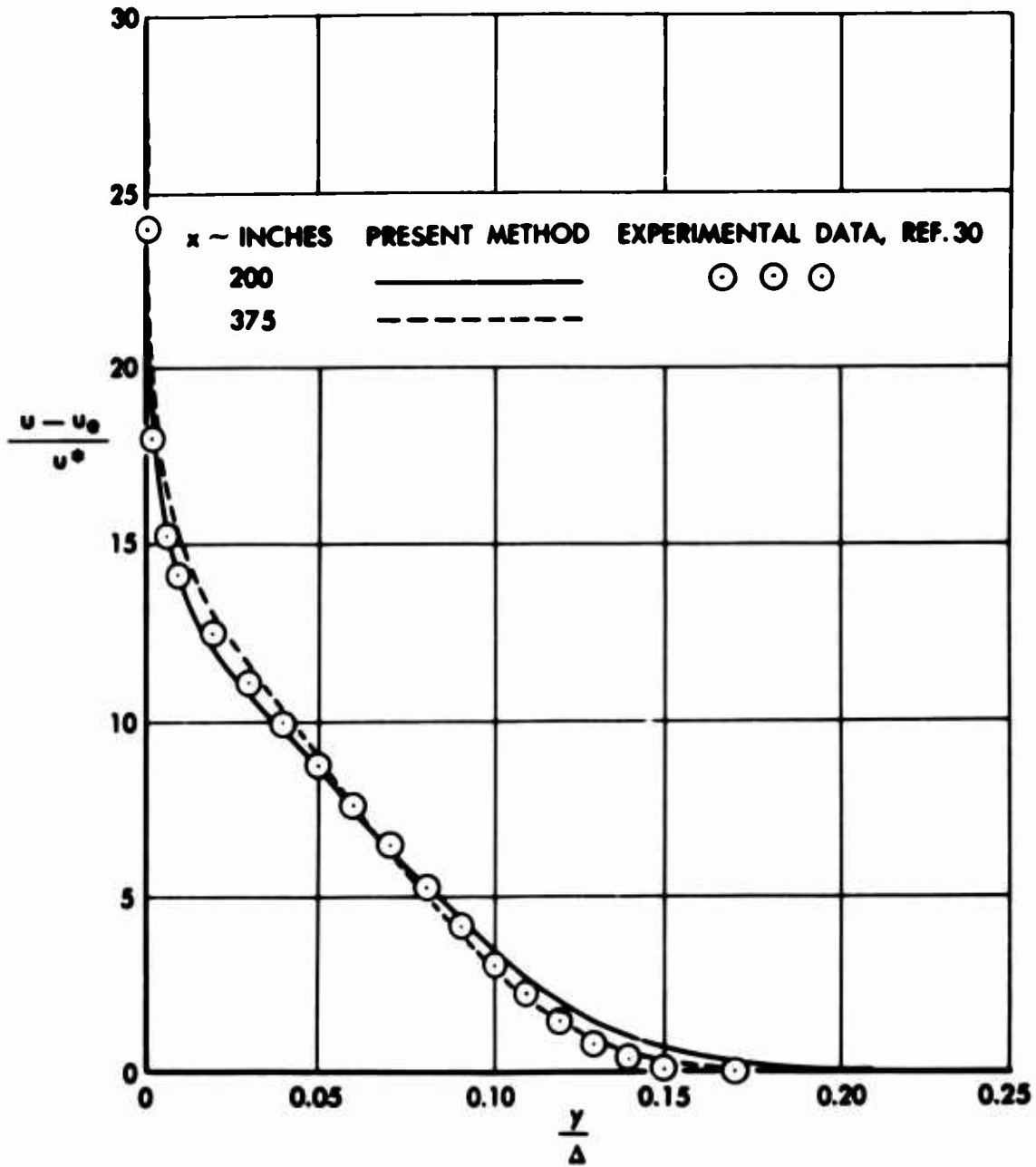


Figure 18.-Continued. (c) Comparison of calculated and experimental velocity profiles in the defect-law coordinates at  $x = 200$  and  $375$  inches.

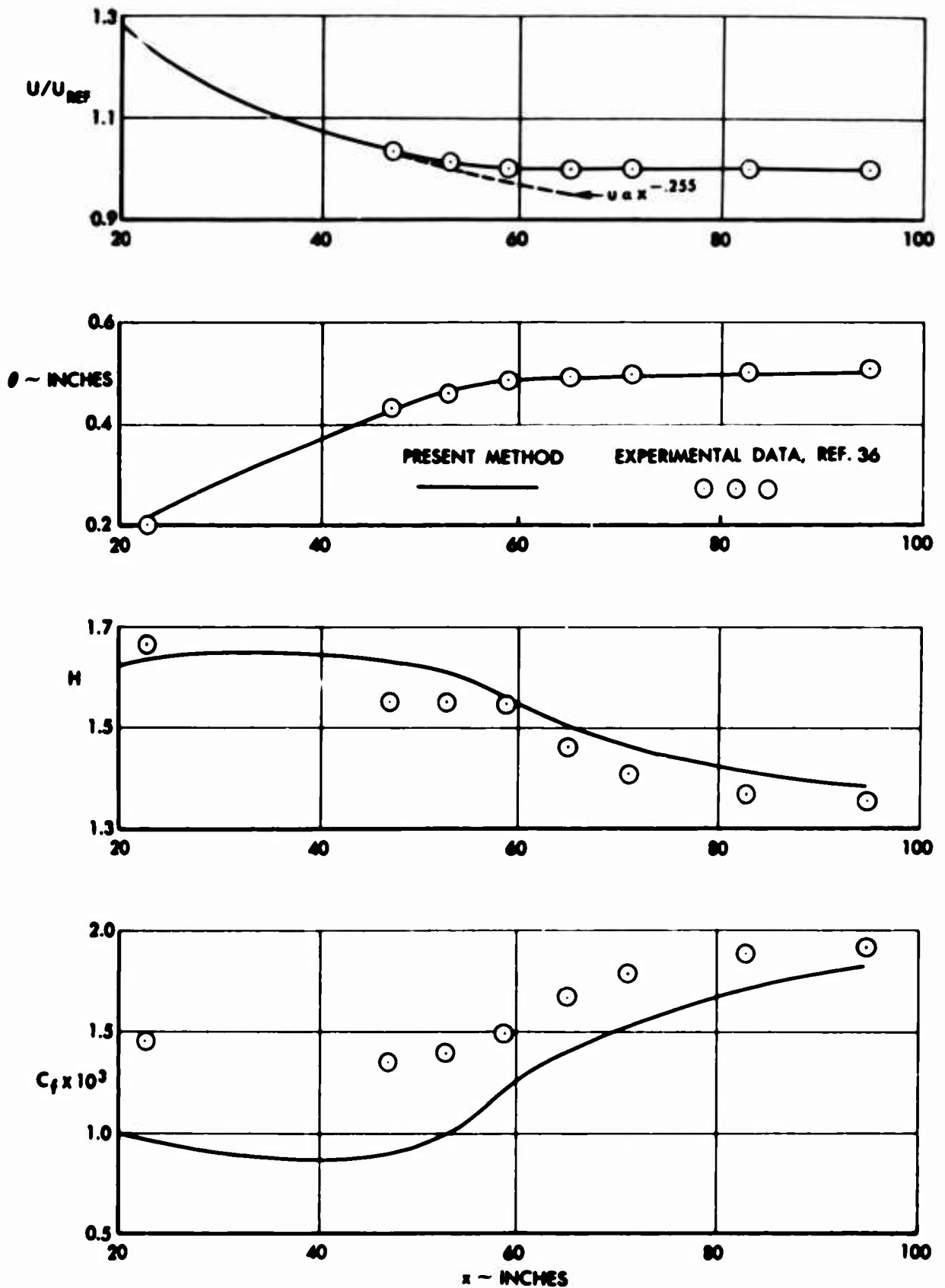


Figure 20.-Results of calculations of an equilibrium flow recovering to constant pressure flow (Experimental data of Bradshaw and Ferriss,  $\alpha = -0.255$  - 0).  
 (a) Experimental velocity distribution and comparisons of calculated and experimental momentum thickness, shape-factor and local skin-friction parameters.

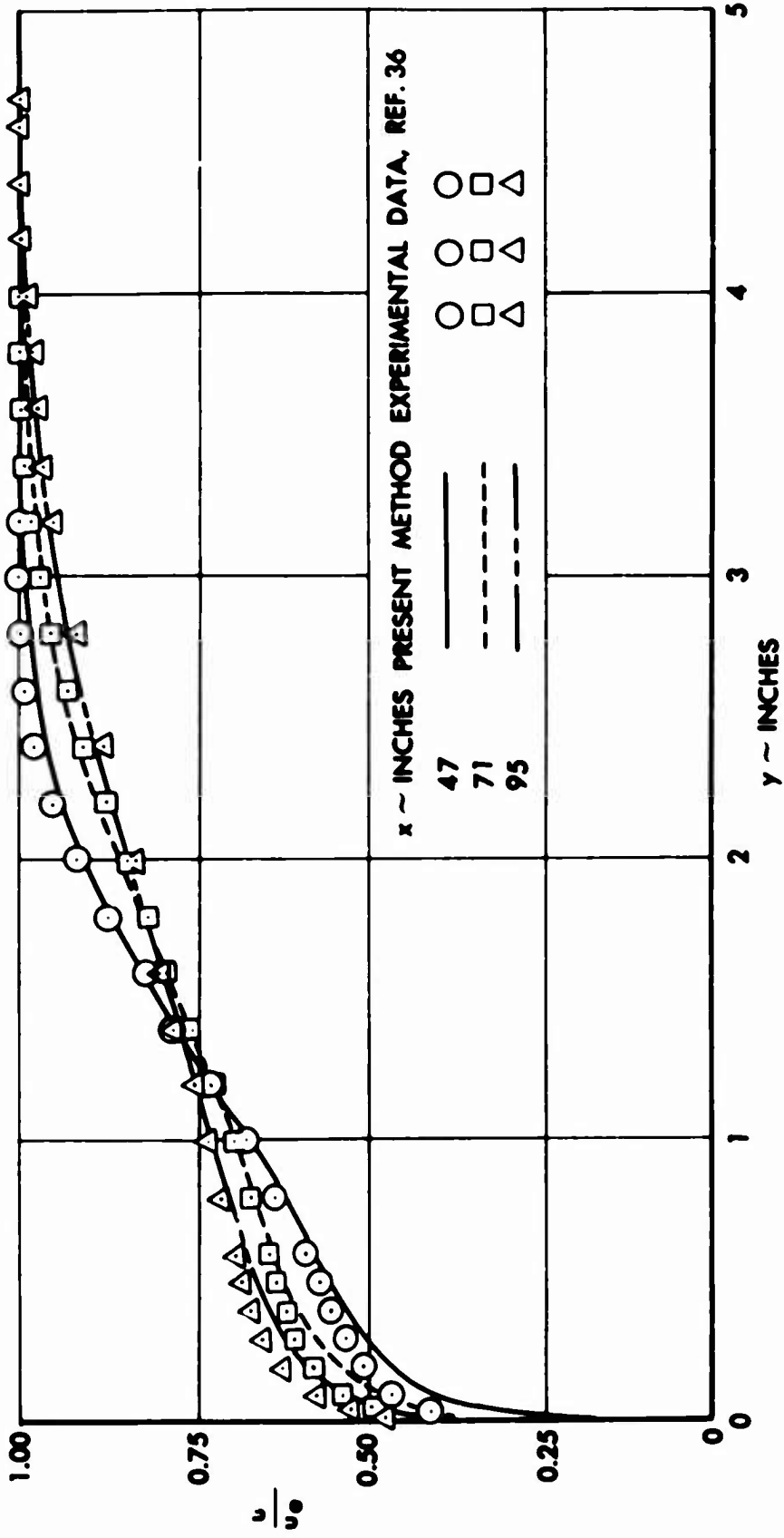


Figure 20.-Continued. (b) Comparison of calculated and experimental velocity profiles at  $x = 47, 71$  and  $95$  inches.

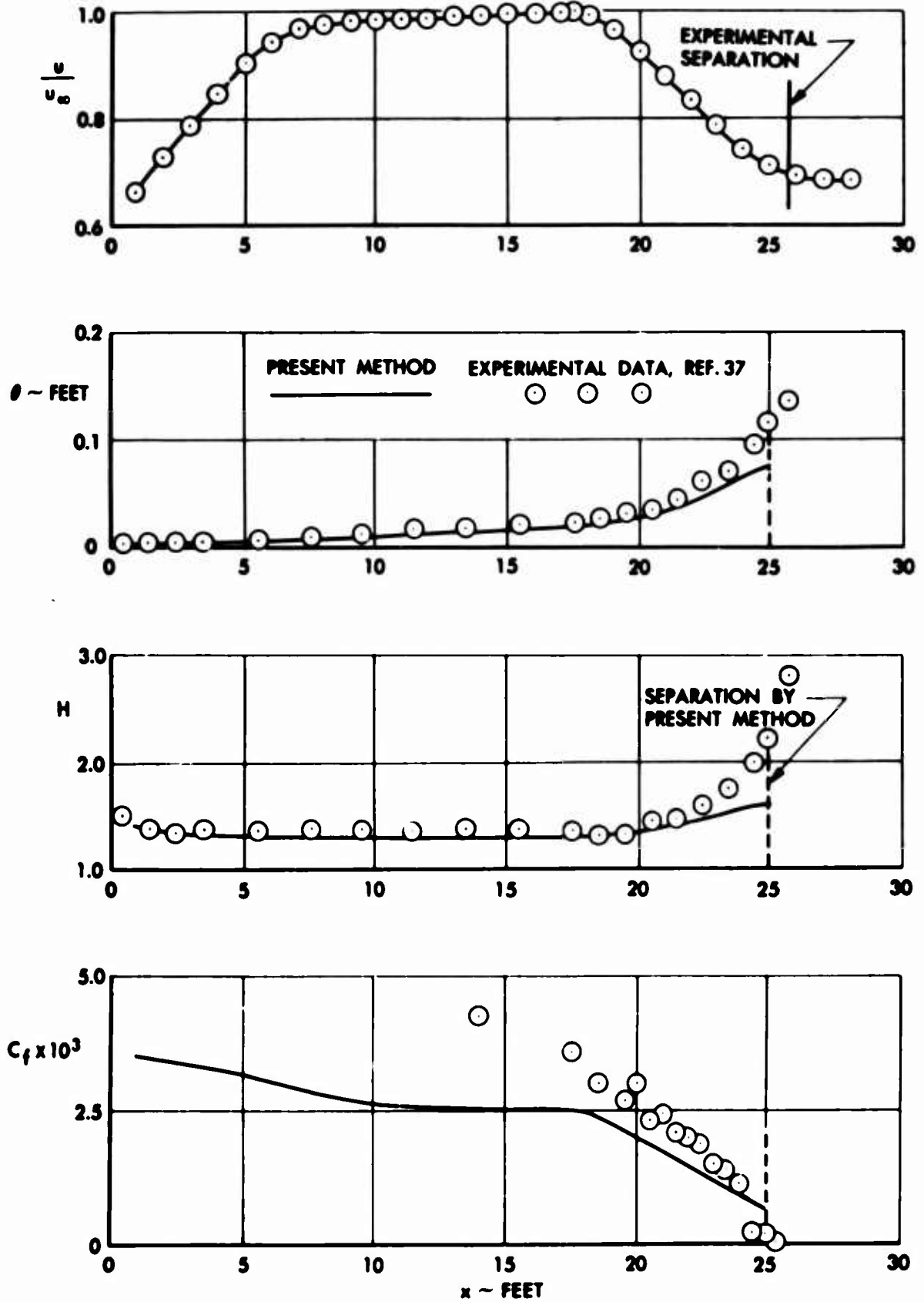


Figure 21.- Results of calculations for favorable and adverse pressure gradients on an airfoil-like body (Experimental data of Schubauer and Klebanoff).  
 (a) Experimental velocity distribution and comparisons of calculated and experimental momentum-thickness, shape-factor, and local skin-friction parameters.

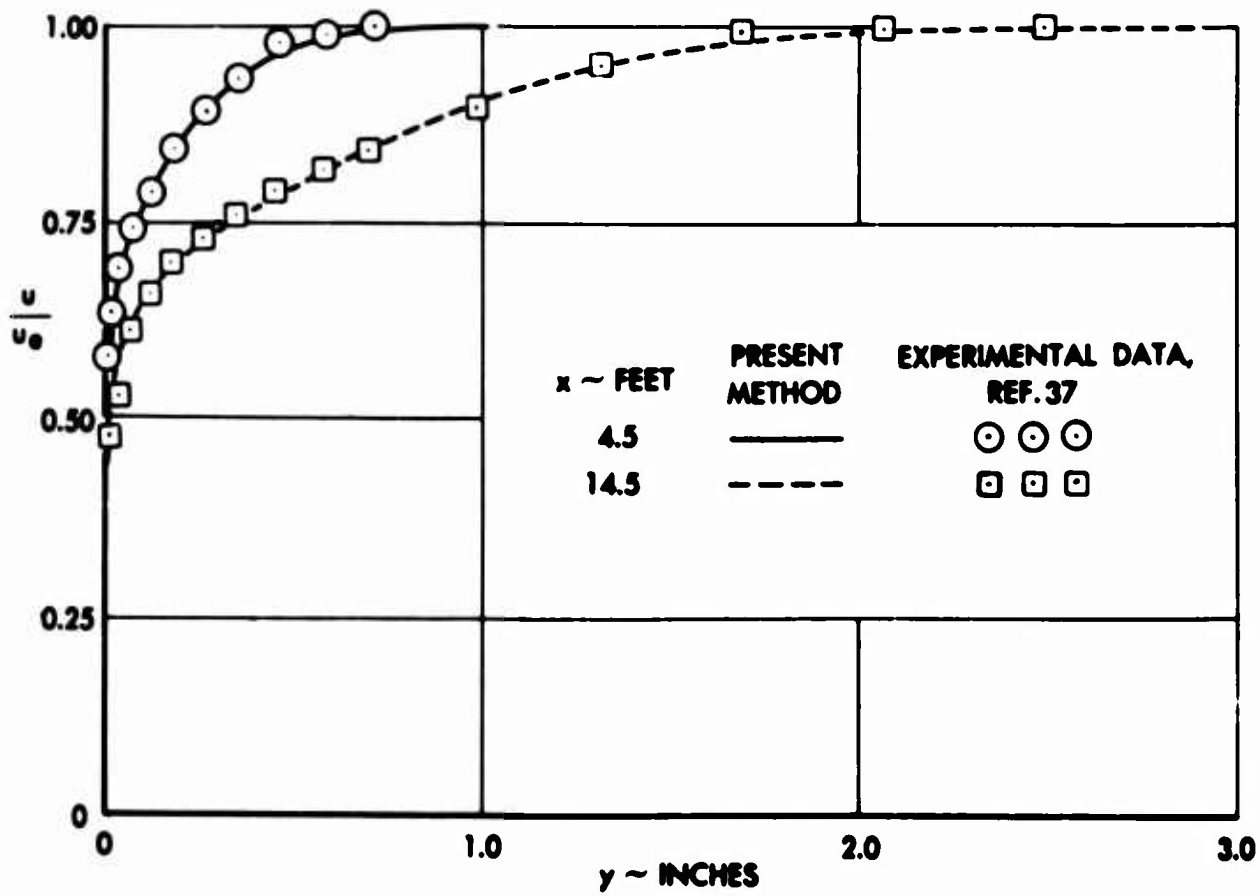


Figure 21.-Continued. (b) Comparison of calculated and experimental velocity profiles at  $x = 4.5$  and 14.5 feet.

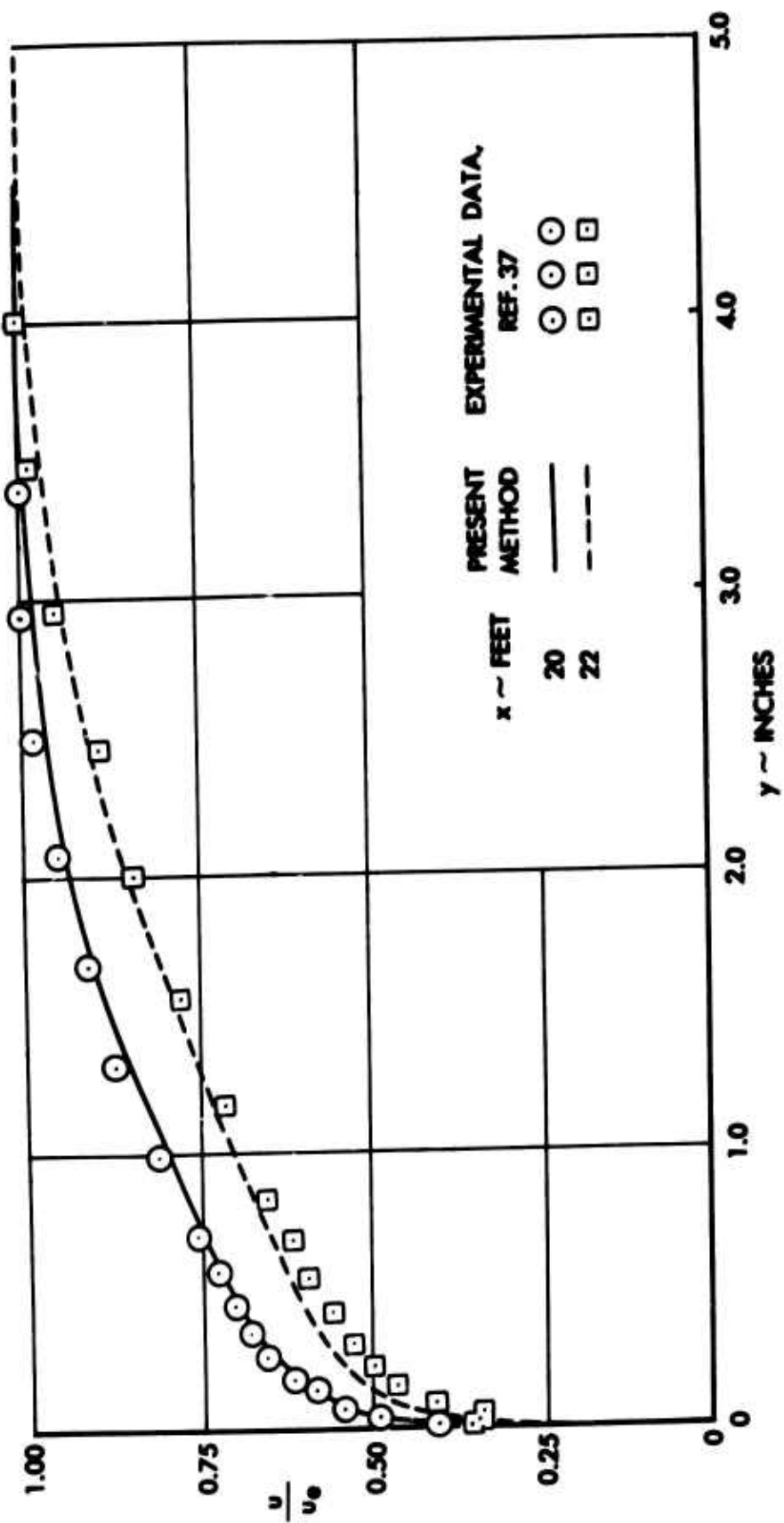


Figure 21.-Continued. (c) Comparison of calculated and experimental velocity profiles at x = 20 and 22 feet.

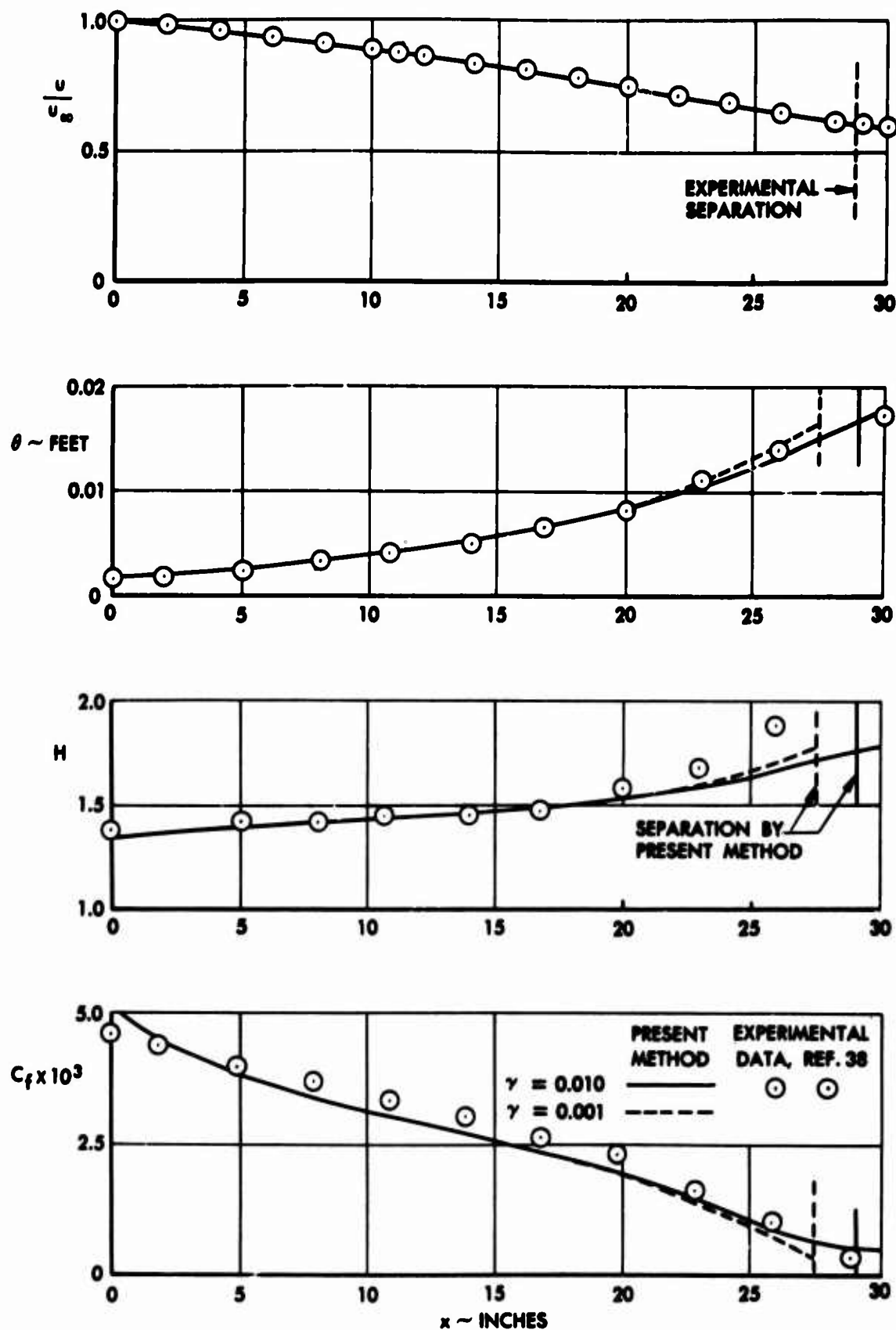


Figure 23.- Results of calculations for a nonequilibrium flow in an adverse pressure gradient (Experimental data of Moses' P.D.2).  
 (a) Experimental velocity distribution and comparison of calculated and experimental momentum-thickness, shape-factor, and local skin-friction parameters.

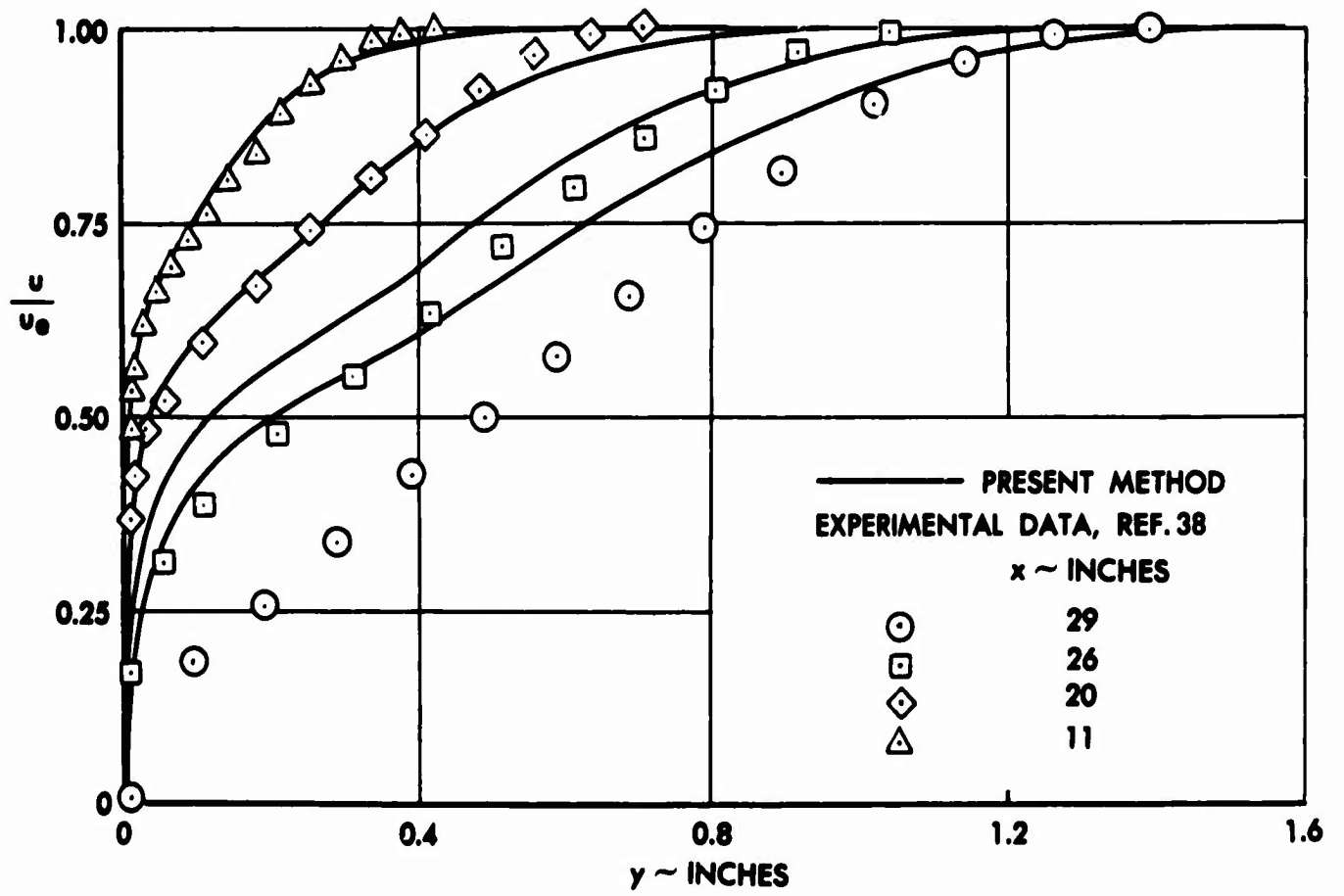


Figure 23.- Continued. (b) Comparison of calculated and experimental velocity profiles at x = 11, 20, 26, and 29 inches.

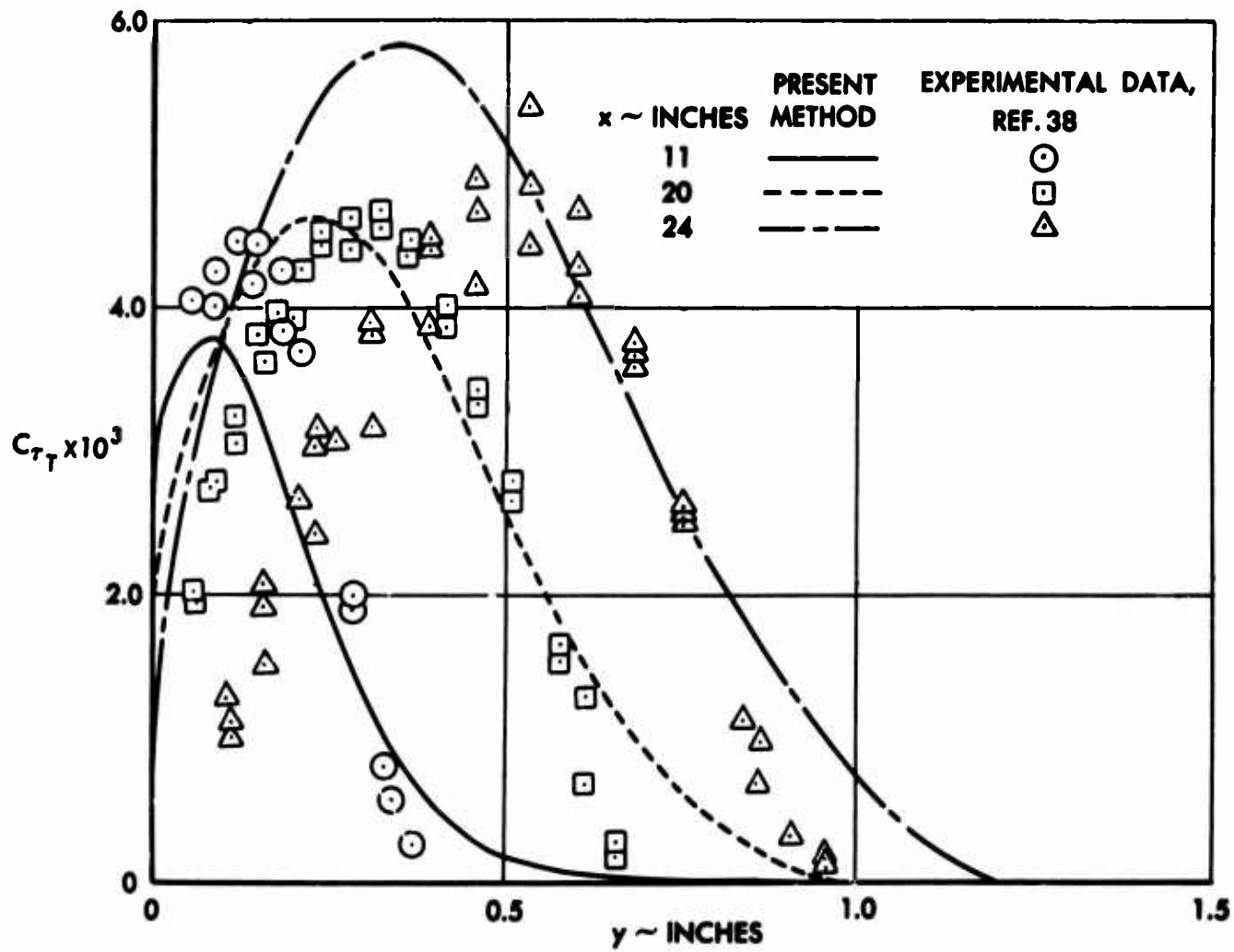


Figure 23.-Continued. (c) Comparison of calculated and experimental turbulent shear-stress coefficients at  $x = 11, 20,$  and  $24$  inches.

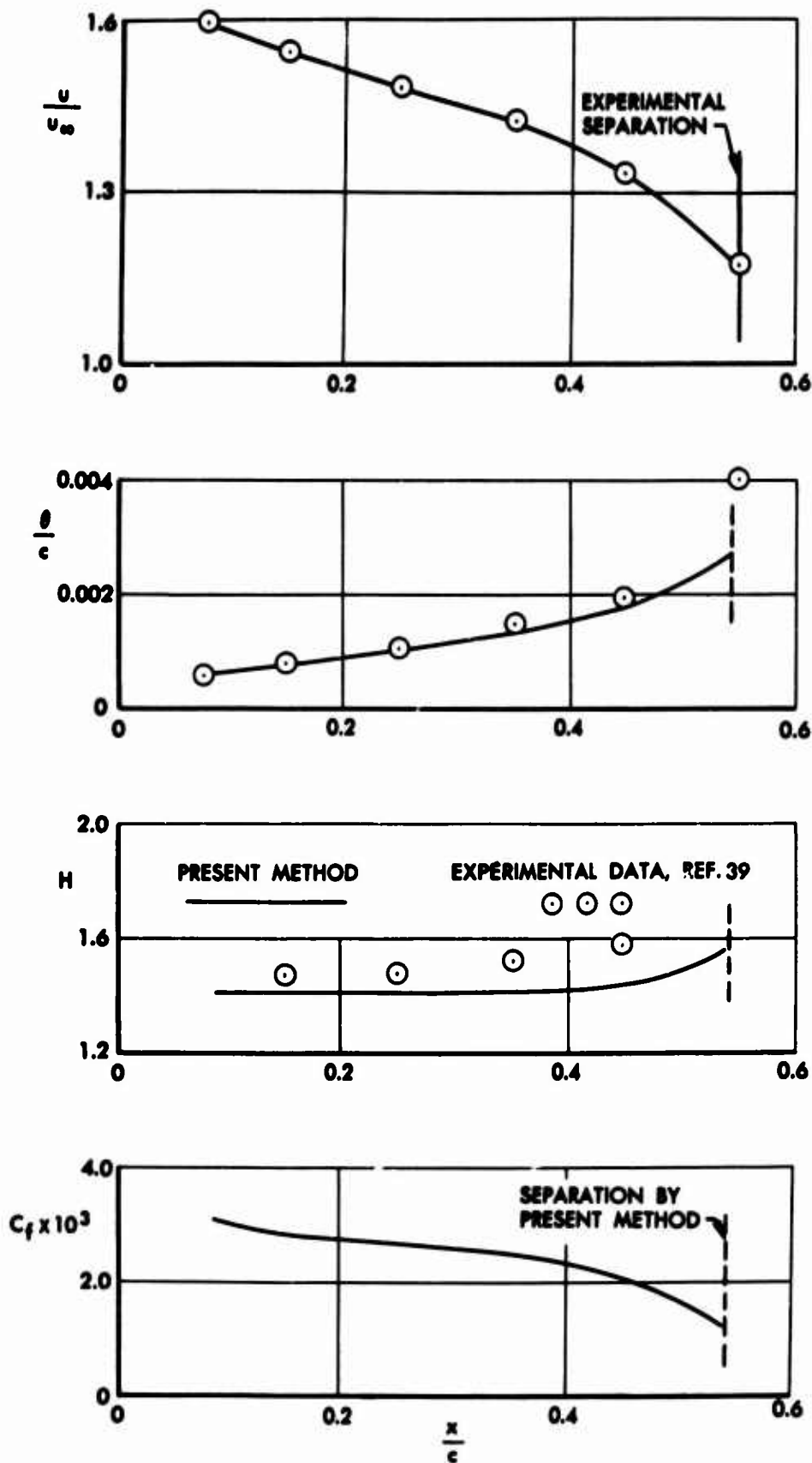


Figure 24.- Results of calculations for an airfoil with separation (Experimental data of von Doenhoff and Tetervin, NACA 65(216)-222 Airfoil).

(a) Experimental velocity distribution and comparisons of calculated and experimental momentum-thickness, shape-factor, and local skin-friction parameters.

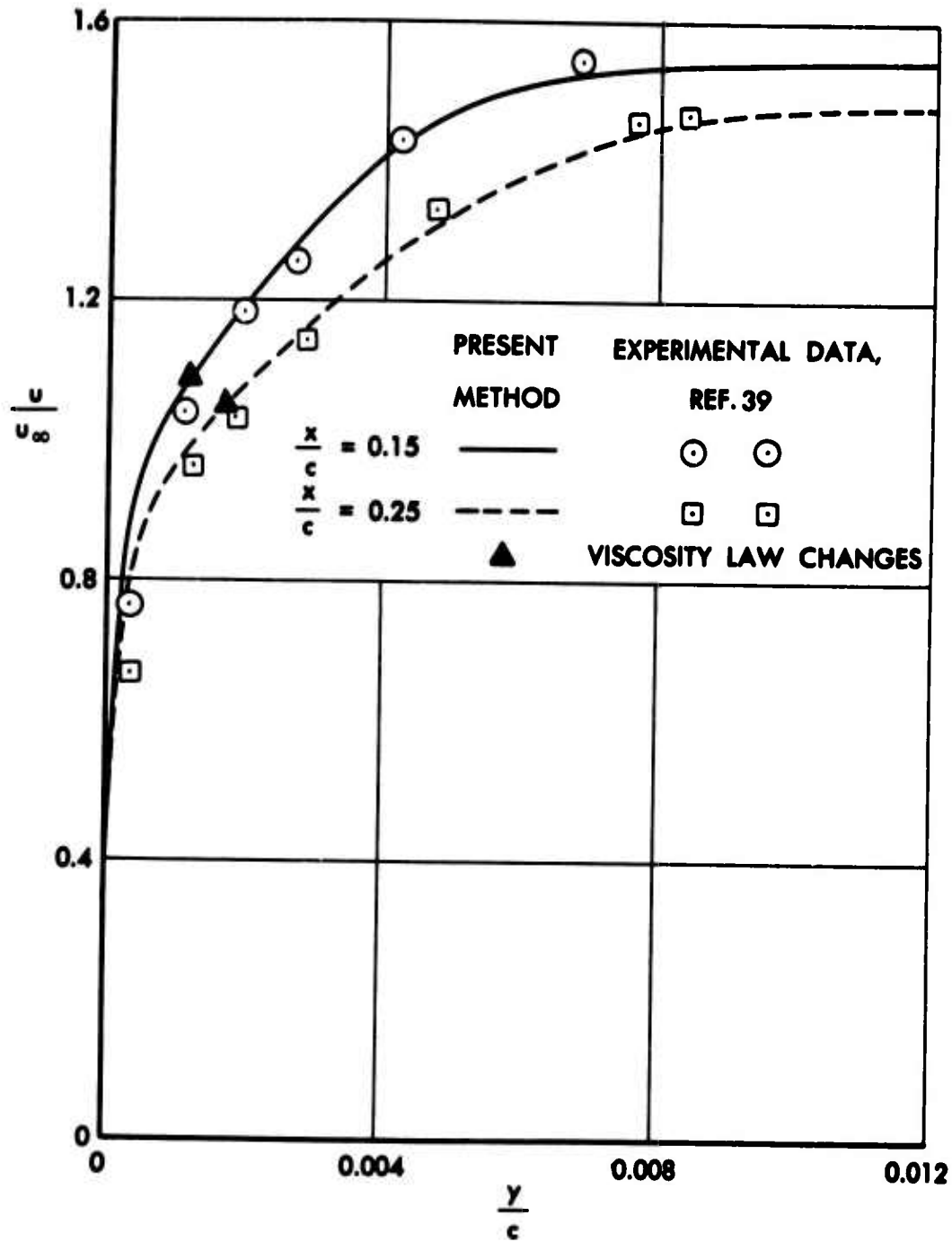


Figure 24.-Continued. (b) Comparison of calculated and experimental velocity profiles at  $x/c=0.15$  and  $0.25$ .

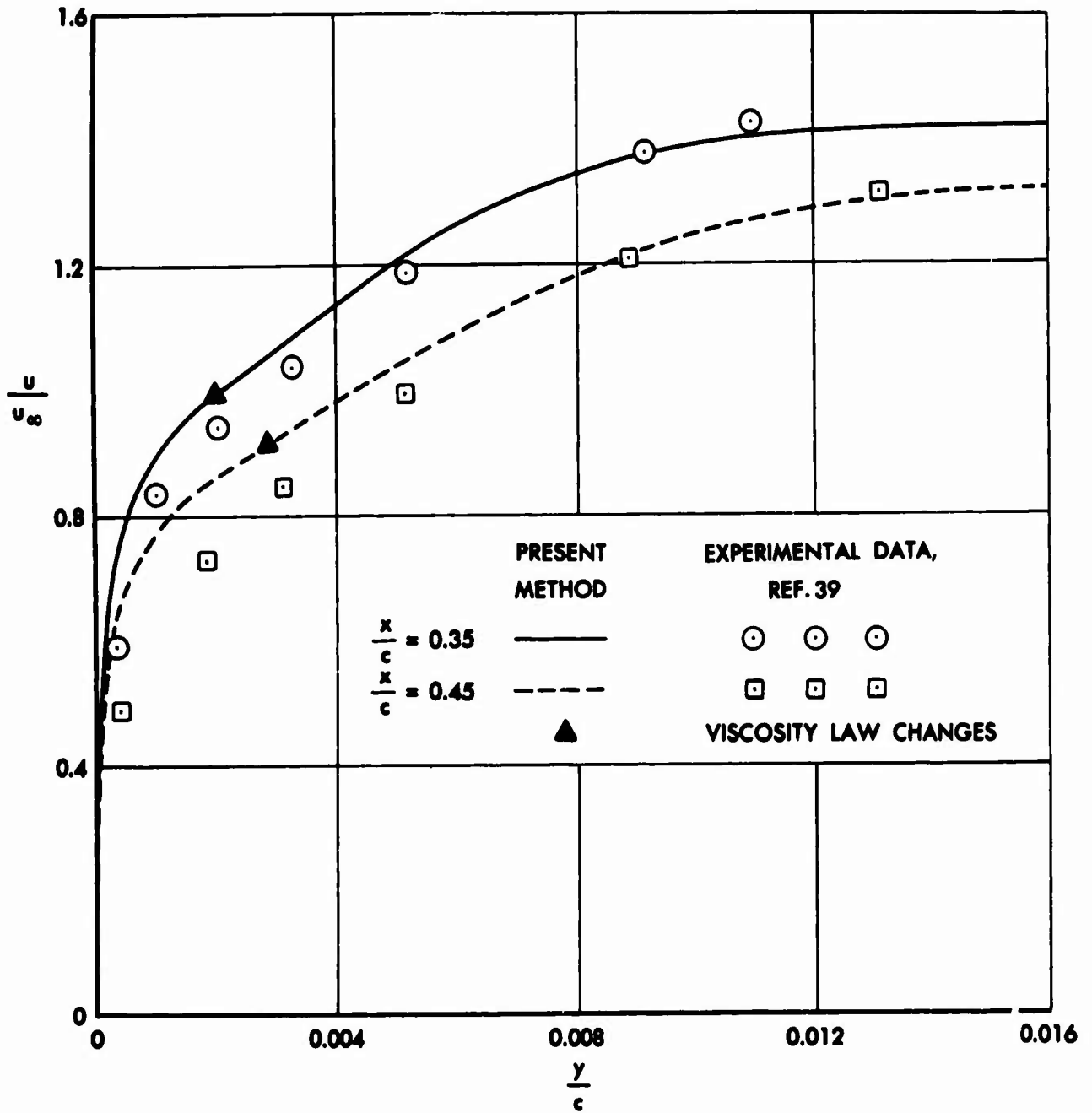


Figure 24.-Continued. (c) Comparison of calculated and experimental velocity profiles at  $x/c = 0.35$  and  $0.45$ .

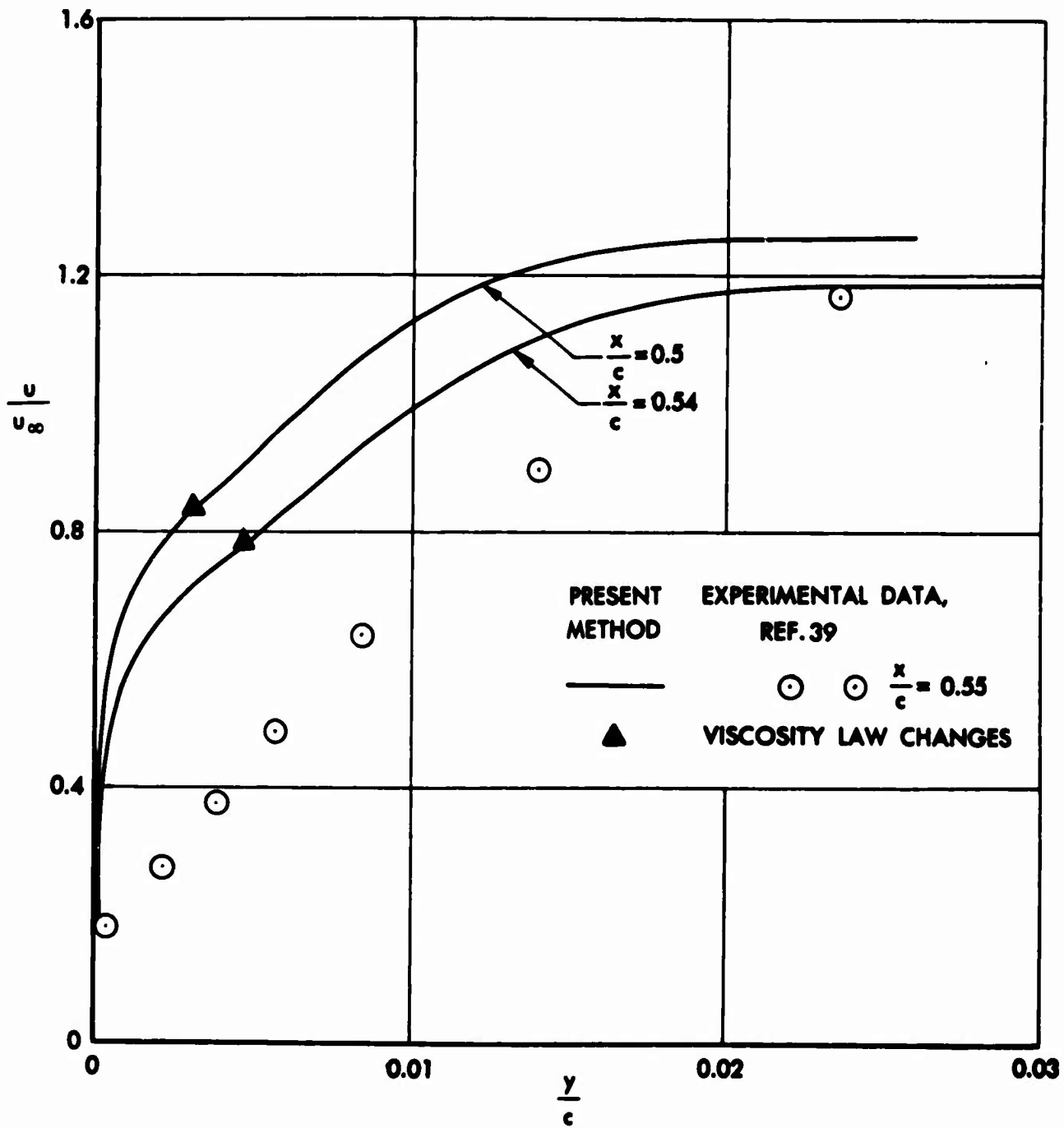


Figure 24.- Continued. (d) Comparison of calculated and experimental velocity profiles at  $x/c = 0.50$ ,  $0.54$ , and  $0.55$ .



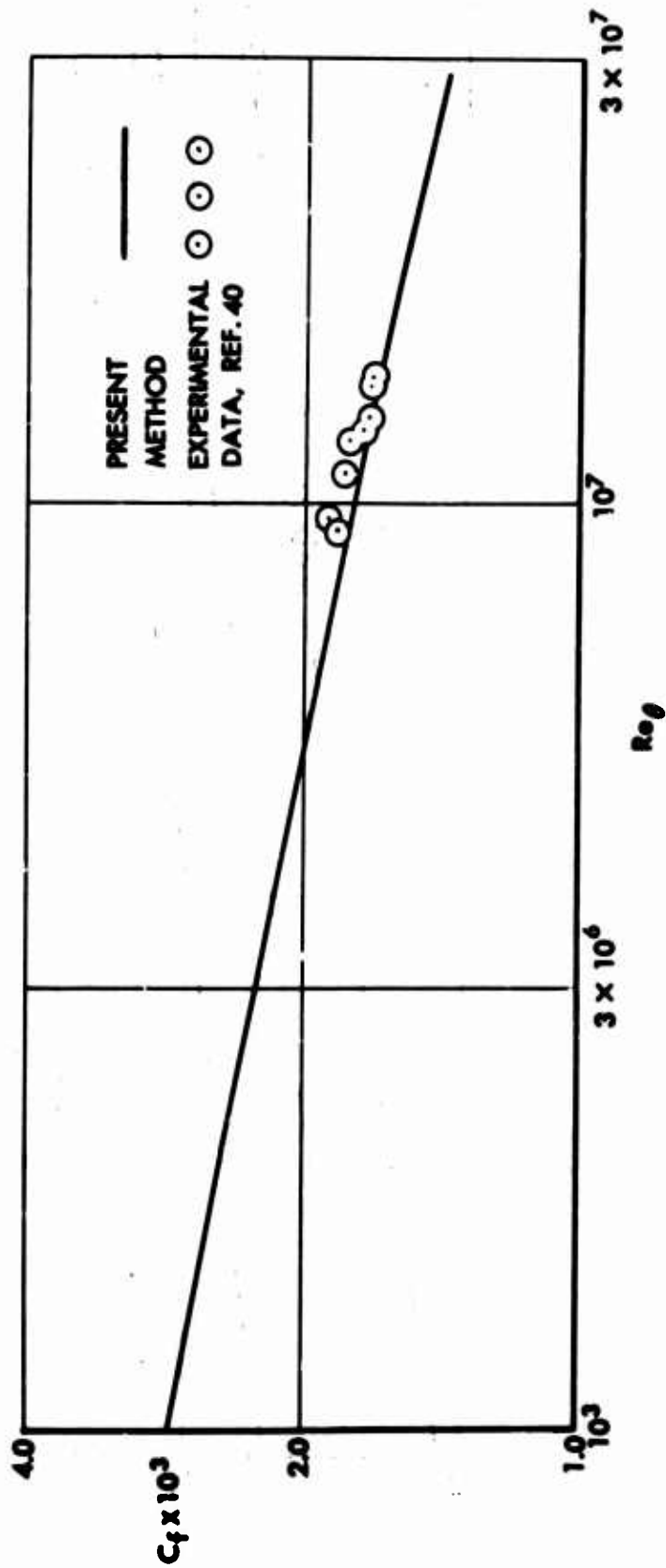


Figure 2.3.- Continued. (b) Variation of local skin friction with Reynolds number based on momentum thickness,  $Re_\theta$ .

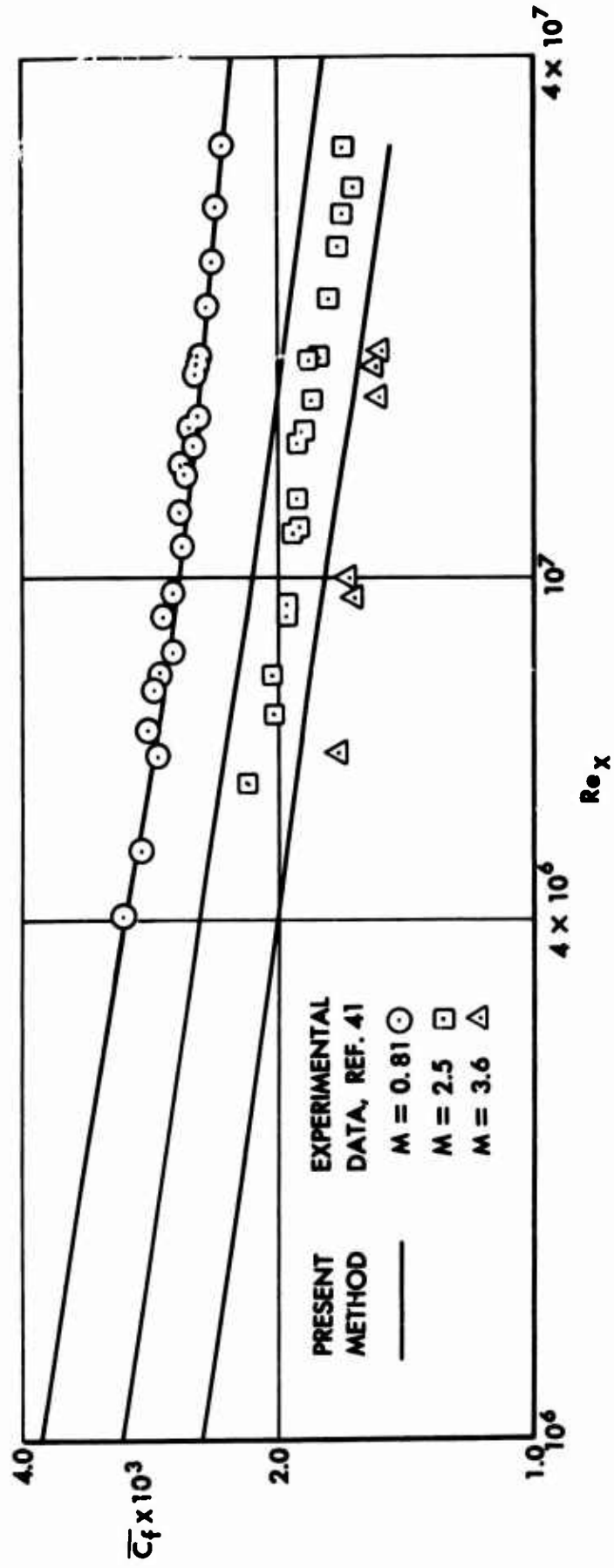
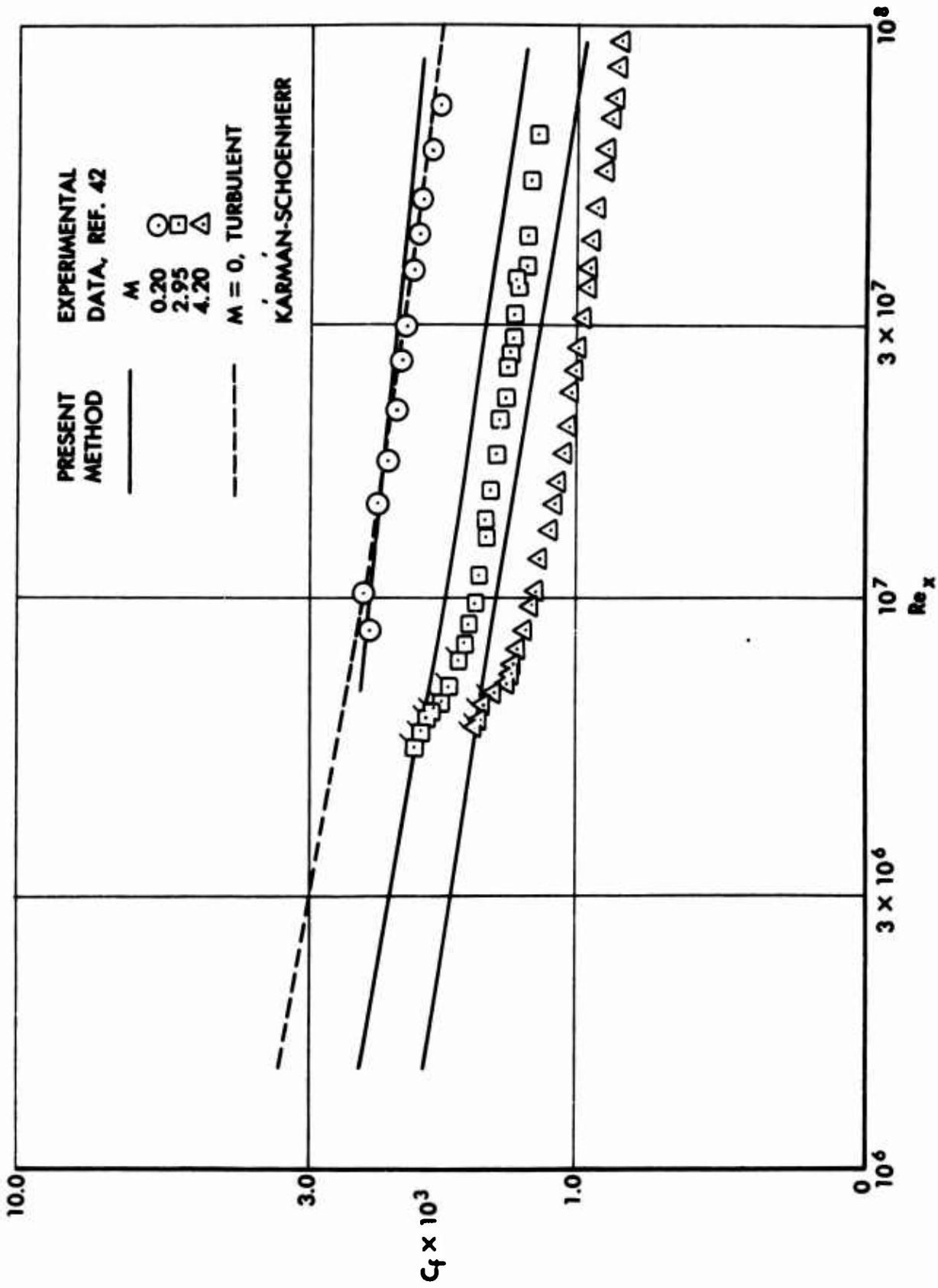


Figure 26.- Comparison of calculated and experimental average skin-friction coefficients for an adiabatic flat plate at  $M=0.81$ , 2.5 and 3.6 (Experimental data of Chapman and Kester).



Figs 27.- Comparison of calculated and experimental local skin-friction coefficients for an adiabatic flat plate at  $M=0.20, 2.95$  and  $4.20$  (Experimental data of Matting et al).

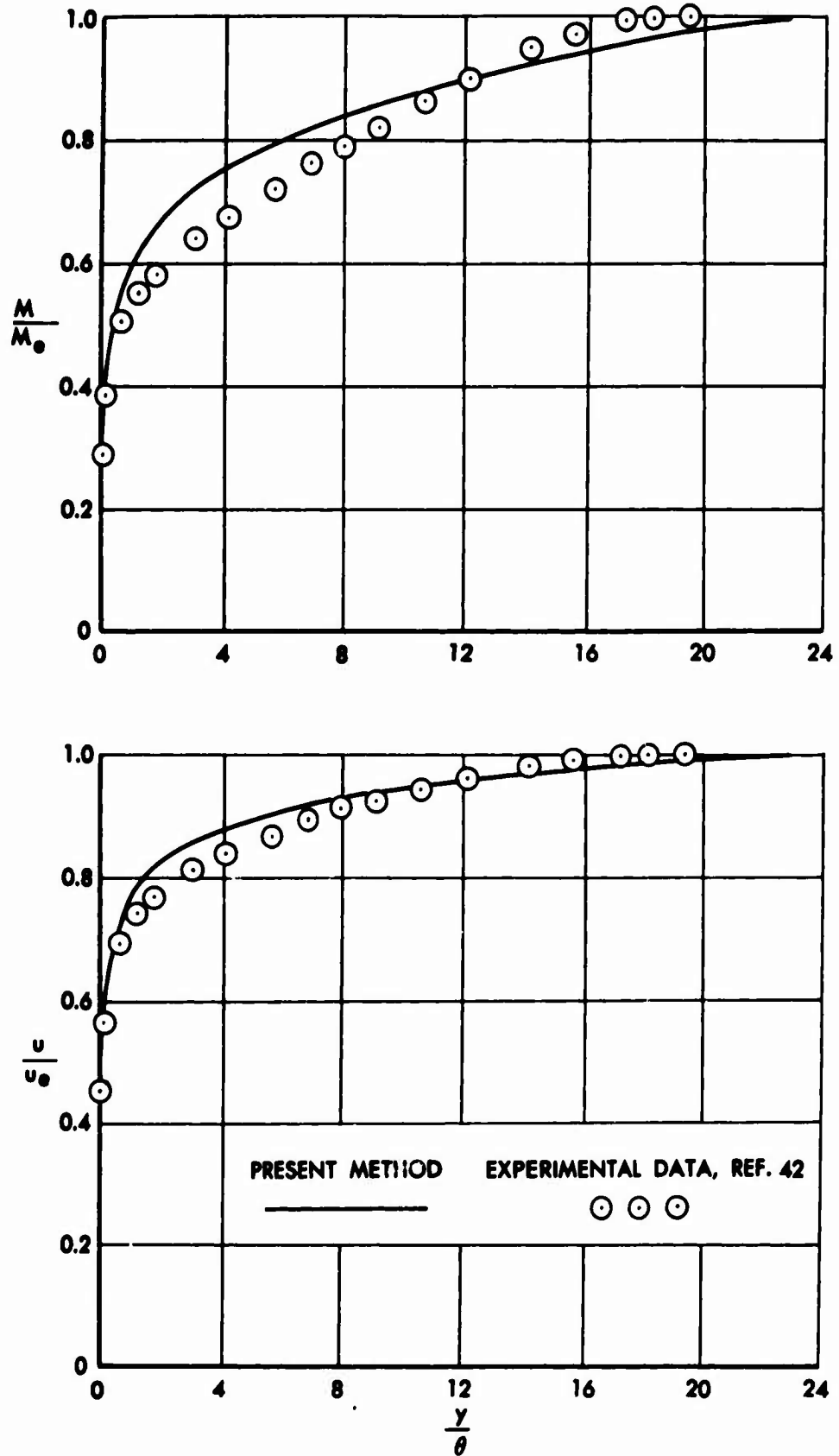


Figure 28.- Comparison of calculated and experimental boundary layer Mach number profiles and velocity profiles (Experimental data of Matting et al).  
(a)  $M=2.95$ ,  $Re_x = 31 \times 10^6$ .

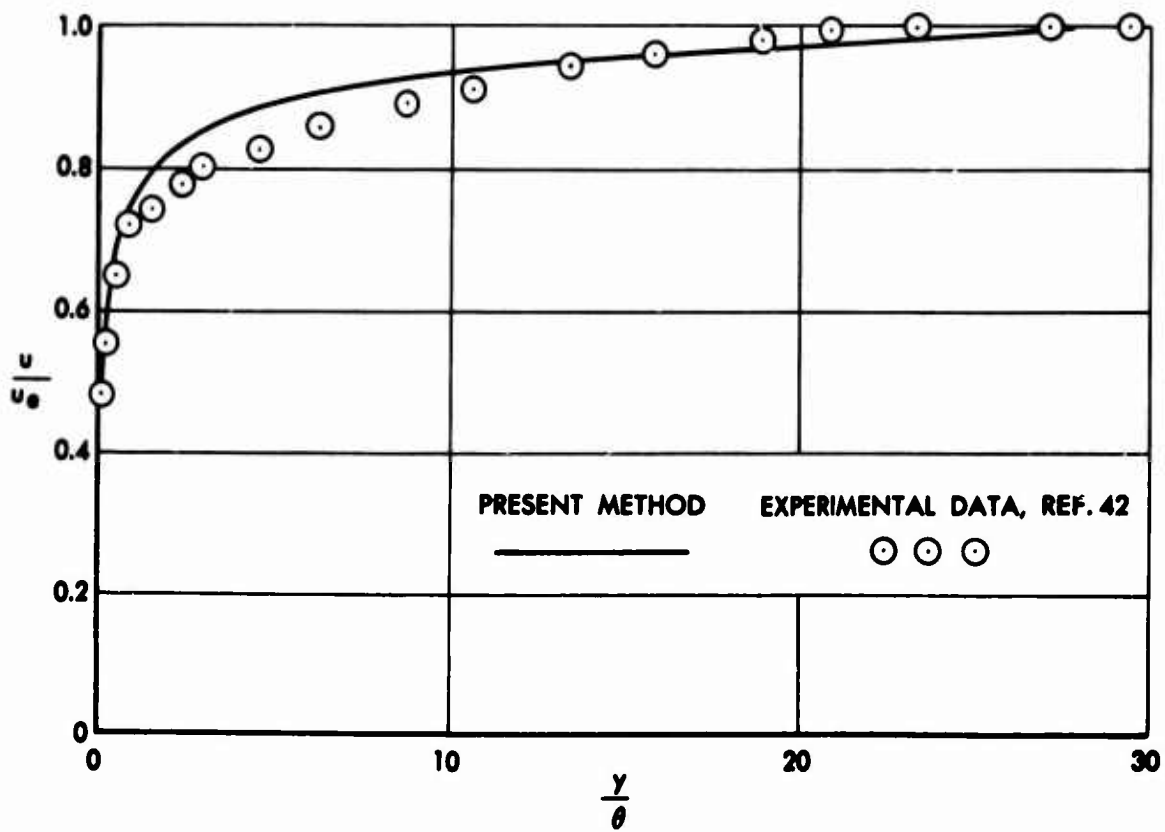
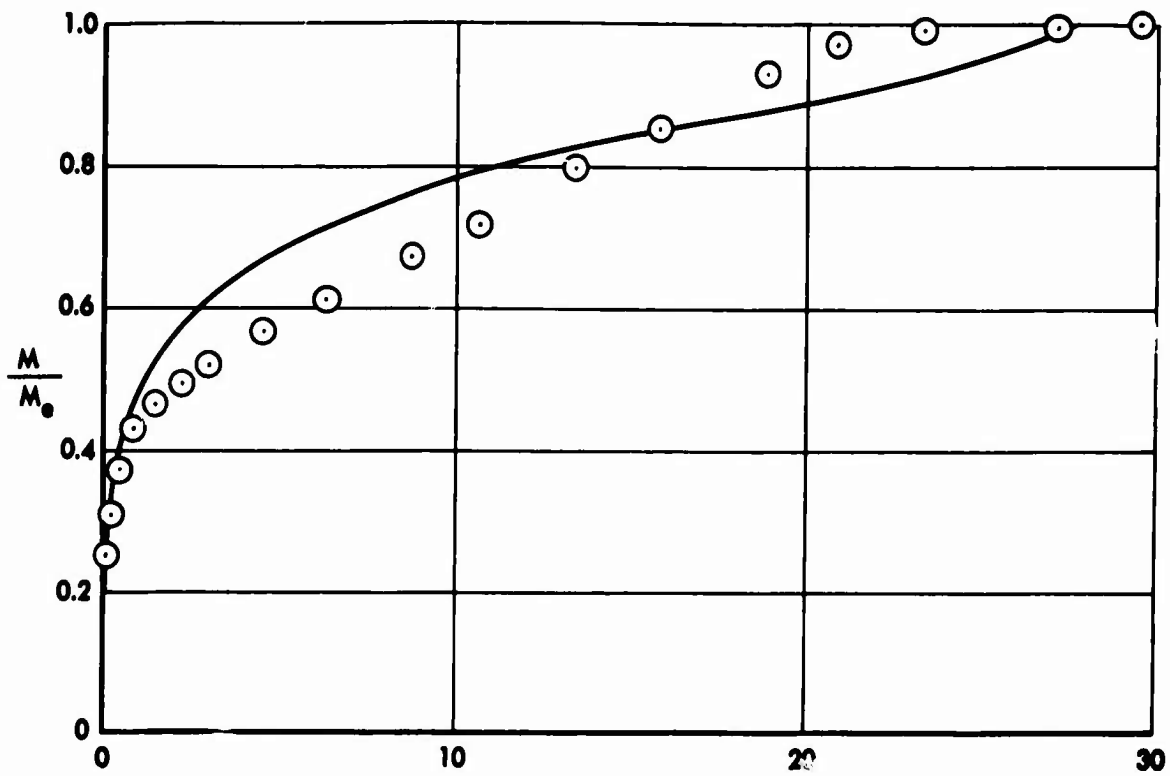


Figure 28.- Continued. (b)  $M = 4.2$ ,  $Re_x = 69 \times 10^6$ .

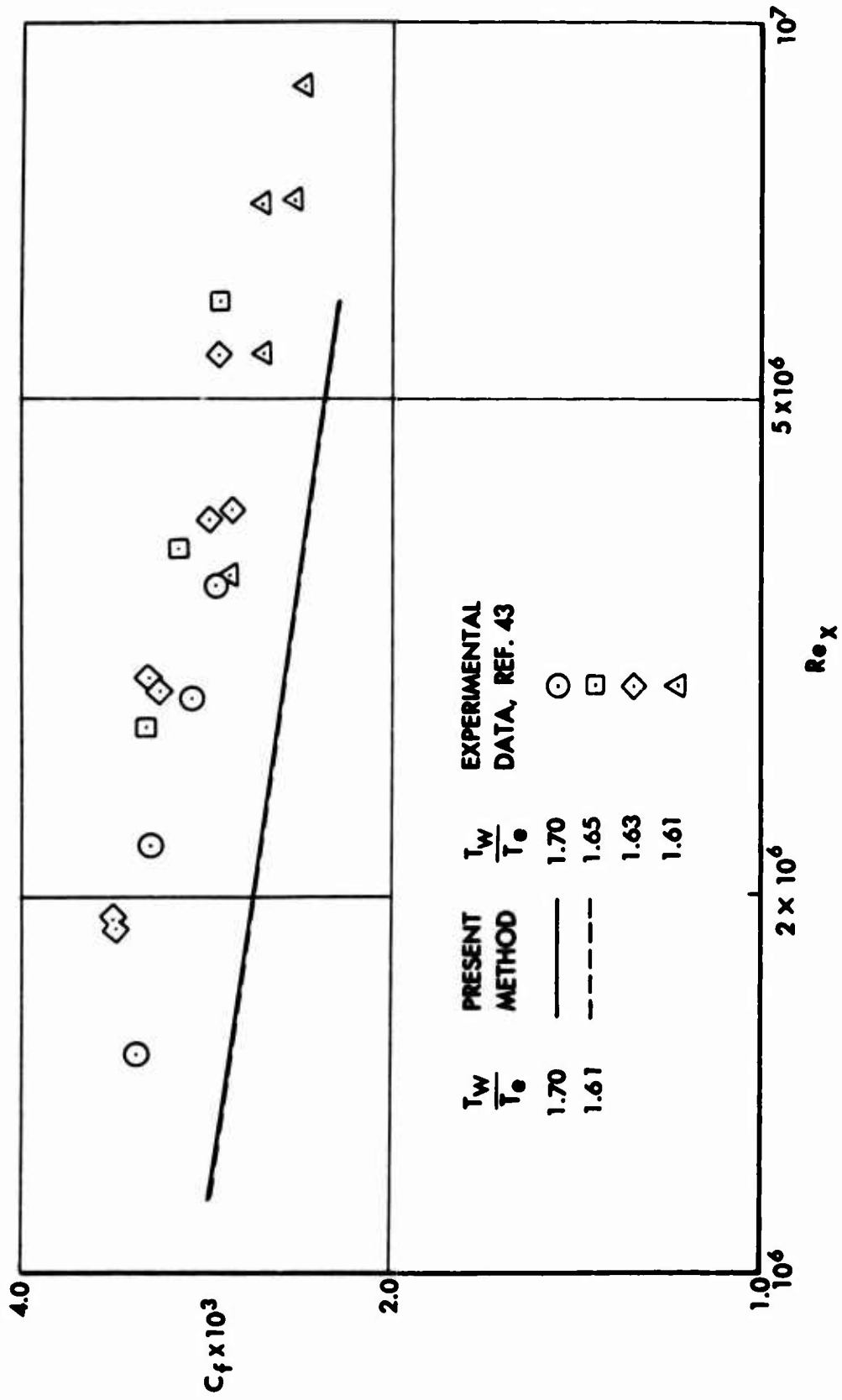


Figure 29.- Comparison of calculated and experimental average skin-friction coefficients for a flat plate with heat transfer at  $M = 1.69$  (Experimental data of Pappas).

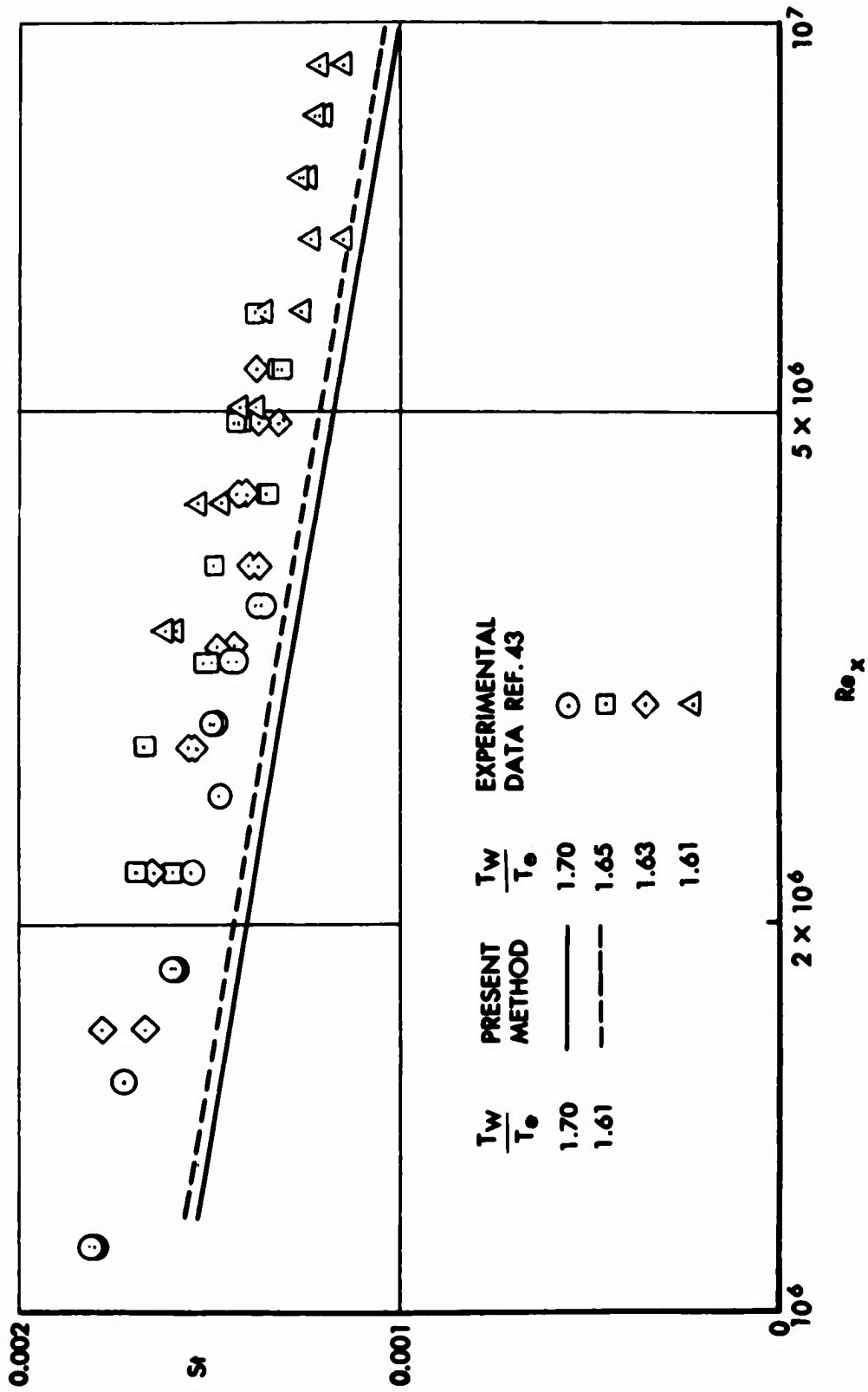


Figure 30.- Comparison of calculated and experimental local Stanton number for a flat-plate with heat transfer at  $M = 1.69$  (Experimental data of Pappas).

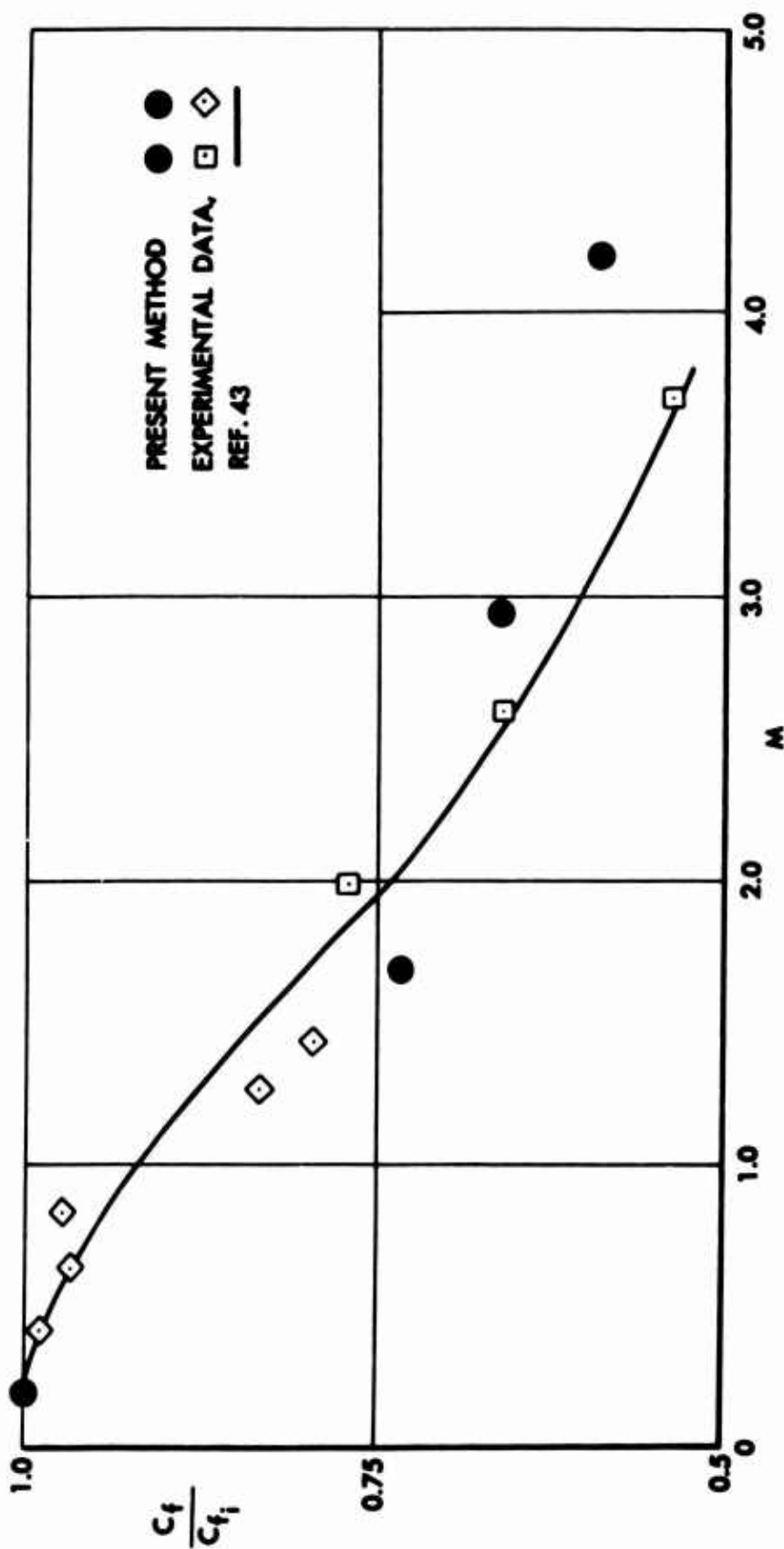


Figure 31.- Comparison of skin-friction variation with Mach number.

Unclassified

Security Classification

**DOCUMENT CONTROL DATA - R&D**

*(Security classification of title, body of abstract and indexing annotation must be entered when the overall report is classified)*

<b>1. ORIGINATING ACTIVITY (Corporate author)</b> Douglas Aircraft Company Aircraft Division Long Beach, California		<b>2a. REPORT SECURITY CLASSIFICATION</b> Unclassified	
		<b>2b. GROUP</b>	
<b>3. REPORT TITLE</b> Numerical Solution of the Turbulent-Boundary-Layer Equations			
<b>4. DESCRIPTIVE NOTES (Type of report and inclusive dates)</b> Technical Report			
<b>5. AUTHOR(S) (Last name, first name, initial)</b> Smith, A. M. O. Cebeci, T.			
<b>6. REPORT DATE</b> May 29, 1967		<b>7a. TOTAL NO. OF PAGES</b> 142	<b>7b. NO. OF REFS</b> 46
<b>8a. CONTRACT OR GRANT NO.</b> NOW 66-0324-c <b>a. PROJECT NO.</b>		<b>8a. ORIGINATOR'S REPORT NUMBER(S)</b> DAC 33735	
<b>c.</b> <b>d.</b>		<b>8b. OTHER REPORT NO(S) (Any other numbers that may be assigned to this report)</b> None	
<b>10. AVAILABILITY/LIMITATION NOTICES</b> Distribution of this document is unlimited			
<b>11. SUPPLEMENTARY NOTES</b> None		<b>12. SPONSORING MILITARY ACTIVITY</b> Naval Ordnance Systems Command Department of the Navy Washington, D. C.	
<b>13. ABSTRACT</b> This report presents a numerical solution of turbulent boundary-layer equations for both compressible and incompressible flows. An eddy viscosity concept is used to eliminate the Reynolds shear-stress term, and an eddy-conductivity concept is used to eliminate the time mean of the product of fluctuating velocity and temperature. The turbulent boundary layer is regarded as a composite layer consisting of inner and outer regions, and a separate expression for eddy viscosity is used in each region. The ratio of eddy-viscosity to eddy conductivity is assumed to be constant. An implicit finite-difference method is used in the solution of both momentum and energy equations after they are linearized.			

DD FORM 1473  
1 JAN 64

Unclassified

Security Classification

14. KEY WORDS	LINK A		LINK B		LINK C	
	ROLE	WT	ROLE	WT	ROLE	WT
Boundary Layer Compressible Incompressible Turbulent						

**INSTRUCTIONS**

1. **ORIGINATING ACTIVITY:** Enter the name and address of the contractor, subcontractor, grantee, Department of Defense activity or other organization (*corporate author*) issuing the report.
- 2a. **REPORT SECURITY CLASSIFICATION:** Enter the overall security classification of the report. Indicate whether "Restricted Data" is included. Marking is to be in accordance with appropriate security regulations.
- 2b. **GROUP:** Automatic downgrading is specified in DoD Directive 5200.10 and Armed Forces Industrial Manual. Enter the group number. Also, when applicable, show that optional markings have been used for Group 3 and Group 4 as authorized.
3. **REPORT TITLE:** Enter the complete report title in all capital letters. Titles in all cases should be unclassified. If a meaningful title cannot be selected without classification, show title classification in all capitals in parentheses immediately following the title.
4. **DESCRIPTIVE NOTES:** If appropriate, enter the type of report, e. g., interim, progress, summary, annual, or final. Give the inclusive dates when a specific reporting period is covered.
5. **AUTHOR(S):** Enter the name(s) of author(s) as shown on or in the report. Enter last name, first name, middle initial. If military, show rank and branch of service. The name of the principal author is an absolute minimum requirement.
6. **REPORT DATE:** Enter the date of the report as day, month, year, or month, year. If more than one date appears on the report, use date of publication.
- 7a. **TOTAL NUMBER OF PAGES:** The total page count should follow normal pagination procedures, i. e., enter the number of pages containing information.
- 7b. **NUMBER OF REFERENCES:** Enter the total number of references cited in the report.
- 8a. **CONTRACT OR GRANT NUMBER:** If appropriate, enter the applicable number of the contract or grant under which the report was written.
- 8b, 8c, & 8d. **PROJECT NUMBER:** Enter the appropriate military department identification, such as project number, subproject number, system numbers, task number, etc.
- 9a. **ORIGINATOR'S REPORT NUMBER(S):** Enter the official report number by which the document will be identified and controlled by the originating activity. This number must be unique to this report.
- 9b. **OTHER REPORT NUMBER(S):** If the report has been assigned any other report numbers (*either by the originator or by the sponsor*), also enter this number(s).
10. **AVAILABILITY/LIMITATION NOTICES:** Enter any limitations on further dissemination of the report, other than those

imposed by security classification, using standard statements such as:

- (1) "Qualified requesters may obtain copies of this report from DDC."
- (2) "Foreign announcement and dissemination of this report by DDC is not authorized."
- (3) "U. S. Government agencies may obtain copies of this report directly from DDC. Other qualified DDC users shall request through \_\_\_\_\_."
- (4) "U. S. military agencies may obtain copies of this report directly from DDC. Other qualified users shall request through \_\_\_\_\_."
- (5) "All distribution of this report is controlled. Qualified DDC users shall request through \_\_\_\_\_."

If the report has been furnished to the Office of Technical Services, Department of Commerce, for sale to the public, indicate this fact and enter the price, if known.

11. **SUPPLEMENTARY NOTES:** Use for additional explanatory notes.
12. **SPONSORING MILITARY ACTIVITY:** Enter the name of the departmental project office or laboratory sponsoring (*paying for*) the research and development. Include address.
13. **ABSTRACT:** Enter an abstract giving a brief and factual summary of the document indicative of the report, even though it may also appear elsewhere in the body of the technical report. If additional space is required, a continuation sheet shall be attached.  
  
It is highly desirable that the abstract of classified reports be unclassified. Each paragraph of the abstract shall end with an indication of the military security classification of the information in the paragraph, represented as (TS), (S), (C), or (U).  
  
There is no limitation on the length of the abstract. However, the suggested length is from 150 to 225 words.
14. **KEY WORDS:** Key words are technically meaningful terms or short phrases that characterize a report and may be used as index entries for cataloging the report. Key words must be selected so that no security classification is required. Identifiers, such as equipment model designation, trade name, military project code name, geographic location, may be used as key words but will be followed by an indication of technical context. The assignment of links, roles, and weights is optional.